

FMH606 Master's Thesis 2024  
Process Technology

**A case study of fire and explosion risk at  
hydrogen facilities, an ignition probability  
study.**

Signe Natten Meland

Faculty of Technology, Natural Sciences and Maritime Sciences  
Campus Porsgrunn



**Course:** FMH606 Master's Thesis 2024

**Title:** *A case study of fire and explosion risk at hydrogen facilities, an ignition probability study.*

**Pages:** 142

**Keywords:** *Hydrogen, QRA, Ignition Probability*

**Student:** *Signe Natten Meland*

**Supervisor:** *Knut Vågsæther*

**External partner:** *Safetec*

### **Summary:**

Hydrogen is an essential energy carrier, making it very important for the global energy decarbonization process. Because of limited knowledge of ignition mechanisms, its elevated ignition risk compared to other gases present is a big issue for safety design. This can result in expensive over-caution or insufficient safety precautions, which can compromise the successful deployment of renewable energy solutions. The SAFEN JIP (Safe Energy Carriers) was made to address these knowledge gaps. The primary aim of the SAFEN model is to calculate realistic ignition probabilities for quantitative risk analysis (QRA) in facilities that handle hydrogen. To achieve this, the model needs to be tested to evaluate its performance and efficacy. This involves assessing how well the SAFEN model functions when applied to larger-scale geometries and more detailed scenarios.

In this thesis, the implementation of the SAFEN ignition probability model in the CFD software KFX-RBM is checked. KFX-RBM is further used to simulate hydrogen leaks in various geometries. The geometries used are a 40' ISO container, a hydrogen refueling station, and a process plant. The geometries were simulated with two different leak rates, 0.1 kg/s and 1 kg/s, and the location of the leak varied from the middle to the corner of the geometry to see if it affected the total ignition probability. For comparison, simulations with methane leaks have also been performed. The simulation of the 40' ISO container resulted in an ignition probability of 3.4 % for the 0.1 kg/s leak rate and 3.72 % for the 1 kg/s leak rate. For the hydrogen refueling station, the 0.1 kg/s leak rate gave an ignition probability of 3.48 %, while the 1 kg/s leak rate gave an ignition probability of 4.67 %. Finally, the process plant showed an ignition probability of 3.01 % for the 0.1 kg/s leakage and 5.66 % for the 1 kg/s leakage.

This thesis contributes to the knowledge of hydrogen ignition probability in various geometries and leak scenarios, presenting new information for improving safety precautions when handling hydrogen.

*The University of South-Eastern Norway accepts no responsibility for the results and conclusions presented in this report.*



# Preface

This thesis marks the end of my journey toward my Master's Degree at the University of South-Eastern Norway (USN). It has been an incredibly rewarding and challenging experience, and I am profoundly grateful for the support and opportunities provided. This thesis was done in collaboration with Safetec in Trondheim, Norway.

I want to thank my supervisor at the University of South-East Norway, Knut Vågsæther, for all the help he has given me, as well as the patience he has shown when I had trouble with software-related delays. I deeply appreciate his guidance on the thesis structure and his valuable feedback throughout the process. I also want to give a big thanks to my supervisor from Safetec, Ingar Fossan, for giving me the opportunity to write this master's thesis. I really appreciate all the help he has provided me, and for always being engaged and offering many great ideas for improving my thesis.

Second, I want to thank Safetec, and especially Safetec in Trondheim, for making me feel as if I were part of the crew. Thank you for letting me sit and write at your offices and for engaging in my thesis. I would like to extend special thanks to Rune Kleiveland at the Trondheim offices for helping me so much and assisting me with every software problem that occurred. I am also grateful to Nils Inge Lilleheie from DNV for helping update the SAFEN model in the software and to Geir Ove Myhr at Safetec for consistently installing the new and improved versions of the software.

Finally, I want to thank my dear family and my boyfriend, Magnus, for all the help and moral support they have provided me.

Porsgrunn, 28th May 2024

Signe Natten Meland



# Contents

<b>Preface</b>	<b>5</b>
<b>Contents</b>	<b>9</b>
List of Figures . . . . .	16
List of Tables . . . . .	18
Nomenclature . . . . .	19
<b>1 Introduction and Background</b>	<b>21</b>
1.1 Introduction . . . . .	21
1.2 Background . . . . .	22
1.3 Objective . . . . .	23
1.4 Report Structure . . . . .	24
<b>2 Theory/ Literature Study</b>	<b>25</b>
2.1 Hydrogen . . . . .	25
2.2 The danger of a hydrogen leak . . . . .	25
2.3 Hydrogen- air cloud formation . . . . .	26
2.4 Vapor Cloud Explosion . . . . .	26
2.5 Cloud size influence on explosion loads . . . . .	27
2.6 Hydrogen Ignition Probability . . . . .	27
2.7 Quantitative risk assessment-QRA . . . . .	28
2.7.1 HyRAM . . . . .	29
2.7.2 MISOF . . . . .	30
2.7.3 Weakness in QRA . . . . .	32
2.8 SAFEN ignition probability model . . . . .	33
2.8.1 Understanding ignition probability calculations . . . . .	33
2.8.2 Ignition by hot surfaces . . . . .	34
2.8.3 Mechanically generated sources . . . . .	34
2.8.4 Electrostatic discharges . . . . .	35
2.8.5 Diffusion ignition . . . . .	35
<b>3 Method</b>	<b>37</b>
3.1 Basic about KFX . . . . .	37
3.2 Background Theory . . . . .	38
3.2.1 Turbulence Model . . . . .	38

3.3	User Interface . . . . .	39
3.3.1	Starting with KFX . . . . .	39
3.4	KFX- Risk and Barrier Management . . . . .	44
3.4.1	Input Parameters for KFX-RBM . . . . .	44
3.4.2	Output Parameters for KFX-RBM . . . . .	45
<b>4</b>	<b>Model Testing</b>	<b>47</b>
4.1	Basic hydrogen leak in open box . . . . .	47
4.1.1	First calculations . . . . .	51
4.1.2	Second calculations . . . . .	52
4.1.3	Third calculations . . . . .	53
4.2	Calculating the ignition probability . . . . .	55
4.2.1	Continuous ignition probability . . . . .	56
4.2.2	Discrete ignition probability . . . . .	57
4.3	Model testing discussion . . . . .	57
<b>5</b>	<b>Simulation set-up</b>	<b>59</b>
5.1	Input parameters and boundary conditions . . . . .	59
5.2	Making a base-case in KFX Wizard . . . . .	60
5.2.1	Powerscan- Creating multiple cases at once . . . . .	61
5.3	Simulation of 40' ISO-container . . . . .	64
5.4	Simulation of hydrogen refueling station . . . . .	66
5.5	Simulation of onshore process unit . . . . .	67
<b>6</b>	<b>Results from 40' ISO-container</b>	<b>69</b>
6.1	Hydrogen . . . . .	69
6.1.1	Gas Dispersion . . . . .	69
6.1.2	Flammable Cloud . . . . .	72
6.1.3	Ignition Probability . . . . .	74
6.1.4	Ignition Probability Contributors . . . . .	76
6.1.5	Sensitivity . . . . .	79
6.2	Methane . . . . .	81
6.2.1	Methane . . . . .	81
<b>7</b>	<b>Result from Hydrogen Refueling Station</b>	<b>85</b>
7.1	Hydrogen . . . . .	85
7.1.1	Gas dispersion . . . . .	85
7.1.2	Flammable cloud . . . . .	88
7.1.3	Ignition Probability . . . . .	90
7.1.4	Ignition Probability Contributors . . . . .	92
7.1.5	Grid Sensitivity . . . . .	94
7.2	Methane . . . . .	96
7.2.1	Methane . . . . .	96



<b>8</b>	<b>Process Plant</b>	<b>99</b>
8.1	Hydrogen . . . . .	99
8.1.1	Gas dispersion . . . . .	99
8.1.2	Flammable Cloud . . . . .	102
8.1.3	Ignition Probability . . . . .	104
8.1.4	Ignition Probability Contributors . . . . .	106
8.1.5	Grid sensitivity . . . . .	108
8.2	Methane leak compared with hydrogen leak . . . . .	110
8.2.1	Methane . . . . .	110
8.3	Comparison with HYEX and DNV model . . . . .	113
8.3.1	DSB . . . . .	113
<b>9</b>	<b>Discussion</b>	<b>115</b>
9.1	Total ignition probability (after 30 sec) . . . . .	115
9.1.1	Variation regarding rate . . . . .	116
9.1.2	Contributors . . . . .	117
9.1.3	Leak Direction . . . . .	118
9.1.4	Location . . . . .	119
9.2	Total ignition probability (at 0 seconds) . . . . .	119
9.2.1	Variation regarding rate . . . . .	120
9.2.2	Contributors . . . . .	120
9.2.3	Direction . . . . .	120
9.3	Total ignition between 1-5 seconds . . . . .	121
9.3.1	Contributors . . . . .	122
9.4	Comparison of Ignition Probability Models . . . . .	122
9.5	Grid sensitivity . . . . .	123
9.6	Methane leak compared to hydrogen leak . . . . .	124
<b>10</b>	<b>Conclusion and further work</b>	<b>127</b>
10.1	Conclusion . . . . .	127
10.2	Further work . . . . .	128
	<b>Bibliography</b>	<b>129</b>
<b>A</b>	<b>Container, xml file</b>	<b>133</b>
<b>B</b>	<b>Container, scn file</b>	<b>137</b>
<b>C</b>	<b>Container, ignprob.log file</b>	<b>139</b>



# List of Figures

- 1.1 Number of accidents each decade.From [6] . . . . . 23
- 2.1 Recommended total ignition probability for hydrogen leaks, from DSB report [19] . . . . . 32
- 3.1 KFX license client window that shows up when KFX is opened . . . . . 39
- 3.2 Message window that displays license validity . . . . . 40
- 3.3 Default KFX user interface . . . . . 40
- 3.4 Fire and Gas cloud simulation . . . . . 41
- 3.5 The KFX Risk and Barrier Management in the Fire ad Gas Cloud wizard with additional options . . . . . 42
- 3.6 User interface for KFXview . . . . . 43
- 3.7 Window terminal that launches when clicking the cmd button . . . . . 43
- 4.1 Geometry of the box used for the basic hydrogen leak where one side is shorter so the hydrogen can escape . . . . . 48
- 4.2 Grid with 50,000 grid cells that was used for the simulation of basic hydrogen leak in open box . . . . . 49
- 4.3 Parameters used to set up the scenario inputs for the base-case in KFX Wizard used to test the ignition model . . . . . 50
- 4.4 Parameters used to calculate the transient leak from the gas segment for the base-case in KFX Wizard used to test the ignition model . . . . . 51
- 4.5 Mechanical ignition probability plotted whit time in seconds on the x-axis, and ignition probability on y-axis . . . . . 54
- 4.6 Discharge ignition probability plotted whit time in seconds on the x-axis, and ignition probability on y-axis . . . . . 55
- 4.7 Diffusion ignition probability plotted with time in seconds on the x-axis, and ignition probability on the y-axis . . . . . 55
- 5.1 Standard 40' ISO-container. Picture from [39] . . . . . 64
- 5.2 3D geometry of the ISO-container used for the simulations . . . . . 65
- 5.3 3D geometry of the ISO-container used for the simulations where the top is cut off to see what it looks like inside . . . . . 65
- 5.4 The figure shows the dimensions of the refueling station. However, the area of interest is the fenced area around the process equipment. From [28] 66

5.5	The figure shows the geometry for the refueling station from kfx view . . .	67
5.6	The figure shows the geometry of the process plant . . . . .	68
6.1	Release profile of 0.1 kg/s downward release where the location is in the middle of the container geometry . . . . .	69
6.2	Surface plots of 4% H2 concentration for 0.1 kg/s downward release at different time points: 10 seconds, 20 seconds, and 30 seconds where the leak locations are in the middle of the container geometry. . . . .	70
6.3	Surface plots of 4% H2 concentration for 1 kg/s downward release at different time points: 10 seconds, 20 seconds, and 30 seconds where the leak locations are in the middle of the container geometry. . . . .	70
6.4	Release profile of 1 kg/s downward release where the location is in the middle of the container geometry . . . . .	71
6.5	Surface plots of 4% H2 concentration for 0.1 kg/s downward release at different time points: 10 seconds, 20 seconds, and 30 seconds where the leak locations are in the corner of the container geometry. . . . .	71
6.6	Surface plots of 4% H2 concentration for 1 kg/s downward release at different time points: 10 seconds, 20 seconds, and 30 seconds where the leak locations are in the corner of the container geometry. . . . .	72
6.7	Stoichiometric equivalent cloud volume for corner (left) and middle (right) leak in all directions with leak rate 0.1kg/s for the container geometry. . .	72
6.8	Stoichiometric equivalent cloud volume for corner (left) and middle (right) leak in all directions with leak rate 1 kg/s for the container geometry. . . .	73
6.9	Flammable cloud volume between lower- and upper flammability limit for corner (left) and middle (right) leak in all directions with leak rate 0.1kg/s for the container geometry. . . . .	73
6.10	Flammable cloud volume between lower- and upper flammability limit for corner (left) and middle (right) leak in all directions with leak rate 1 kg/s for the container geometry. . . . .	73
6.11	Ignition probability for the different leaks and their locations at the start of the leak (t=0) . . . . .	74
6.12	Ignition probability for the different leaks and their locations at the end of the leak for the container scenario. . . . .	74
6.13	Average total ignition probability for the 1 kg/s leak and 0.1 kg/s for the container scenario. . . . .	75
6.14	Logarithmic representation of the contributors that contribute to the total ignition probability for the container scenario. . . . .	76
6.15	Contributors to the total ignition at the start of the leak for the container scenario. . . . .	77
6.16	Contributors to the total ignition after the leak has exceeded in 30 sec for the container scenario. . . . .	77

6.17	Contributors to the total ignition where the ignition probability is plotted against the cloud volume, for the middle leak with 0.1 kg/s leak rate. . . .	78
6.18	Contributors to the total ignition where the ignition probability is plotted against the cloud volume, for the middle leak with 1 kg/s leak rate. . . .	78
6.19	Grid sensitivity for the 0.1 kg/s leak with the different contributors . . . .	79
6.20	Grid sensitivity for the 1 kg/s leak with the different contributors . . . .	80
6.21	Flammable cloud volume for the 0.1 kg/s (left) and 1 kg/s (right) leaks . .	80
6.22	Flammable cloud volume between lower- and upper flammability limit for the 0.1 kg/s (left) and 1 kg/s (right) leaks . . . . .	81
6.23	Surface plots of 4% methane concentration for 1 kg/s downward release at different time points: 10 seconds, 20 seconds, and 30 seconds where the leak locations are in the middle of the container geometry. . . . .	81
6.24	Stoichiometric equivalent cloud volume for both hydrogen and methane, compared to the ignition probability . . . . .	82
6.25	Flammable cloud volume between lower- and upper flammability limit for both methane and hydrogen compared to the ignition probability . . . . .	82
6.26	Average ignition probability at t=30 for methane and hydrogen . . . . .	83
7.1	Release profile of 0.1 kg/s downward release where the location of the leak is in the middle of the refueling station geometry. . . . .	85
7.2	Surface plots of 4% H <sub>2</sub> concentration for 0.1 kg/s downward release at different time points: 10 seconds, 20 seconds, and 30 seconds where the leak locations are in the middle of the refueling station geometry. . . . .	86
7.3	Surface plots of 4% H <sub>2</sub> concentration for 0.1 kg/s downward release at different time points: 10 seconds, 20 seconds, and 30 seconds where the leak locations is in the corner of the refueling station geometry. . . . .	86
7.4	Release profile of 1 kg/s downward release where the location of the leak in in the middle of the refueling station geometry. . . . .	87
7.5	Surface plots of 4% H <sub>2</sub> concentration for 0.1 kg/s downward release at different time points: 10 seconds, 20 seconds, and 30 seconds where the leak locations is in the middle of the refueling station geometry. . . . .	87
7.6	Surface plots of 4% H <sub>2</sub> concentration for 1 kg/s downward release at different time points: 10 seconds, 20 seconds, and 30 seconds where the leak locations is in the corner of the refueling station geometry. . . . .	88
7.7	Surface plot of 4% H <sub>2</sub> concentration for 0.1 kg/s releases at 10 seconds in x, y and z direction. . . . .	88
7.8	Flammable cloud volume for corner (left) and middle (right) leak in all directions with leak rate 0.1kg/s for the refueling station geometry. . . . .	88
7.9	Flammable cloud volume for corner (left) and middle (right) leak in all directions with leak rate 1kg/s for the refueling station geometry. . . . .	89
7.10	Stoichiometric equivalent cloud volume for corner (left) and middle (right) leak in all directions with leak rate 0.1 kg/s for the refueling station geometry.	89

7.11	Stoichiometric equivalent cloud volume for corner (left) and middle (right) leak in all directions with leak rate 1 kg/s for refueling station geometry. . . . .	89
7.12	Average ignition probability for all leaks with their leak rate at the start of the leak (t=0) for the refueling station geometry. . . . .	90
7.13	Average ignition probability for all leaks with their leak rate at the end of the leak for the refueling station geometry. . . . .	90
7.14	Average total ignition probability for the two leak rates for the refueling station geometry. . . . .	91
7.15	Logarithmic representation of the contributors that contribute to the total ignition probability for the refueling station geometry. . . . .	92
7.16	Contributors to the simulation at the start of the leak (t=0) for the refueling station geometry. . . . .	93
7.17	Contributors to the simulation at the end of the leak (t=30) for the refueling station geometry. . . . .	94
7.18	Grid sensitivity for the 0.1 kg/s leak with the different contributors. . . . .	95
7.19	Grid sensitivity for the 1 kg/s leak with the different contributors. . . . .	95
7.20	Stoichiometric equivalent cloud volume for the 0.1 kg/s (left) and 1 kg/s (right) leaks. . . . .	96
7.21	flammable cloud volume cloud for the 0.1 kg/s (left) and 1 kg/s (right) leaks.	96
7.22	Surface plots of 4% CH <sub>4</sub> concentration for 1 kg/s downward release at different time points: 10 seconds, 20 seconds, and 30 seconds where the leak locations are in the middle of the geometry. . . . .	97
7.23	Stoichiometric equivalent cloud volume compared to the ignition probability for the hydrogen and methane comparison. The leak is done for the middle leak, in the negative z-direction for the refueling station geometry. . . . .	97
7.24	Flammable cloud volume for the middle leak, zn-direction, compared to the ignition probability for the hydrogen and methane comparison for the refueling station geometry. . . . .	98
7.25	Histogram presenting the ignition probability for the methane leak, compared to the hydrogen leak for the refueling station geometry. . . . .	98
8.1	Release profile of 0.1 kg/s downward release where the location is in the middle of the geometry . . . . .	99
8.2	Surface plots of 4% H <sub>2</sub> concentration for 0.1 kg/s downward release at different time points: 10 seconds, 20 seconds, and 30 seconds where the leak locations are in the corner of the process plant geometry. . . . .	100
8.3	Surface plots of 4% H <sub>2</sub> concentration for 01 kg/s downward release at different time points: 10 seconds, 20 seconds, and 30 seconds where the leak locations are in the middle of the process plant geometry. . . . .	100
8.4	Release profile of 1 kg/s downward release where the location is in the middle of the geometry . . . . .	101

8.5	Surface plots of 4% H <sub>2</sub> concentration for 0.1 kg/s downward release at different time points: 10 seconds, 20 seconds, and 30 seconds where the leak locations are in the corner of the process plant geometry. . . . .	101
8.6	Surface plots of 4% H <sub>2</sub> concentration for 0.1 kg/s downward release at different time points: 10 seconds, 20 seconds, and 30 seconds where the leak locations are in the corner of the process plant geometry. . . . .	102
8.7	Flammable cloud volume for corner (left) and middle (right) leak in all directions with leak rate 0.1kg/s for the process plant geometry. . . . .	102
8.8	Flammable cloud volume cloud for corner (left) and middle (right) leak in all directions with leak rate 1 kg/s for the process plant geometry. . . . .	103
8.9	Stoichiometric equivalent cloud volume for corner (left) and middle (right) leak in all directions with leak rate 0.1kg/s for the process plant geometry. . . . .	103
8.10	Stoichiometric equivalent cloud volume for corner (left) and middle (right) leak in all directions with leak rate 0.1kg/s for the process plant geometry. . . . .	103
8.11	Average ignition probability for the 1 kg/s leak and 0.1 kg/s for the start of the leak. . . . .	104
8.12	Ignition probability for the different leaks and their locations after 30 sec. . . . .	104
8.13	Average ignition probability for the 1 kg/s leak and 0.1 kg/s . . . . .	105
8.14	Logarithmic representation of the contributors that contribute to the total ignition probability for the process plant geometry. . . . .	106
8.15	Contributors to the total ignition at the start of the leak for the process plant geometry. . . . .	107
8.16	Contributors to the total ignition after the leak has exceeded in 30 sec . . . . .	107
8.17	Contributors to the total ignition probability where the ignition probability is plotted against the cloud volume, for the middle leak with 0.1 kg/s leak rate for the process plant geometry. . . . .	108
8.18	Contributors to the total ignition probability where the ignition probability is plotted against the cloud volume, for the middle leak with 1 kg/s leak rate for the process plant geometry. . . . .	108
8.19	Grid sensitivity for the 0.1 kg/s leak with the different contributors. . . . .	109
8.20	Grid sensitivity for the 1 kg/s leak with the different contributors. . . . .	109
8.21	Stoichiometric equivalent cloud volume cloud for the 0.1 kg/s (left) and 1 kg/s (right) leaks. . . . .	110
8.22	Flammable cloud volume for the 0.1 kg/s (left) and 1 kg/s (right) leaks. . . . .	110
8.23	Surface plots of 4% CH <sub>4</sub> concentration for 1 kg/s downward release at different time points: 10 seconds, 20 seconds, and 30 seconds where the leak locations are in the middle of the geometry. . . . .	111
8.24	Surface plots where the process plant is cut after 3 meters to present the 4% CH <sub>4</sub> concentration for 1 kg/s downward release at different time points: 10 seconds, 20 seconds, and 30 seconds where the leak locations are in the middle of the geometry. . . . .	111

8.25	Stoichiometric equivalent cloud volume for both hydrogen and methane, compared to the ignition probability . . . . .	112
8.26	Flammable cloud volume between lower- and upper flammability limit for both methane and hydrogen compared to the ignition probability . . . . .	112
8.27	Average total ignition probability for methane and hydrogen . . . . .	113
8.28	Comparison of DSB's figure about Recommended total ignition probability for hydrogen leaks for the HYEX and DNV model compared to the ignition probability for the three geometries in this thesis . . . . .	114
8.29	Visual representation indicating the ignition probabilities for the three geometries based on the DNV model and HYEX model from [19] . . . . .	114
B.1	Figure shows a picture of the .scn file for the container geometry- part 1 . . . . .	137
B.2	Figure shows a picture of the .scn file for the container geometry- part 2 . . . . .	137
B.3	Figure shows a picture of the .scn file for the container geometry- part 3 . . . . .	137
B.4	Figure shows a picture of the .scn file for the container geometry- part 4 . . . . .	137
B.5	Figure shows a picture of the .scn file for the container geometry- part 5 . . . . .	137
C.1	Figure shows a picture of the ignition probability log (donated ignprob.log) file for the container geometry- part 1 . . . . .	140
C.2	Figure shows a picture of the ignition probability log (donated ignprob.log) file for the container geometry- part 2 . . . . .	141
C.3	Figure shows a picture of the ignition probability log (donated ignprob.log) file for the container geometry- part 3 . . . . .	142



# List of Tables

- 1.1 Summary of the biggest hydrogen-related accidents [2] . . . . . 22
- 2.1 Ignition probability for methane versus flow rate ranges for methane . . . . . 29
- 2.2 HyRAM default ignition probabilities for hydrogen . . . . . 30
- 3.1 Part of the output parameters from ignprob log. . . . . 45
- 4.1 Parameters used for calculating the ignition probability by hand . . . . . 51
- 4.2 Comparison of Hand vs. Computer Calculations . . . . . 52
- 4.3 Comparison of Hand vs. Computer Calculations after DNV fixed the model 53
- 4.4 Comparison of Hand vs. Computer Calculations after DNV fixed the model  
a second time . . . . . 54
- 4.5 Hand calculations compared to the computer calculations for the continu-  
ous ignition probability, *Prob\_C* . . . . . 56
- 4.6 Hand calculations compared to the computer calculations for the discrete  
ignition probability, *Prob\_D* . . . . . 57
- 5.1 Parameter overview of all the directions the two leak rates will be simulated  
in. . . . . 60
- 5.2 Constant parameters used for setting up the ISO container simulation in  
KFX . . . . . 61
- 5.3 Tank temperature, pressure and leak rate for the jet inlet calculated by  
KFX for the 0.1 kg/s leak rate . . . . . 61
- 5.4 Tank temperature, pressure and leak rate for the jet inlet calculated by  
KFX for the 1 kg/s leak rate . . . . . 61
- 5.5 Parameters for the scenario file- Part 1. From [34] . . . . . 62
- 5.6 Parameters for the scenario file- Part 2. From [34]. . . . . 63
- 5.7 RBM parameters for the scenario file. From [34] . . . . . 63
- 5.8 SAFEN hydrogen ignition model parameters for Ex-rated equipment used  
in the XML file for every case . . . . . 66
- 6.1 Total probability for the ignitors placed in the area of the container for the  
0.1 kg/s leak. . . . . 75
- 6.2 Total probability for the ignitors placed in the area of the container for the  
1 kg/s leak. . . . . 76

7.1	Total probability for the ignitors placed in the area of the fueling station for the 0.1 kg/s leak. . . . .	91
7.2	Total probability for the ignitors placed in the area of the fueling station for the 1 kg/s leak. . . . .	92
8.1	Total probability for the ignitors placed in the area of the process plant for the 0.1 kg/s leak. . . . .	105
8.2	Total probability for the ignitors placed in the area of the process plant for the 1 kg/s leak. . . . .	106
9.1	Total ignition probability for the container, hydrogen refueling station, and process plant. Values averaged for all release directions. . . . .	115
9.2	Summary of the total ignition probability for the container, hydrogen refueling station, and process plant at t=0. Values averaged for all release directions. . . . .	119
9.3	Total ignition probability for the container, hydrogen refueling station, and process plant at 5 seconds. Values averaged for all release directions. . . . .	121
9.4	Summary of the ignition probability for methane and hydrogen, for the middle leak in the negative z-direction. All these are mentioned in Chapter 6.2.1, 7.2.1 and 8.2.1 . . . . .	124

# Nomenclature

Symbol	Explanation
BD	Blow Down
CAD	Computer Aided Design
DDT	Deflagration to Detonation
EDC	Eddy Dissipation Concept
ESD	Emergency Shut Down
ETA	Event Tree Analysis
FTA	Fault Tree Analysis
HIAD	Hydrogen Incident and Accident
HyRAM	Hydrogen Risk Assessment Models
ISO	International Organization for Standardization
JIP	Joint Industry Project
KFX	Kameleon FireEX
KFX-RBM	Kameleon FireEx - Risk and Barrier Management
LFL	Lower Flammability Limit
MIE	Minimum Ignition Energy
MISOF	Modeling of Ignition Source On offshore oil and gas facilities
P	Probability
$P_C$	Ignition probability from a continuous source
$P_D$	Ignition probability from a discrete source
$P_i$	Ignition probability for immediate ignition
QRA	Quantitative Risk Assessment
RCS	Regulations, codes and standards
SAFEN	Safe Energy Carriers (JIP)
UFL	Upper Flammability Limit
VCE	Vapor Cloud Explosion
$\lambda_C$	Expected number of ignition due to continuous ignition mechanisms per volume
$\lambda_D$	Expected number of ignition due to discrete ignition mechanisms per volume
$ftf_{vol}$	New flammable volume within the new time-step
$LeL_{vol}$	Flammable volume, also denoted $V_{LFL:UFL}$



# 1 Introduction and Background

## 1.1 Introduction

Today, the world is in desperate need for energy, and especially for renewable energy. The need to address climate change is becoming more and more tangible by the day. This is causing a worldwide shift away from fossil fuels and towards sustainable methods for energy. One element standing out as a solution to the worldwide problem can be the answer to finding a greener, cleaner future for energy- hydrogen. The United Nations claims that in 2030 the world's population will reach 8.5 billion, while in 2050 it will be 9.7 billion. In 2030, there will be one billion more people than there are today [1].

The need for energy is growing together with population growth, and the discernible need for energy carriers is big. One of the most promising materials with several benefits is hydrogen. Hydrogen is an environmentally friendly fuel [2].

When hydrogen is burned in an internal combustion engine only water is produced. Hydrogen can be stored in high-pressure gas cylinders or the form of a cryogenic liquid fuel, or carbon filters. However, as a raw material, hydrogen has many applications like it can be used in the production of fertilizers, dyes, and plastics, to name a few [3] [2].

Regardless of all the above-mentioned advantages, there is always a risk to the surrounding environment when producing, storing, transporting, and using hydrogen as a secondary fuel. The reason for this comes from hydrogen's wide range of flammability and because of the amount of energy that is released if the hydrogen burns or explodes. [2] Throughout history, there have been several hydrogen-related accidents resulting in fatal deaths and severe damage. One notable incident occurred in 2019 at Uno-X station in Sandvika, where a hydrogen filling station exploded. According to Nel Hydrogen Manager Jon André Løkke, the root cause for the explosions was a failure mechanism of a plug assembly of a hydrogen tank in the high-pressure storage unit. This led to a hydrogen leak. The hydrogen that was released mixed air and eventually ignited[4].

After this situation, the question then arises: is hydrogen safe? Or, is it safer than our current energy sources like gasoline and natural gas? The problem with the word safe is that it is difficult to define and different populations perceive the word in different ways. So then a better approach might be to ask: what are the hazards and risks associated

with the use of hydrogen, and how do these compare to our traditional energy sources [5]?

## 1.2 Background

This chapter presents the foundational framework that this thesis is built upon.

The hydrogen accident in Sandvika is just one of several hydrogen-related accidents that have happened over the years. Table 1.1 presents a summary of the major hydrogen-related accidents that have occurred in the last 100 years or so.

Table 1.1: Summary of the biggest hydrogen-related accidents [2]

Year	Location	Origin of accident/activity	Death/injury
1999	Panipat, India	Fire/Refinery	5/-
1999	Hillsborough, Tampa, Florida	Fire and explosion/Power station	3/50
1992	Sodeguara, Japan	Explosion/ Refinery	10/7
1992	Hong Kong	Explosion/Power Plant	2/19
1990	Czechoslovakia	Explosion	15/26
1989	USA	Jet Fire/ Pipeline	7/8
1989	Pasadena, Texas	Explosion/ Chemical Plant	23/314
1986	Genoa, Italy	Explosion	3/2
1986	Kennedy Space Central, Florida	Challenger Explosion/ Space Center	7/119
1977	Gujarat, India	Explosion/Chemical Plant	5/35
1972	Netherlands	Explosion	4/40
1937	Hindenburg, Lakehurst	Fire	36/-

To prevent accidents like the one in Sandvika, it is important to properly determine the risk of all activities related to hydrogen with new and more accurate risk analysis tools.

In 2018, a non-profit organization named the International Association for Hydrogen Safety “HySafe” posted a database for the European Hydrogen Incident and Accident, HIAD 2.0, with over 700 hydrogen events – accidents, incidents, and near misses [6].

The majority of the events in HIAD 2.0 occurred in a period from the 1990s to the 2000s, as illustrated in Figure 1.1. According to Wen and al. [6], the reason for the decrease in accidents after the 2000s is an improved safety design and operative provisions both in the chemical and petrochemical industries. They also claim that a reason can be because of under-reporting or delay in reporting of the events [6].

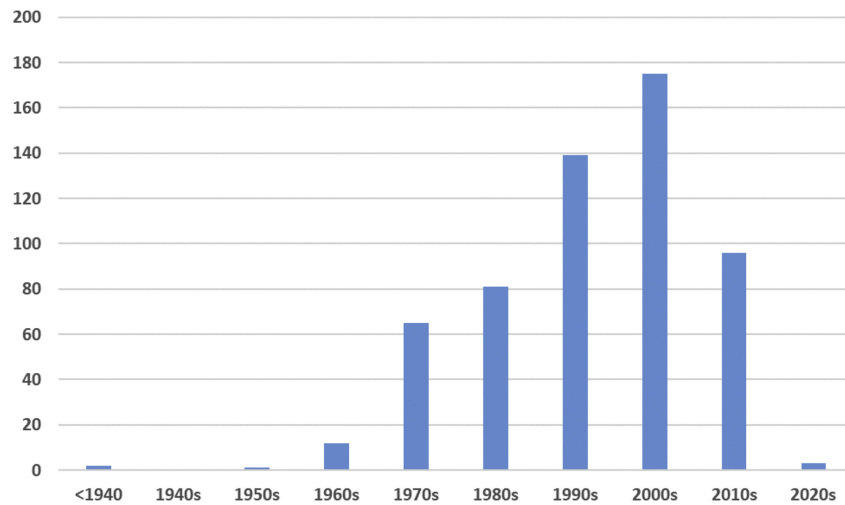


Figure 1.1: Number of accidents each decade. From [6]

Safety issues are severely important because insufficient control for loss prevention can result in catastrophic accidents that can extend beyond the plant boundary. Large-scale hydrogen utilization will require a reliable risk analysis process. The traditional risk assessment is not sufficient to analyze risks in more complex systems. For this, a QRA methodology is a genuine tool that can be used to achieve this. [2]

A much-used QRA methodology is the HyRAM which is described more in 2.7.1 and has been a good tool for development and revision of hydrogen regulations, codes and standards (RCS). [7]

### 1.3 Objective

This Master's Thesis is a part of the SAFEN project. SAFEN is a Joint Industry Project (JIP) with several industry partners including Asker Horizons, Vår Energi, Yara, DSB, Equinor, Gassco, Gen2 Energy, BW Offshore, Origin Energy, and others. Safetec leads the project in close cooperation with other consultancy companies like DNV and Gexcon.

The main objectives of the SAFEN project are to share experiences and knowledge in understanding failure mechanisms, hazards, and accident situations for hydrogen, ammonia, and  $CO_2$ . Hydrogen is an essential energy carrier, making it very important for the global energy decarbonization process. Because of limited knowledge of ignition mechanisms, its elevated ignition risk compared to other gases present is a big issue for safety design. This can result in expensive over-caution or insufficient safety precautions, which can compromise the successful deployment of renewable energy solutions. The SAFEN JIP (Safe Energy Carriers) was made to address these knowledge gaps [8].

The first phase of the SAFEN project ended in 2023 and delivered models for leak frequencies and ignition probabilities. The SAFEN project intends to address the knowledge gaps in our understanding of risk derived in the hydrogen industry [8].

The main objective of this thesis entails looking into the performance and efficacy of the SAFEN model and how it performs concerning larger-scale geometries and more detailed models. To achieve this, several sub-objects need to be fulfilled.

- Update the SAFEN model with the newest ignition probabilities and add the new equipment, so this can be used with the Risk and Barrier Management to calculate the total ignition probability.
- Gather information about KFX-RBM and how to use the software to simulate hydrogen leaks.
- Make sure that the SAFEN model in KFX-RBM is accurate and verify that it has been computed correctly.
- Research ignition probability.
- Simulate gas expansion and hydrogen leakage, analyzing how the gas expands within the geometries while simultaneously calculating the ignition probability with KFX-RBM.

## 1.4 Report Structure

This thesis consists of 10 chapters. The first chapter is the introduction to the thesis. Chapter 2 is the literature study done on hydrogen and hydrogen leaks, together with quantitative risk assessment Chapter 3 discusses the methodology used, specifically focusing on KFX and KFX-RBM. The purpose of this section is to give insight into the toolbox KFX-RBM which is still under development and for this reason, doesn't have any manual. The chapter introduces the underlying theory that RBM is built upon, as well as shows how the fire and explosion risk are reconstructed. Chapter 4 is about testing KFX-RBM. Where an open box was used to simulate a basic hydrogen leak. Chapter 5 presents the simulation done in KFX. It presents some of the tools used with KFX, as well as it presents the input parameters and geometries used for the simulations. Chapters 6 through 8 present the findings and main results from the three geometries. Chapter 9 presents the discussion around the main results. Chapter 10 presents the conclusion and present briefly future work that can be done.



## 2 Theory/ Literature Study

### 2.1 Hydrogen

Hydrogen is a substance made up of the element hydrogen, which only consists of one proton and one electron. It is the most abundant element in the universe. The colorless, odorless, tasteless, and non-toxic element is usually found in gaseous form in the atmosphere [9]. Hydrogen can be produced in many different ways such as from water, oil, natural gas, biofuels, and sewage slurs, to mention a few [10]. Much effort has been made to develop hydrogen storage that is safe, environmentally- friendly, affordable, and most importantly, with high energy densities. Hydrogen fuels can be stored in gaseous, liquid, and solid-state [11]. Gaseous storage involves compressing hydrogen gas at high pressure in tanks for a shorter period, or it can be stored through natural gas pipelines. Gaseous storage is mainly used for hydrogen fuel cells. Liquid storage mainly converts hydrogen gas into liquid hydrogen by compressing it at a low temperature ( $-253^{\circ}\text{C}$ ). Liquid hydrogen is mainly used in aviation, while solid-state storage stores hydrogen gas in metallic hybrids or nanostructured materials in a solid form. This type of storage is usually used for the preparation and utilization of materials [10].

### 2.2 The danger of a hydrogen leak

As the substance with the smallest relative molecular mass, hydrogen is more likely to leak from high-pressure environments than natural gas is. The flammable and explosive nature with a wide range of flammability, wide range of explosion volume fractions, lowest ignition energy, high diffusion coefficient, and very fast flame speed make hydrogen severely hazardous to use. As a general rule, the high-pressure gaseous hydrogen jet will leak in the direction of the leak, and it will subsequently rise under the effect of air buoyancy. The accumulations are formed at the top of the confined space. When the hydrogen concentration in air is 4-75 %, the hydrogen will easily burn or explode in contact with an external ignition source. After the incident of combustion or explosions, its flame propagation speed increases, and it will easily ignite the surrounding objects. As the flame continues to grow more and more rapidly, a deflagration to detonation (DDT) transition occurs, typically within a few seconds. Normally a small leak will spread more

rapidly without causing danger, while a large leak may produce jet flames and explosions [12] [10].

## 2.3 Hydrogen- air cloud formation

Like every other flammable gas, hydrogen is highly dangerous in a confined space. In an open space, hydrogen's probability of exploding is lower than what it would be in a confined space as the buoyancy speed is high. When hydrogen is involved in combustion, water vapor is generated by absorbing heat from the air. However, hydrogen does not generate carbons during combustion [13].

Hydrogen has a wider range of flammable concentrations than hydrocarbons. Factors like temperature, pressure, presence of diluent, absence of diluent, and shape of structure could all affect the flammability limit of hydrogen, which is between 4-75 %. To trigger an explosion of a hydrogen-air cloud, the concentration of hydrogen in the air has to be within a restricted concentration of the hydrogen limit. While existing studies on the detonation limit for hydrogen vary, the ISO (International Organization for Standardization) recommends the detonation range for hydrogen-air cloud to be around 18 % to 58%. While a study by Dorofeev, Sidorov, Dvoinishnikov *et al.* [14] recommends a minimum of 12.5 % of hydrogen concentration ratio for transition to detonation [15].

## 2.4 Vapor Cloud Explosion

Vapor cloud explosions (VCE) are a serious hazard in the chemical process industries. When a substantial quantity of flammable gas or vapor is accidentally released into the atmosphere it could form a vapor cloud and if the ignition is delayed about 5-10 min, it could produce a VCE [16]. Hydrogen release is presumably to be ignited before the flammable hydrogen-air cloud with sufficient volume to produce VCE blast loads can form. The low MIE of hydrogen means that the prompt ignition is presumably more likely than for hydrocarbon fuels, which simply does not insinuate that a delayed ignition will occur. Hydrogen is also discounted as a VCE hazard because of its buoyancy, which indicates that a hydrogen release will "float away" before the flammable cloud with adequate volume to produce a blast load can form. Even if the hydrogen-air mixture is normally buoyant, assuming the release of hydrogen is not very cold, the dispersion of a hydrogen leak with high pressure will not be influenced by the buoyancy during the momentum-dominated dispersion phase. This can result in a large flammable hydrogen-air cloud being formed at ground level [17]. The VCE could have serious damage effects due to the over-pressure that is created from the fast expansion of the combustion process. The over-pressure created is one of the most important causes of damage to facilities, equipment, and people [16].

## 2.5 Cloud size influence on explosion loads

Every events that can lead to a rapid build-up of pressure have to be considered. Things like gas, liquid, and dust can contribute to explosions. There are two explosive mechanisms that should be considered when evaluating combustible vapor incidents, known as detonations and deflagration. A deflagration is an explosion where the flammable speeds are lower than the speed of sound. They are known as low explosives, while detonations are often more destructive than deflagration. Detonation is an explosive where the flame speed is greater than the speed of sound [18] [19].

In most cases, the explosions will be deflagration, but for equipment of higher density and longer paths, the detonation can switch to an over-pressure in the range of 15-20 barg throughout the cloud. Detonations that occur in environments that are not at atmospheric pressure, the detonation will increase because of the pressure, and it can increase up to 20 times higher than the initial over-pressure [19].

Usually, the flammable cloud volume is much smaller than the distance to the boundary of the plant, and because of that the over-pressure is mainly propagation beyond the flammable cloud that decides the societal risk contours. The over-pressure external to the gas cloud is regulated by the explosion over-pressure inside the cloud as well as the cloud's shape and size. The over-pressure is reduced outside of the cloud so that the over-pressure inside the cloud surpasses 0.5-1 barg further increase in over-pressure will only apply a moderate impact on the over-pressure outside the cloud. This suggests that it is extremely crucial to regulate the size of the cloud during ignition, as this ascertains how quickly the over-pressure decreases outside the cloud. [19]

## 2.6 Hydrogen Ignition Probability

The lower flammability limit, known as LFL, is the leanest limit that a continuous flame can be preserved for a fuel-air mixture. As the amount of fuel in a fuel-air mixture is reduced, a limit is reached below the LFL where the mixture of fuel and air won't be able to burn. This "lean limit" exists because as the mixture becomes more lean the heat production from the combustion process decreases. As a result, the temperature rise caused by the fuel oxidation is reduced. If a fuel-air mixture is leaner than the lean limit the temperature rise is insufficient to sustain the combustion process. The fuel-air mixture's local temperature, or internal energy, must be high enough to generate enough active radicals to support the ignition of the next layer of unburned gasses. As hydrogen is being consumed during the combustion, the unburned hydrogen is being consumed during the combustion zone, this increases the local concentration of hydrogen, which allows the combustion to continue [20].

Hydrogen is highly flammable over an immense flammability range. It requires special models to determine the ignition of hydrogen since it is flammable in concentrations between 4% and 75% in air, it also has an order of magnitude lower ignition energy than for instance hydrocarbons that have a concentration in air above 20% [19].

## 2.7 Quantitative risk assessment-QRA

A Quantitative Risk Assessment (QRA) is a tool for determining risks linked to the use, handling, transportation, and storage of dangerous substances. QRA's are often used to show the risk associated with an activity to give relevant data to authorize decisions if the developments on-site or off-site are acceptable. The QRA's are made based on similar starting-point models, and basic data, so the differences in QRA should only appear due to differences in process- and site-specific information [21].

There are different methodologies to conduct quantitative risk assessment [22] [23]. Examples of this are:

- Fault Tree Analysis (FTA)
- Event Tree Analysis (ETA)
- Bow Tie Analysis

There are five main questions that should be asked and answered when performing a QRA [24]:

- What can go wrong? (What are the start events, hazard, and accident events)
- What happens in that case? (Analysis of impact/consequences)
- How often can it happen? (Frequency analysis)
- Is the risk level acceptable? (This should be measured against the company's criteria as well as the PSA criteria)
- If not, what needs to be done to make it acceptable?

HyRAM and MISOF are two methodologies used when conducting a QRA. While MISOF is not regarded as a standalone methodology, it is an important part of the QRA that focuses on the assessment of ignition risks. The following chapters discuss these two methodologies [7].

## 2.7.1 HyRAM

HyRAM is a QRA methodology for analyzing the the safety of hydrogen fueling and storage infrastructure [7]. HyRAM, developed at Sandia National Laboratories in California, is a proven model for detecting hydrogen leaks. For a long time, it has been used in the industry, however is still considered uncertain[25]. Sandia National Laboratories suggests a model for hydrogen ignition that involves 2/3 of the total ignition probability is immediate ignition, while 1/3 is delayed ignition. If an immediate ignition happens a fire will occur, while if a delayed ignition happens an explosion with a following fire will occur [19].

HyRAM presents the ignition probability as a step function, and it has no refining of leaks above 6.25 kg/s. In HyRAM, all leaks above 6.25 kg/s have the same total ignition probability of 35 % while a numerously amount of literature shows that the ignition probability for hydrogen can be a lot higher than what is stated in HyRAM if the leak both has a high back pressure and has a high leak rate. Table 2.2 shows the default ignition probability for hydrogen for different leak rates where all leaks above 6.25 kg/s have the same ignition probability. The data is based on work done by Groth and Hecht [7].

Immediate ignition releases of hydrogen have different consequences than delayed ignition. For a continuous leak, immediate ignition will lead to jet fires and fireballs for rupture, while delayed ignition of a continuous or instantaneous leak leads to a deflagration or a flash fire. For this reason, it is important to have separate ignition probabilities for the different events, which should be obedient with historical ignition probability data [26] [27]. The data for hydrocarbons shows that the ignition probability for gas leaks lower than 1 kg/s is 0.01. This can be seen in Table 2.1. The probabilities in Table 2.1 need to be a better fit for hydrogen since this only shows methane. To make this better fit for hydrogen, three steps are conducted [26] [28].

Table 2.1: Ignition probability for methane versus flow rate ranges for methane

Class	Leak Rate	Ignition probability
Small	<1 kg/s	0.001
Medium	1-50 kg/s	0.007
Large	50 kg/s	0.30

The first step is to reduce the flow ranges by a factor of 8 for hydrogen, This is done because the difference in molecular weight between hydrogen and methane is 8, which directly affects the flammable cloud size [26] [28].

Step 2 is to increase the ignition probabilities by 16%. This is carried out because hydrogen has a much wider flammable range than hydrocarbons. Methane has a flammability range

from 5.3-14%. Allowing that the 15 vol.% to 75 vol.% of any hydrogen cloud, due to the pressure being released when ignited, constitutes of 16% of the total cloud size of the LFL [26] [28].

The last step consists of increasing the ratio of immediate to delayed ignition in a 2:1 ratio [26]. The result from these changes can be seen in 2.2.

Table 2.2: HyRAM default ignition probabilities for hydrogen

Release Rate (kg/s)	Immediate Ignition Prob.	Delayed Ignition Prob.
<0.125	0.008	0.004
0.125-6.25	0.053	0.027
>6.25	0.230	0.120

## 2.7.2 MISOF

Together with the HyRAM ignition probability models, introduced in Chapter 2.7.1, the much-used model called MISFO (Modeling of Ignition Source On offshore oil and gas facilities.) is also used when performing QRA, the only difference between HyRAM and MISOF is that MISOF is used as an important part of the QRA. Both these two models will be used in this thesis.

The MISOF model is based on the idea that ignition leaks are governed by ignition mechanisms materialized by an interaction between the exposed objects and the combustible mixture facilitating the initiation of the combustion process. Mechanisms that could trigger this initiating could be heat transfer due to excessive temperature of the objects or it could be the release of electrostatic discharges due to components having different potentials. The model was developed by Lloyd's Register and Lilleaker Consulting AS on behalf of Equinor and it was originally recommended for use on land-based oil and gas facilities [27].

The P(I) is the ignition probability and it is the product of two probabilities; the probability for exposure of a live ignition source to a flammable atmosphere, P(E), together with the ignition probability given such exposure, P(I given E). The ignition probability can by this means be expressed as [29]:

$$P_{ignition} = P(E) \cdot P(I \text{ given } E) \quad (2.1)$$

The main objective of the ignition model is to define P(I given E) as the most important potential source of ignition. The MISOF model is made from data collected from reported offshore leak and ignition incidents. For land-based facilities, some adaptations have been

made to the model. For offshore installations, the equipment density is usually higher since the space is more limited on offshore facilities compared to onshore facilities [29].

To model the time-dependent behavior of the ignition mechanism in MISOF, there are two different types of ignition mechanisms, continuous and discrete. A continuous ignition mechanism can be such ignition mechanisms that are present continuously, like a flame or a hot surface, and ignite the flammable atmosphere when it is exposed. Discrete ignition sources are effective in a short moment. These could be things like an electric spark due to static electricity or be generated by switching something on and off [30].

The distinction between gas and liquid leaks is not stated in the MISOF model. What matters in the MISOF model is the explosive environment created by the leak and its volumetric distribution. On a conceptual level, the ignition model consists of these main categories [8].

- Immediate ignition: Probability for ignition before the formation of the flammable gas cloud. This is a special case where the ignition mechanisms are related to the characteristics of the discharged fluid or the item from which is released.
- Delayed ignition: Probability of ignition resulting from an object being exposed to environments that could ignite when they come into contact with a flammable gas cloud. In this instance, ignition will occur after the start of the release, and a flammable environment has developed.

Furthermore, the two groups are divided into categories that depend on the type of equipment and ignition mechanisms. For the "immediate ignition" group, there are two categories [8].

- Generic immediate ignition: ignition that occurs immediately after the start of the leak. This works for any type of equipment except for pumps.
- Pump immediate ignition. This is only applicable to leaks from pumps.

For delayed ignition the equipment categories are broken down into the following groups [8]:

- Rotating equipment, for use in explosive atmosphere (Ex-rated equipment)
- Electrical equipment, for use in explosive atmosphere (Ex-rated equipment)
- Other equipment, for use in explosive atmosphere (Ex-rated)
- Objects not intended for use in explosive atmosphere (Non-Ex equipment)

There are two ways to conduct modeling of the ignition probability given exposure to Ex-rated equipment. The most used way is to apply the generic parameter named "Ignition sources in the area" this is denoted ( $\lambda_i$ ). The ( $\lambda_i$ ) is the expected number of ignitions per volume unit. This makes it a volumetric parameter that represents the likelihood of encountering an effective potential ignition source in the classified area [27].

Following, the ignition model have two types of idealized ignition mechanisms that are accepted. These are the:

- Continuous ignition mechanisms: They include sources that are present continuously, such as flames or hot surfaces.
- Discrete ignition mechanisms: These are effective at only a specific time. They can be things like electric sparks due to static electricity or they could be sparks due to a switch being turned on/off.

The modeling of the exposure probability (P(E)) in equation 2.1 for the two ignition mechanisms the model accepts varies, requiring the time-dependent expose model to be modified to take these variations into account [27].

### 2.7.3 Weakness in QRA

Different QRA's that are conducted are often inconsistent. This is because the person conducting the QRA analysis tends to choose different models to use. The models are often different in how relevant they are and how valid they are. One example of this can be seen in the DSB article where they compare the HYEX model with the HyRAM model [19]. This can be seen in Figure 2.1.

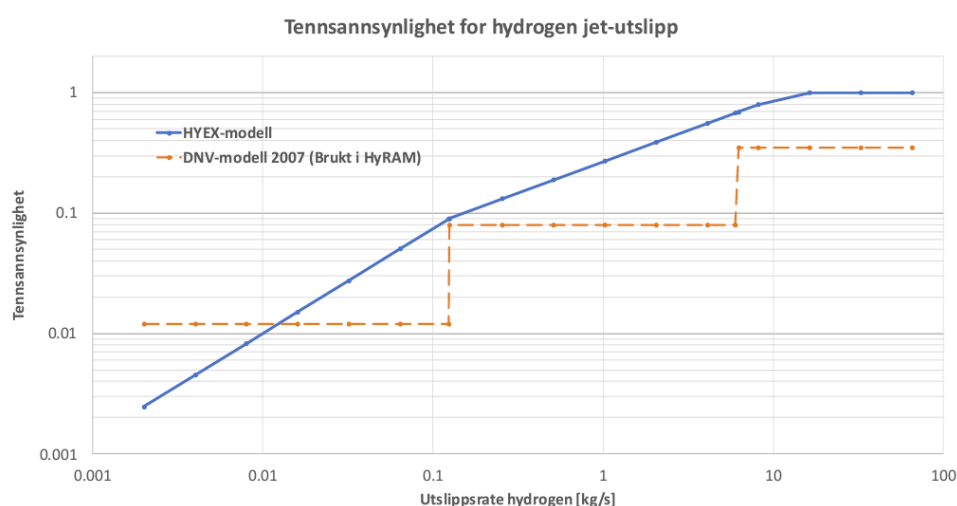


Figure 2.1: Recommended total ignition probability for hydrogen leaks, from DSB report [19]



## 2.8 SAFEN ignition probability model

The proposed SAFEN model for hydrogen is rooted in MISOF, as detailed in Section 2.7.2, which says that leak ignition is controlled by the interactions of ignition mechanisms between the combustible mixture and the exposed objects [8].

The SAFEN model provides insight to the magnitude of the hydrogen ignition probability. The model says that the overall ignition probability that is correlated to all hydrogen leaks with a leak rate exceeding 0.01 kg/s that is released in an industrial environment has a much higher ignition probability than hydrocarbon leaks and they are much lower than 100 %. Since hydrogen is much more prone to ignition because of its ignition mechanisms and low minimum ignition energy, SAFEN suggests that the expected average ignition probability for all leak rates is between 1 and 10 % if the leak occurs in an environment where the objects are made for exposure to a combustible atmosphere (ATEX directive) and not exposed to equipment labeled Non- Ex [8] [27].

The SAFEN model is based on MISOF, but several modifications have been made. These changes are detailed in Sections 2.8.2, 2.8.3, 2.8.4 and 2.8.5.

### 2.8.1 Understanding ignition probability calculations

To understand how to model and calculate ignition probability, envision this scenario: Consider a road where two cars are driving in each lane. Suddenly, there is a hydrogen leakage from the process plant near the road, after some seconds this leak results in a gas cloud. If the cloud comes in contact with the car, assume that the probability of the car igniting the cloud is 50 %. One of the cars (Car A) is driving in the right lane, which is the lane closest to the leaking process plant, while the other car (Car B) is in the left lane. The cloud from the hydrogen leak reaches Car A first. This makes the ignition probability go to 50 %. However, when the cloud subsequently reaches Car B after impacting Car A, the combined ignition probabilities do not sum up to 100 %. If you then have a third car (Car C) on the road the ignition probability will exceed 100 % giving an ignition probability of 150 %. However, this is not correct. The model calculates the ignition for the first two cars as 75 % ( $1 - 0.5^2$ ). With car C on the road, the ignition probability becomes 87.5 %. This value tends towards 100 asymptotically. An easier way to calculate the ignition probability ( $P_i$ ) is to consider the total probability ignition, ( $P_{tot}$ ), minus the ignition probability of the event not occurring, ( $P_n$ ) [8] [27], as presented in Equation 2.2.

$$P_i = P_{tot} - P_n \quad (2.2)$$

## 2.8.2 Ignition by hot surfaces

When a flammable mixture is heated locally to the point where its volume exceeds the ignition temperature, the combustion reaction is triggered, which results in a hot surface ignition. The ability of ignition by a hot surface is influenced by factors such as type, temperature, pressure, and the concentration of the flammable mixture. The ignition temperature is also affected by the size and shape of the heated object, the concentration gradient around the hot surface, the flow velocity, and the turbulence of the flammable atmosphere surrounding the hot surface. To some extent, it is also affected by the surface material. [27] Ignition by hot surfaces is covered in MISOF, but it is assumed that the probability is significantly higher for hydrogen. This is mainly due to the low minimum ignition energy for hydrogen [27] [30].

One example of a hydrogen leak ignited by a hot surface is the incident at Herøya in Porsgrunn in 1985 where a hydrogen-air explosion occurred in an ammonia plant. The event started when a gasket in a water pump located inside a building failed, leading to a backflow of water coming into a vessel containing hydrogen gas with a pressure of 30 bars. Around 3 minutes after the failure, the hydrogen reached the leak point. This resulted in a discharge that lasted about 30 seconds before an explosion occurred. It was estimated that the explosion involved around 10-20 kg of hydrogen being released because of a hot bearing [31] [8].

## 2.8.3 Mechanically generated sources

The ignition probability due to mechanically generated sources (denoted `Prob_mech`) is the ignition probability caused by mechanical impact leading to a hot surface or burning particles that possibly could cause ignition. Examples of these are things like granulate or particles such as sand or gravel. It can be things like fragments or debris generated by a leak. The MISOF models do not include parameters that describe ignition by mechanical impact, but SAFEN has decided to include it in their work for hydrogen. [27] The model suggested by SAFEN is

$$P_{\text{event, impact}} = \frac{1}{200} \times Q_{1s}^{\frac{1}{4}} \quad (2.3)$$

It describes how the ignition is distributed uniformly over the first 5 seconds of the leak. The  $Q_{(1s)}$  is the average leak rate over the first seconds after the leak has started. The reasoning behind that the probability is distributed uniformly over the first five seconds is to make the model capture that this ignition mechanism is a consequence of the onset of the leak, and will materialize quite immediately after the leak has started. One example of this is the hydrogen refueling station in Sandvika, Norway that generated a large explosion within a few seconds of the leak [27].

## 2.8.4 Electrostatic discharges

The leak event may lead to electrostatic discharges which can cause ignition. The ignition probability for such phenomena is denoted `Prob_disch`. Three different types of electrostatic discharges are considered: spark discharges, brush discharges, and corona discharges. The suggested model is

$$P_{\text{event, electrostatic}} = \frac{1}{100} \times Q_{1s}^{\frac{1}{4}} \quad (2.4)$$

This describes how the ignition is distributed uniformly over the first 5 seconds of the leak, where  $Q_{(1s)}$  is the average leak rate over the first seconds after the leak has started. This is similar to the model for ignition probability for mechanical sources.

## 2.8.5 Diffusion ignition

The `Prob_diff` is diffusion ignition. It is assumed that diffusion ignition happens when the pressure is above 15 barg and the pressure in the system has to be released immediately, this means that for example opening a pressure relief valve is not sufficient to materialize a diffusion ignition. Diffusion ignition happens instantly upon release due to mixing between the leak substances and surrounding air, which renders combustion. [27] The ignition probability associated with small and moderate hydrogen leaks is most likely zero if no object is exposed, and the diffusion ignition mechanism cannot materialize. The mathematical model is suggested to be

$$P_{\text{event, diffusion}} = A_p \times \log(d + 1) + B_p \quad (2.5)$$

where  $d$  is the hole diameter in meters, while  $P$  is the pressure in bar gauge.

$$A_p = A'_p \times \ln P \quad (2.6)$$

$$B_p = B'_p \times \ln P \quad (2.7)$$

$$A'_p = \frac{1}{500} \quad (2.8)$$

$$B'_p = \frac{1}{5000} \quad (2.9)$$

The total model can be formulated as

$$P_{\text{event, diffusion}}(P, d) = \frac{\ln P}{5000} \times ((\ln d + 1) + 10) \quad (2.10)$$



## 3 Method

### 3.1 Basic about KFX

The software Kameleon FireEx KFX, known as KFX, was used for this thesis. KFX is recognized in the oil and gas industry as one of the leading industrial CFD programs for simulating flares, gas dispersion, fire mitigation, and fire development for highly realistic conditions for all varieties of structures. [32] KFX is a CFD simulator originally developed by SINTEF, ComputIT and NTNU with partners from the industry, but presently it is DNV that develops it further. KFX is in particular developed for applications associated with safety, addressing scenarios like gas dispersion, explosions, and fire, in addition to other industrial challenges [33]. It is the leading CFD simulation for simulating dispersion, fire, and explosions. KFX exploits a finite volume technique to solve the Navier-Stokes equations and integrate three-dimensional (3D) and transient simulations. KFX employs a porosity technique to enable the resolution of smaller objects than the grid cells, making the code very efficient. The Eddy Dissipation Concept (EDC) is distributed as the CFD program's framework for combustion modeling. [33] KFX is well known to be one of the powerful tools used in the Offshore Oil and Gas Industry for investigating post-accidents. Some of KFX's many simulation capabilities [33] [34] would include:

- Types of fires like jet fires and pool fires in many different geometries like complex geometries, in open space, in windy or still air conditions.
- Fire impact on structures
- Evaluation of escape routes
- Gas dispersion
- LNG fires
- Leaks of LNG with pool spreading
- Fire mitigation that is water-based by deluge
- Gas and smoke analysis
- Calculation of explosive gas cloud size

## 3.2 Background Theory

This section presents the basic background for KFX. To solve the averaged basic transport equations from fluid dynamics, KFX uses a Cartesian finite volume technique. With KFX the main gas-phase governing equation as the primary equation is developed to analyze the combustion phenomenon with complex geometry, while the mass species fractional equation or the conservation of mass is expressed by the continuity equations, momentum conservation along the coordinate direction by the Navier-Stokes equation, and total energy equation for compressible gas flow [35].

### 3.2.1 Turbulence Model

Turbulent flow is irregular with rapid fluctuations in velocity, temperature, density, and composition. These fluctuations make turbulent flow very diffusive and result in increased transport of momentum, mass, and energy. Navier-Stokes equation describes the basic physics of the transport mechanisms for laminar flow. On the other hand, for most practical turbulent flows, it would require an extremely fine grid and high time resolution to be able to resolve the turbulent fluctuations. This is a difficult, if not impossible, task for even modern computers. To overcome this difficulty, a turbulence model must be used. To compute the effect of turbulence KFX uses the  $k$ - $\epsilon$ . [35] [36]. The  $k$ - $\epsilon$  model is one of the most used turbulence models in engineering. In the  $k$ - $\epsilon$  model two transport equations need to be solved. One for turbulence kinetic energy  $k$ , and one for the dissipation of turbulence kinetic energy  $\epsilon$ . The following two equations 3.1 and 3.2 are the two that are being solved in the  $k$ - $\epsilon$  model. [35] [36]

$$\frac{\partial(\rho k)}{\partial t} + \text{div}(\rho k U) = \text{div}\left[\frac{\mu_t}{\sigma_k} \times \text{grad}k\right] + 2\mu_t \times S_{ij} \cdot S_{ij} - \rho \epsilon \quad (3.1)$$

$$\frac{\partial(\rho \epsilon)}{\partial t} + \text{div}(\rho \epsilon U) = \text{div}\left[\frac{\mu_t}{\sigma_\epsilon} \cdot \text{grad}\epsilon\right] + C_{1\epsilon} \times \frac{\epsilon}{k} 2\mu_t \cdot S_{ij} \cdot S_{ij} - C_{2\epsilon} \rho \frac{\epsilon^2}{k} \quad (3.2)$$

The five constant given in Equations 3.1 and 3.2  $C_\mu$ ,  $\rho_k$ ,  $\rho_\epsilon$ ,  $C_{1\epsilon}$ ,  $C_{2\epsilon}$  have the following values:

$$C_\mu = 0.09, \rho_k = 1.00, \rho_\epsilon = 1.30, C_{1\epsilon} = 1.44, C_{2\epsilon} = 1.92 \quad (3.3)$$

$\sigma_k$  and  $\sigma_\epsilon$  are the Prandtl numbers that connect the diffusivity of  $k$  and  $\epsilon$  to the eddy viscosity term  $\mu_t$  [37].

The effect of turbulence on the fluid flow is considered by introducing a turbulence viscosity that is dependent on the value of  $k$  and  $\epsilon$ .

The computation of turbulence combustion uses the eddy dissipation concept (EDC) turbulent combustion models. These models distinguish the residence times of the structures and the mean reaction rates as a function of a mass fraction of reacting structures and the mean reaction rates as a function of a mass fraction for reacting structures [36] [35]. However, this is irrelevant to this thesis as it focuses on gas dispersion and not combustion.

### 3.3 User Interface

This section is informed by the findings and methodologies presented in Govindarajan [34].

#### 3.3.1 Starting with KFX

In Windows KFX license client is launched by selecting the KFX program icon, while in Linux KFX is started by typing KFX into the command line. To open the Risk and Barrier Management version of KFX, it is needed to type "kfxrbm" in the Linux terminal. When this is done, the KFX license client shows up on the screen, shown in Figure 3.1 [34].



Figure 3.1: KFX license client window that shows up when KFX is opened

A license message window will also appear with the license client, as shown in Figure 3.2. This message window will display the license validity and error messages.

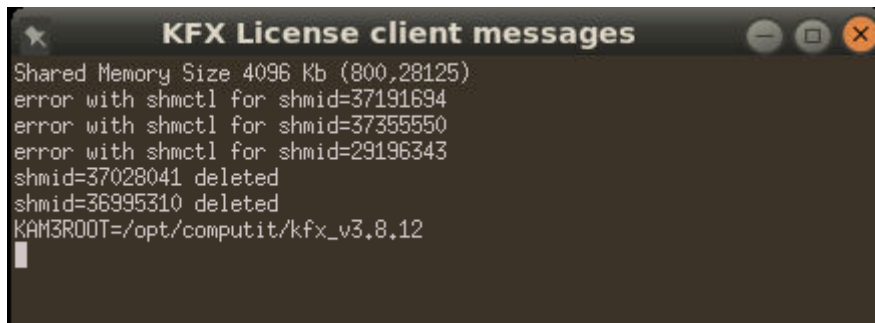


Figure 3.2: Message window that displays license validity

When a valid license is obtained for KFX, various applications with their manuals can be started from the license client window.

The **KFX** button to the left will open the default KFX user interface with a default case. This can be seen in Figure 3.3. The window to the left is the KFX window manager. It presents all of the information that is required to be set up by the user to make various simulations, choose what result to be logged as well as visualize the results while the simulation is running. The window on the right side shows the geometrical model in a selected plane together with the chosen grid resolution [34].

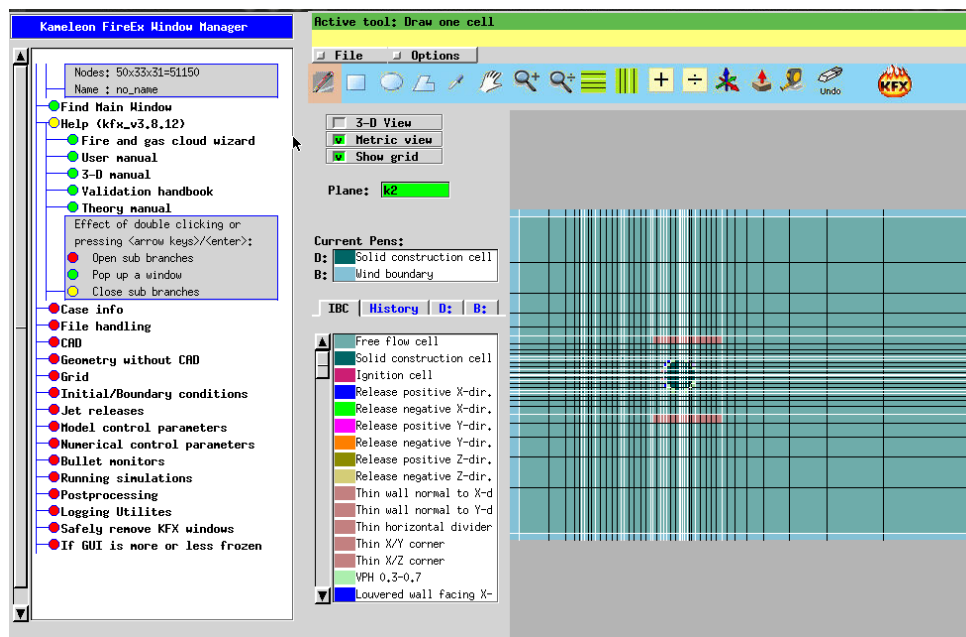


Figure 3.3: Default KFX user interface

By clicking the **Wizard** the **Fire and Gas Simulation Wizard** opens. This is the most efficient way to set up a case for a accurate simulation. As shown in Figure 3.4,



the wizard presents various categories such as simulation type, geometry file loading or creation, wind conditions, temperature parameters, leak characteristics (e.g., rate, size, location), fuel composition, grid data, and domain boundaries. Calculation buttons will compute parameters like the Upper Explosive Limit (UEL), Lower Explosive Limit (LEL), and equivalent hole diameter [34].

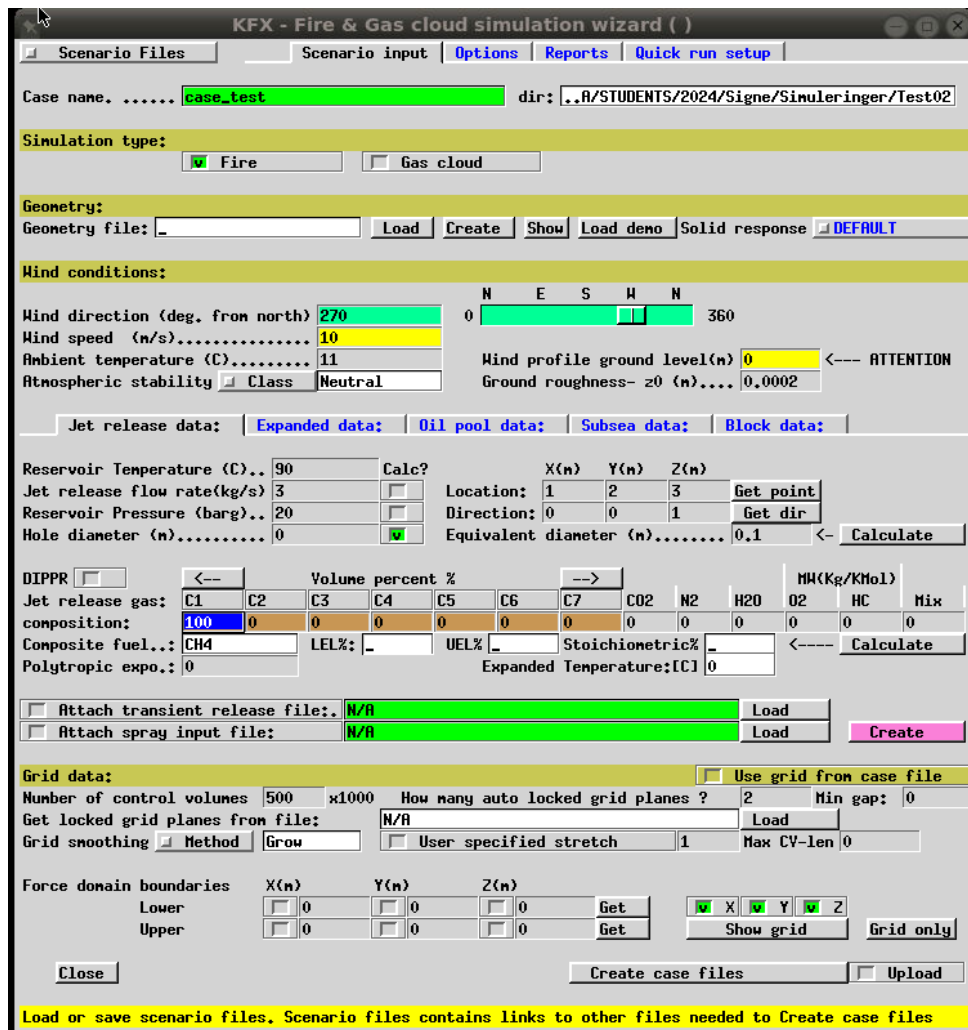


Figure 3.4: Fire and Gas cloud simulation

KFX-RBM is the Risk and Barrier management version of KFX. These additional input options allow the calculation of the transient leak from gas segments or vessels while considering factors like blowdown and Emergency shutdown (ESD). The Wizard analyzes crucial variables such as blowdown activation delays and ESD valve closure time [34]. This is presented in Figure 3.5

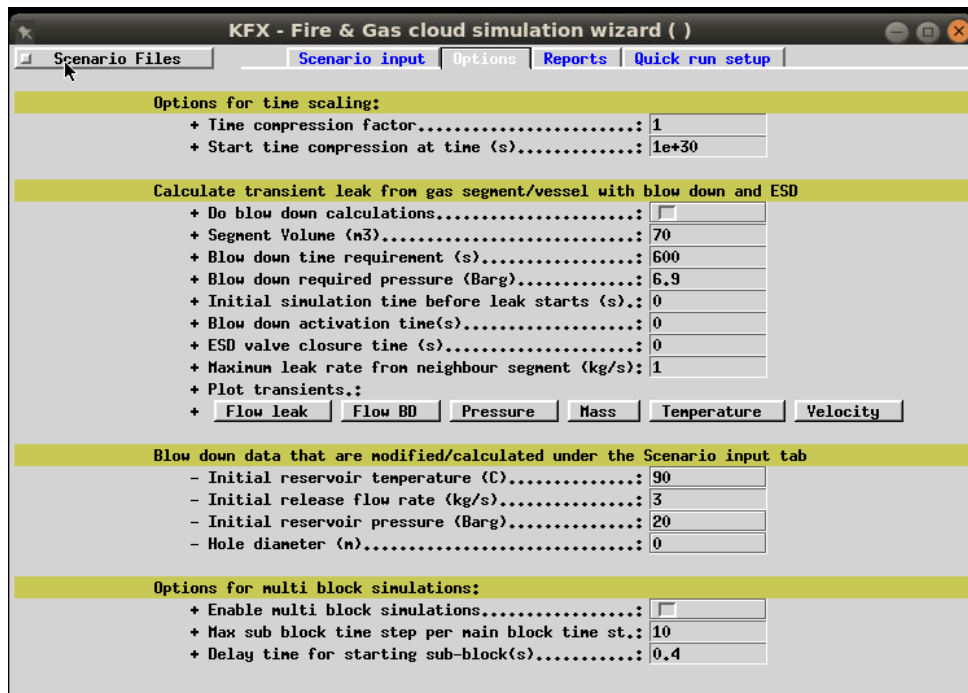


Figure 3.5: The KFX Risk and Barrier Management in the Fire and Gas Cloud wizard with additional options

The tab named "Reports" in the upper bar in Figure 3.5 lets the user select their preferred domain for logging the results as well as to choose when the simulation should stop. While the tab named "Quick run setup" allows the user to specify the text and visualize the output files from the simulation [34]. .

The **KFXview** button in the license client opens the interface for KFXview as seen in Figure 3.6 In KFXview it is possible to post-process data for simulations in KFX. The files can be viewed in 3D and it is possible to adjust various contours [34]. .

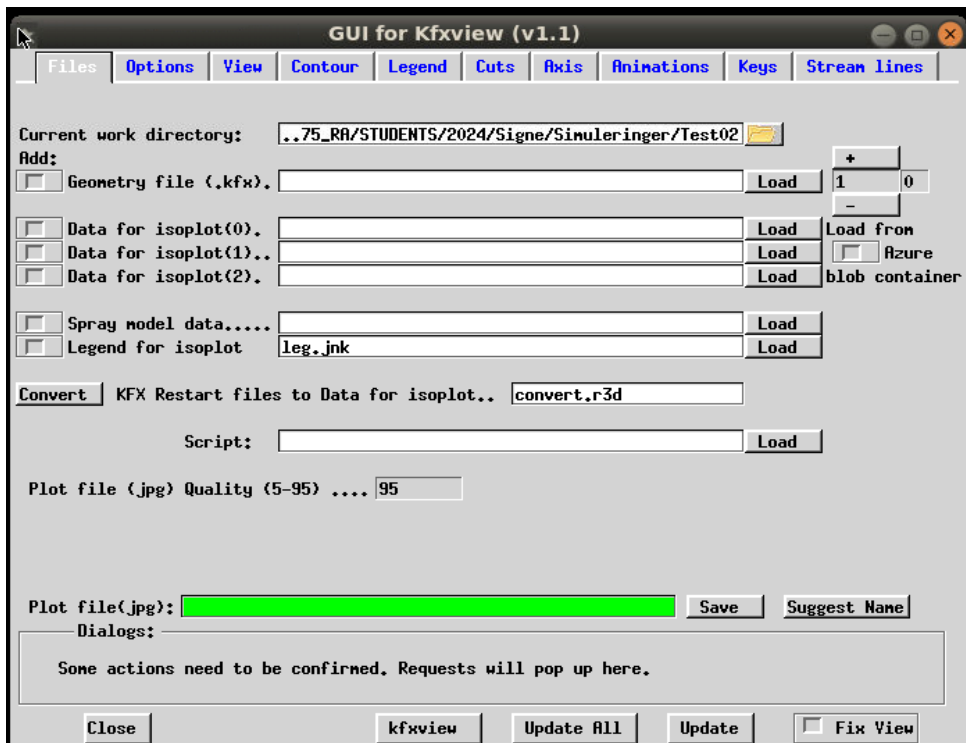


Figure 3.6: User interface for KFXview

The **cmd**> button will launch a Windows or Linux terminal window, as shown in Figure 3.7

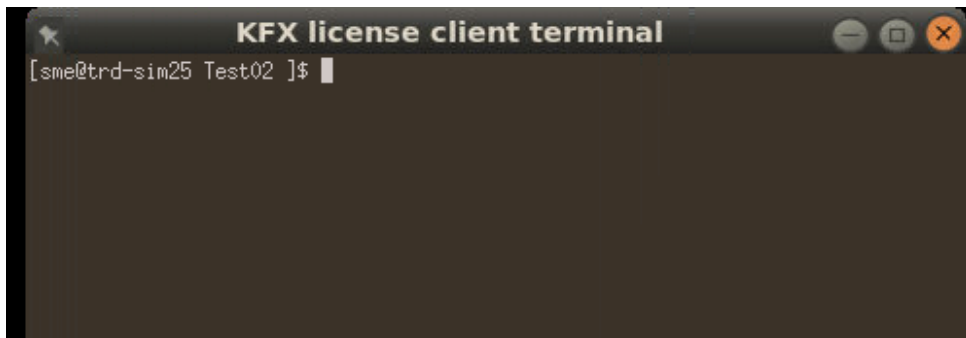


Figure 3.7: Window terminal that launches when clicking the cmd button

The bottom row of the buttons in the KFX license client opens the user manuals. These user manuals are

- **KFX- manual** which shows how to operate the KFX simulation with demos and example cases with additional tools for the result files

- **3-D manual** that informs about the geometry modeling, how to translate various CAD formats into KFX geometry as well as post-processing 3-D calculation results with the **KFXview**.
- **KFX-Exism manual** on how to simulate explosions.

## 3.4 KFX- Risk and Barrier Management

This section will provide information about the KFX-RBM tool and presents how the parameters and equations are used to analyze the ignition probability. KFX-RBM is still under development and has currently no official manual. For this reason, it is important to understand the underlying theory about KFX-RBM and how it works. Most of this work is described by a former Master's thesis Impoco [38] who wrote a thesis with a detailed description of how the KFX-RBM works [38].

The RBM part of KFX is primarily a toolbox that matches the MISOF model's ignition probability with an extensive description of an accidental hydrocarbon leak scenario. For this thesis, KFX-RBM is based on ignition probability from Safetec's SAFEN for hydrogen [38].

KFX Risk and Barrier Management is an extension to KFX that includes a way to calculate ignition possibilities. This is done by placing the ignition source inside the geometry. KFX will then calculate to see if the ignition source is hit by the gas cloud from the gas dispersion simulation. If that is the case, the ignition source will contribute to the total ignition probability [30].

### 3.4.1 Input Parameters for KFX-RBM

It is important to understand the difference in how KFX-RBM models and calculates ignition, compared to what happens in the real world. Like any other computational fluid dynamics software, KFX divides the computational domain into a discretized grid. To get a grid good enough to replicate the real world, it will be needed a grid with a number of grid cells that reach infinity [38].

KFX-RBM placed ignition sources inside this grid as boxes to calculate the ignition probability from each of the boxes. Each ignition source will be designated the expected number of ignitions given exposure as input. This parameter is divided into:

- $\lambda_C$ : Expected number of ignitions due to continuous ignition mechanisms per volume.
- $\lambda_D$ : Expected number of ignitions due to discrete ignition mechanisms per second per volume.

The continuous expected number of ignitions,  $\lambda_C$ , has the unit  $\frac{1}{m^3}$  while the discrete expected number of ignitions,  $\lambda_D$ , has the unit  $\frac{1}{s \cdot m^3}$ .

Detectors can be defined in KFX-RBM. They can detect an ignited leak depending on the type. An IR detector can also detect a gas leak that has not yet ignited. Any number of detectors can be placed in KFX-RBM. Upon detection, a specific amount of the ignitors can be switched off. The parameter  $P_{iso}$  has a value between 0 and 1 and indicates the amount of ignition sources that are switched off. When  $P_{iso}$  is zero, no ignitors will be switched off. When  $P_{iso}$  is 1, all the ignition sources are turned off. [30] [38]. In this thesis switching off ignitors upon detection has not been used.

### 3.4.2 Output Parameters for KFX-RBM

The output from the KFX-RBM simulation is in the ignprob file. KFX-RBM creates one file for each simulation. This file presents the continuous and discrete ignition probabilities, as well as the total ignition probability. The remaining columns in the file are used to calculate the total ignition probability. Table 3.1 shows an example of the ignition probability log (ignprob.log) showing the ignition probabilities.[27] The total ignition probability is the column under *Prob*. A more detailed ignprob.log file can be seen in the Appendix C.

Table 3.1: Part of the output parameters from ignprob log.

time	Prob	P_i	P_C	P_D	ftf_vol	LeL_vol	Leak_rate
5.00E-02	1.83E-02	2.35E-03	8.08E-05	4.68E-09	2.26E+00	2.42E+00	2.00E+01
1.01E-02	1.83E-02	2.35E-03	1.75E-04	1.50E-08	2.81E+00	5.24E+00	2.00E+01
1.54E-02	1.84E-02	2.35E-03	3.17E-04	3.44E-08	4.28E+00	9.51E+00	2.00E+01

Each row represents a time-step in the simulation. The columns is as follows:

- time: The time in seconds
- Prob: Total ignition probability
- Prod\_i: Ignition probability for immediate ignition
- Prod\_C: Ignition probability from a continuous source
- Prod\_D: Ignition probability from a discrete source
- ftf\_vol: New flammable volume within the new time-step
- LeL\_vol: Flammable volume, also denoted  $V_{LFL:UFL}$
- Leak\_rate: Rate of leakage

The continuous ignition probability for one ignition source is given as Prob\_C. This is found by using a Poisson distribution.  $\lambda_C$  is the input variable, the expected number of ignitions per volume, and  $ftf_{vol}$  is the new flammable volume within the time-step. The Poisson distribution gives the following equation for one or more ignitions [28] [30]:

$$P_{C,n} = P(1 \text{ or more ignitions}) = 1 - P(\text{Zero ignitions}) = 1 - e^{-E_C} \cdot \frac{E_C^0}{0!} = 1 - e^{-E_C} \quad (3.4)$$

where  $E_C$  is the expected number of ignition

$$E_C = \lambda_C \cdot ftf_{vol} \quad (3.5)$$

The discrete ignition probability for only one source is:

$$P_{D,n} = 1 - e^{-\lambda_D \cdot V_{LFL:ULF} \cdot \Delta t} \quad (3.6)$$

$P_{D,n}$  is in general found by using a Poisson distribution where  $\lambda_D$  is the expected number of ignitions per volume and time.  $V_{LFL:ULF}$  is the combustible volume and  $\Delta t$  is the time-step.

## 4 Model Testing

The ignition probability model used in this thesis is made and updated regularly by DNV. In this section, the model will be tested through manual calculations of the ignition probability, thereby evaluating its accuracy.

After discussion with experts from Safetec and DNV, it was found to be the best way to test the model was to make a simple box where the leak source was placed inside the box facing one of the walls. The objective was to ensure that the leak should be big enough to rapidly fill the box with hydrogen over the flammable limit. The grid for the simulations should be coarse enough to ensure that the simulation completes within a few minutes.

### 4.1 Basic hydrogen leak in open box

To execute the test, a box with a specific volume is created using coordinates in KFX. The box consists of six sides, with one side made shorter to allow the hydrogen to escape, as illustrated in Figure 4.1.

The whole area box was covered as an "other generic" ignition probability, indicating that ignition occurs immediately upon the start of the leak, and is directly related to the leak. Four infrared point detectors were added to the geometry. This was done in an xml file (Example in Appendix A). Before running the simulations with the correct xml file, the ignition probability for continuous ignition was set to  $5.0E-07$  for easier to calculate the probability by hand.

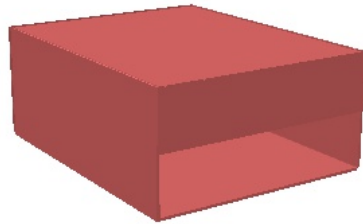


Figure 4.1: Geometry of the box used for the basic hydrogen leak where one side is shorter so the hydrogen can escape

The parameters used for the model testing are given in Figure 4.3 and 4.4. Figure 4.3 shows the basic case scenario input for the gas cloud simulation. The only parameters that are changed from the standard simulation are the jet release flow and the reservoir pressure, together with the location of the leak and the direction of the leak. The grid is relatively coarse to make the simulation run fast. The domain boundaries are made to be slightly outside the box to make the simulation more accurate and ensure that the entire area of interest, including the wall will be looked at. By extending the boundaries to outside of the box we will see any potential leaks or other types of interactions with the environment surrounding the box, as seen in Figure 4.2.



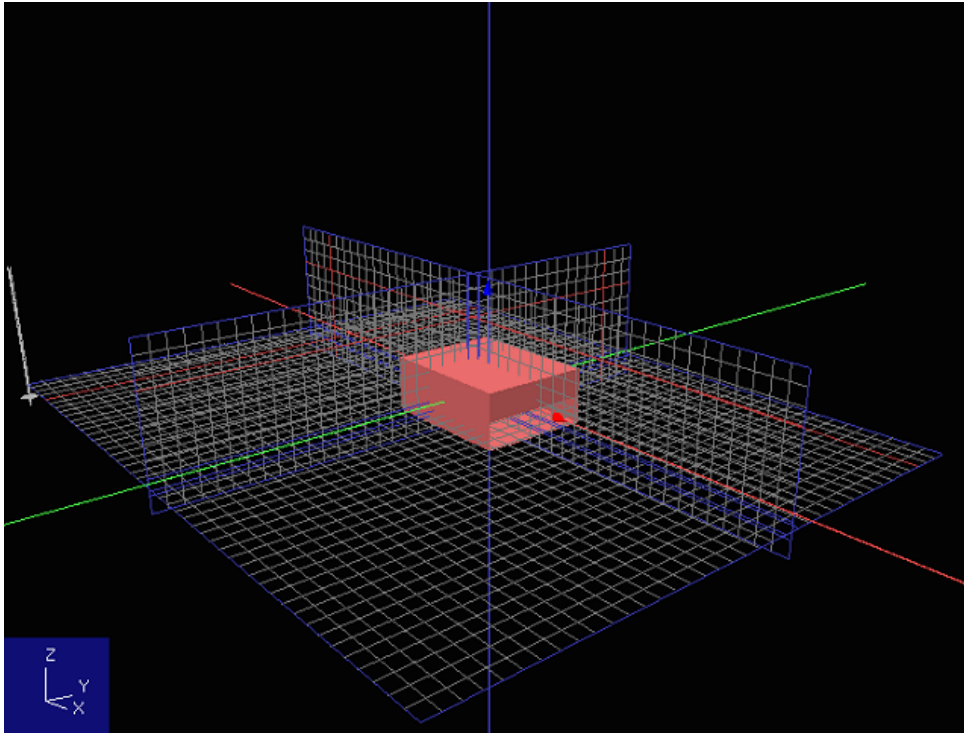


Figure 4.2: Grid with 50,000 grid cells that was used for the simulation of basic hydrogen leak in open box

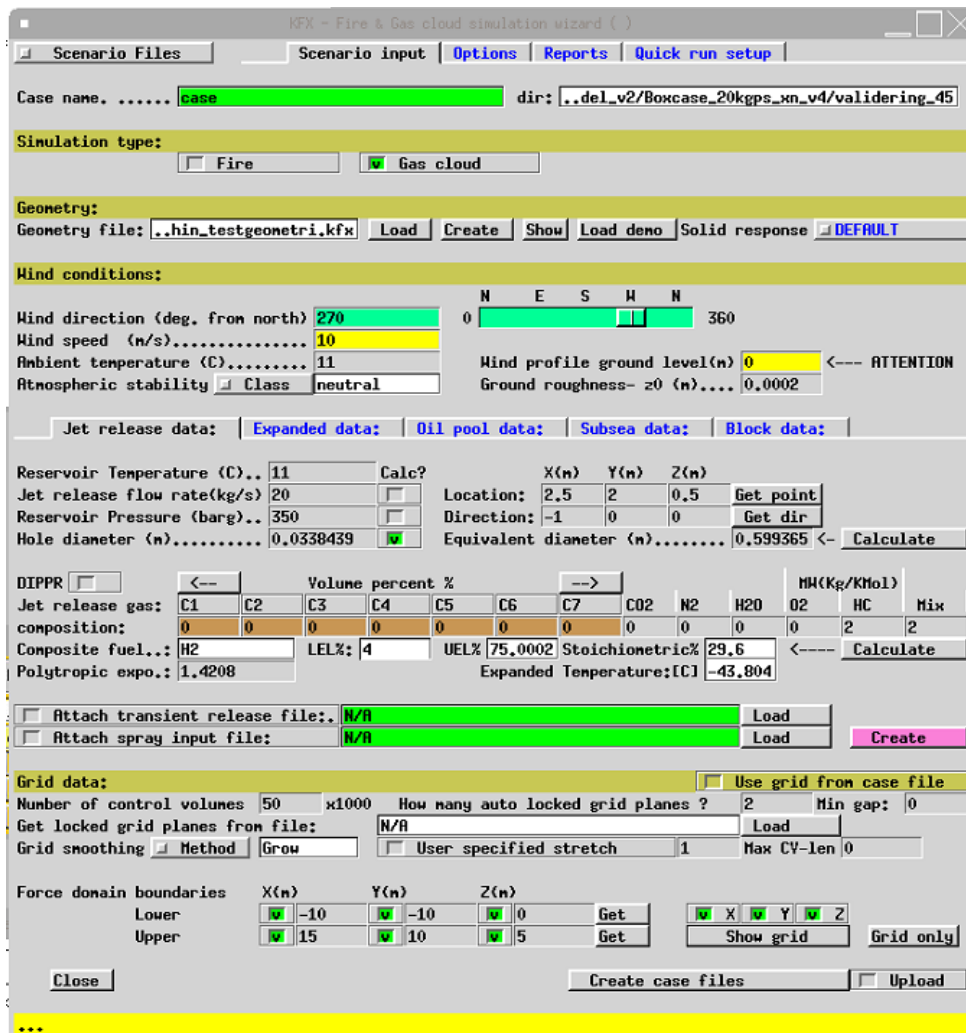


Figure 4.3: Parameters used to set up the scenario inputs for the base-case in KFX Wizard used to test the ignition model

To ensure that the hydrogen leak in the simulation happens fast, the transient leak is set to have a high segment volume with a long blow-down time, as illustrated in Figure 4.4. This is done so that there will be a steady state release of 20 kg/s and the test box will quickly be filled with hydrogen gas.

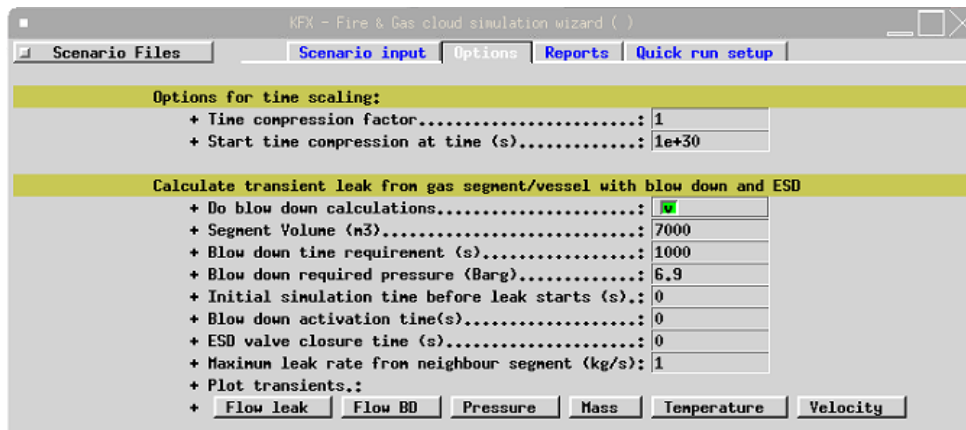


Figure 4.4: Parameters used to calculate the transient leak from the gas segment for the base-case in KFX Wizard used to test the ignition model

The leak is set in a negative x-direction, this is done to make the gas fill the entire box, by first going toward the wall before escaping through the opening on the lower side of the direction of the leakage.

#### 4.1.1 First calculations

To be able to do the ignition probability calculation by hand, some of the numbers for the ignition probability were changed in the xml file to make it easier to calculate them by hand. KFX only calculates the expected number of ignitions that are due to continuous ignition mechanisms per volume and the expected number of ignitions due to discrete ignition mechanisms per second per volume. These numbers were changed to make the calculations easier.

To see if KFX did the correct calculations the box case was run with the KFX Risk and Barrier Management. When the case was run, a file named "ignprob" was accumulated. Here KFX saves all the ignition parameters that it calculates for every millisecond of the simulation. There are several things being calculated but the matter of interest is the Prob\_diff Prob\_mech and prob\_disch. The parameters used to calculate this by hand can be seen in 4.1.

Leak [kg/s]	Pressure [barg]	Hole Diameter [mm]
20	350	33.8439

Table 4.1: Parameters used for calculating the ignition probability by hand

The Prob\_mech can be calculated by using the 2.3 where the answer was as follows

$$P_{\text{event, impact}} = \frac{1}{200} \times 20_{1s}^{\frac{1}{4}} = 1.0573 \times 10^{-2} \quad (4.1)$$

The Prob\_disch can be calculated from 2.4 above. This gave the result:

$$P_{\text{event, electrostatic}} = \frac{1}{100} \times 20_{1s}^{\frac{1}{4}} = 2.1147 \times 10^{-2} \quad (4.2)$$

While the last equation for the Prob\_diff which can be calculated from equation 2.10

$$P_{\text{event, diffusion}}(P, d) = \frac{\ln 350}{5000} \times ((\ln 33.8439 + 1) + 10) = 1.5876 \times 10^{-3} \quad (4.3)$$

The results from the ignprob log compared to the hand calculations can be seen in Table 4.2

	Prob_mech	Prob_disch	Prob_diff
Hand Calculation	$1.0573 \times 10^{-2}$	$2.1147 \times 10^{-2}$	$1.5876 \times 10^{-3}$
Computer Calculation	$1.1497 \times 10^{-2}$	$2.2862 \times 10^{-2}$	$9.5514 \times 10^{-2}$

Table 4.2: Comparison of Hand vs. Computer Calculations

As depicted in Table 4.2, the outcome shows a noticeable difference between the calculations done by hand and those that come from KFX. The log file related to the ignition probability (ignprob) exhibits a recurring display of data at every time-step until approximately 30 seconds. As predicted by the computational model, the probabilities associated with mechanical ignition (prob\_mech), diffusion ignition (prob\_diff), and discharge ignition (prob\_disch) should finish at dynamic variation after 5 seconds, stabilizing at constant values. However, inspection of the ignprob file reveals a continuous alteration in these probabilities beyond the 5 seconds. Specifically, observations regarding the deviation of prob\_mech and prob\_disch from expected behaviors, with their values descending into negative values after approximately 5.3 seconds. Consequently, this variance suggests potential irregularity within the computational code that needs to be looked into more.

### 4.1.2 Second calculations

After discussion with DNV, the model was changed to make sure KFX calculates the correct ignition probabilities.

The hand calculations are the same as in section 4.1.1 whereas the outcome of the computer calculations and the hand calculations can be seen in Table 4.3 below. The calculations for Prob\_disch and Prob\_mech are correct the only parameter that still seems off is the Prob\_diff

	Prob_mech	Prob_disch	Prob_diff
Hand Calculation	$1.057 \times 10^{-2}$	$2.1147 \times 10^{-2}$	$1.588 \times 10^{-2}$
Computer Calculation	$1.057 \times 10^{-2}$	$2.1147 \times 10^{-2}$	$4.7078 \times 10^{-2}$

Table 4.3: Comparison of Hand vs. Computer Calculations after DNV fixed the model

After some iterative troubleshooting procedures to identify what is wrong, trial and error to try to find what was wrong. It appeared that the potential sources of error were either the pressure parameter or the diameter of the hole. Given that the probability attributed to diffusion ignition only depends on the hole diameter and the pressure, it follows that one of these variables could have been wrong. Assuming that the calculation of the hole diameter was conducted in meters rather than millimeters, the ensuing corrected expression gives:

$$P_{\text{event, diffusion}}(P, d) = \frac{\ln 350}{5000} \times ((\ln 0.00338439 + 1) + 10) = 1.170 \times 10^{-2} \quad (4.4)$$

This answer is not close to the computer calculations, see Table 4.3. However, if we reconsider the pressure parameter in a different unit, such as Pascal (Pa) rather than Bar gauge (Barg), the ensuing calculation yields:

$$P_{\text{event, diffusion}}(P, d) = \frac{\ln 35000000}{5000} \times ((\ln 33.8439 + 1) + 10) = 4.7078 \times 10^{-2} \quad (4.5)$$

This answer is much closer to what we got from the computer calculations, see Table 4.3.

### 4.1.3 Third calculations

After DNV's second revision of the model, calculations are presented in Table 4.4. Remarkably, the computational outputs closely align with the results of hand calculations. It is imperative to acknowledge that hand calculations only represent an approximation method for ignition assessment, so perfect concordance between hand and computational outcomes is not anticipated.

	Prob_mech	Prob_disch	Prob_diff
Hand Calculation	$1.057 \times 10^{-2}$	$2.1147 \times 10^{-2}$	$1.588 \times 10^{-2}$
Computer Calculation	$1.0596 \times 10^{-2}$	$2.0942 \times 10^{-2}$	$1.5967 \times 10^{-2}$

Table 4.4: Comparison of Hand vs. Computer Calculations after DNV fixed the model a second time

By plotting the ignition probability against time for the three probabilities, it is evident that both mechanical ignition (Figure 4.5) and discharge ignition (Figure 4.6) indicate a stop of dynamic variation beyond the five-second mark, whereby the probabilities stabilize.

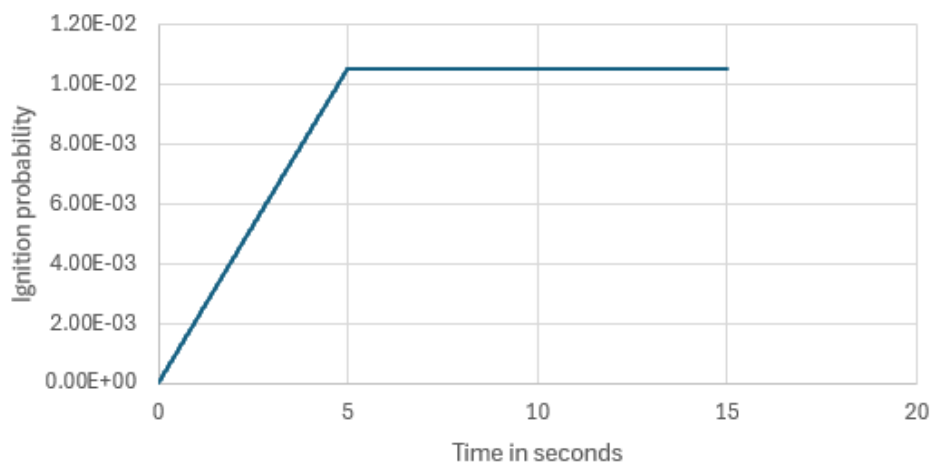


Figure 4.5: Mechanical ignition probability plotted with time in seconds on the x-axis, and ignition probability on y-axis

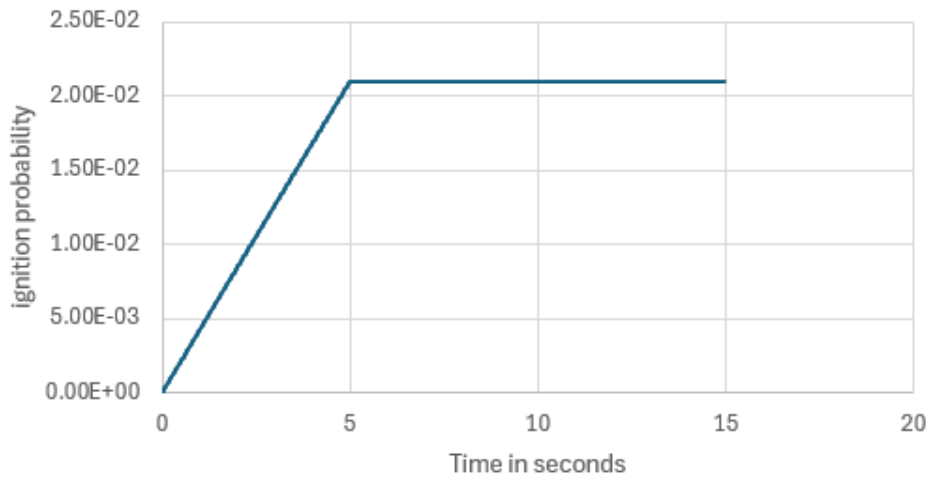


Figure 4.6: Discharge ignition probability plotted with time in seconds on the x-axis, and ignition probability on y-axis

The graph spans from the initial time step for the diffusion ignition probability, depicting continuous variation throughout the simulation.

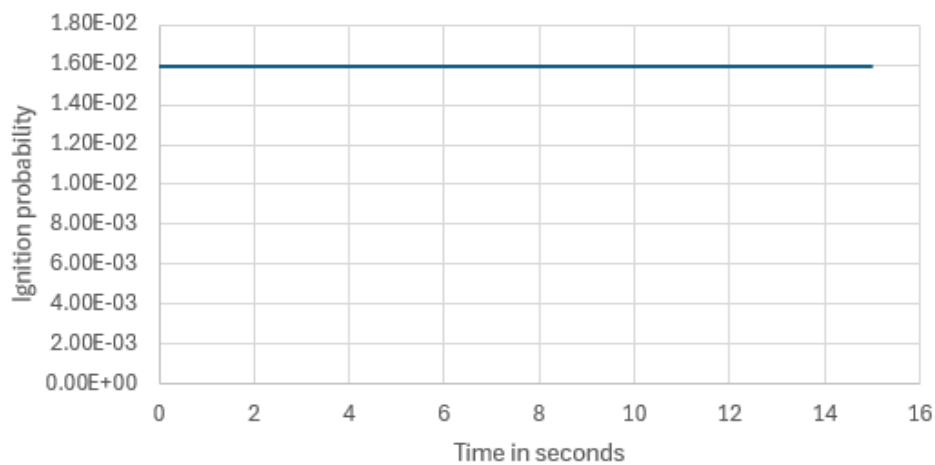


Figure 4.7: Diffusion ignition probability plotted with time in seconds on the x-axis, and ignition probability on the y-axis

## 4.2 Calculating the ignition probability

The next part of the model testing was to calculate the continuous and discrete ignition probabilities in the *ignprob.log*

### 4.2.1 Continuous ignition probability

For the sake of making the hand calculations easier, the continuous ignition probability per equipment is changed to 1.00E-07 while the discrete ignition probability was set to zero. The hand calculations was done by following the equations in Chapter 3.4.2 for a continuous ignition. Keep in mind that for this test we only have one ignition source making the calculations much easier.

For the initial time-step, t=0 seconds, Equation 3.4 and 3.5 was used and gave following:

$$Prob_{C1} = 1 - e^{-1.69E-01 \cdot 1.00E-07} = 1.69E - 08 \quad (4.6)$$

To check that KFX-RBM calculates the correct contribution for the next time steps manual calculations were performed by using the input from the ignprob.log file form KFX-RBM (shown in Table 3.1). The continuous ignition probability for time-step 2 was calculated by adding the contribution during time-step 2 to the value from time-step 1 and all numbers used can be seen in Table 3.1

$$Prob_{C2} = Prob_{C1} + (1 - e^{E_c}) \cdot (1 - Prob_{tot1}) \quad (4.7)$$

This last parenthesis in Equation 4.7 is needed to apply the condition that ignition has not already occurred at time-step 1.  $E_c$  is calculated from Equation 3.5 with data from Table 3.1.

$$Prob_{C2} = Prob_{C1} + (1 - e^{-2.26 \cdot 1.00E-07}) \cdot (1 - 1.83E - 02) = 2.38E - 07 \quad (4.8)$$

For the third time-step at 0.012 seconds, equation 4.7 was used and gave following:

$$Prob_{C3} = Prob_{C2} + (1 - e^{-2.81 \cdot 1.00E-07}) \cdot (1 - 1.83E - 02) = 5.19E - 07 \quad (4.9)$$

The rest of the time steps follow this same pattern. Table 4.5 shows the hand calculations compared to the computer calculations for the first three time steps.

Table 4.5: Hand calculations compared to the computer calculations for the continuous ignition probability,  $Prob_C$

Time [sec]	0.00E+00	5.00E-03	1.02E-02
Computer_calc	1.69E-08	2.42E-07	5.24E-07
Hand_calc	1.69E-08	2.38E-07	5.19E-07
Correct [%]	100	98.3	99.18



### 4.2.2 Discrete ignition probability

To check the discrete ignition probability, the expected discrete ignition probability was set to 1.00E-07 while the continuous ignition probability was set to zero.

For the the initial time-step at t=0 seconds, equation 3.6 was used:

$$Prob_{D1} = 0.00 \cdot 1.69E - 01 \cdot 1.00E - 07 = 0 \quad (4.10)$$

To check that KFX-RBM calculates the correct contribution for the next time steps a similar procedure as used for the continuous probability was employed. The discrete ignition probability for time-step 2 was calculated by adding the contribution during time-step 2 to the value from time-step 1 and all numbers used can be seen in Table 3.1

$$Prob_{D2} = Prob_{D1} + (1 - e^{E_D}) \cdot (1 - Prob_{tot1}) \quad (4.11)$$

This last parenthesis in Equation 4.11 is needed to apply the condition that ignition has not already occurred at time-step 1.  $E_D$  is calculated from Equation 3.6 with data from Table 3.1.

$$Prob_{D2} = 0 + (1 - e^{-1.00E-07 \cdot 2.42 \cdot 5.00E-03}) \cdot (1 - 1.83E - 02) = 1.19E - 09 \quad (4.12)$$

The third time-step at 0.001 seconds was calculated by

$$Prob_{D3} = 1.13E - 09 + (1 - e^{-1.00E-07 \cdot 5.24 \cdot (1.02E-02 - 5.00E-03)}) \cdot (1 - 1.83E + 02) = 3.80E - 09 \quad (4.13)$$

Table 4.6: Hand calculations compared to the computer calculations for the discrete ignition probability,  $Prob_D$

Time [sec]	0.00E+00	5.00E-03	1.02E-02
Computer_calc	0.00E+00	1.13E-09	3.60E-09
Hand_calc	0.00E+00	1.19E-09	3.80E-09
Correct [%]	100	106	105

## 4.3 Model testing discussion

In the basic hydrogen leak test within an open box simulation, the model was tested and it was found that the hand calculations for continuous ignition probability closely matched the result from the computer in the finished model. However, the hand and computer

calculations are significantly more uneven for the discrete ignition probability. The box case was simulated with Powerscan, and as mentioned in Chapter 5.2.1 powerscan uses a grid generator named Meshmerize that has an algorithm for automatically locking grid planes to large surfaces. In the majority of instances, this is desired because the Computer-Aided Design (CAD) files tend to be pretty cluttered with duplicates, automatically locked planes are often located differently from what is desired. The user can mark which grid planes to lock. However, Meshmerize does not always permit the desired locked lines because a smooth grid takes priority [33].

Both grid deviation done by powerscan or manual creation can lead to errors, affecting the simulation results. This is particularly critical in the context of KFX-RBM calculations of ignition probability, which rely on interpolation. Even minor deviations in interpolation placement outside the area of interest can result in inaccuracies, affecting the results' reliability.

This is particularly crucial for small-scale cases since the need for large grid cells is highly important. Since the area is so small, even minor errors in the interpolation cause big differences in the ignition probability, which again gives a wrong picture of the real-world conditions. Accurate interpolation becomes highly important to preserve the authenticity of the real phenomenon being studied. So for a small-scale case, making the grid by manual creation will be the best since it requires careful consideration to ensure a good result without reducing the effectiveness of the simulation. But in most cases, many cases are being simulated, and changing the grid for each one of the simulations will be severely time-consuming compared to using Powerscan to quickly create several cases.

## 5 Simulation set-up

This chapter presents the base case input parameters used to set up the simulations for the three geometries. It also details the parameters necessary for executing the simulations.

### 5.1 Input parameters and boundary conditions

To get results that are as accurate as possible there is a need to have a wide spread of parameters. This makes it possible to give an overall risk picture of the situation. Having an accurate overall risk picture is very important when designing a project as well as operating it [34].

Together with the generic input parameters, each leak scenario will be analyzed for two different locations, two different leak rates, and six different directions. The leak rates chosen are 0.1 kg/s and 1.0 kg/s. The two different leak locations are set to be in the middle of each of the three geometries as well as in the corner of them. In addition, every scenario will be simulated in every direction. This means that 72 cases will be simulated [34] [38].

Base-case describes an instance where the selected module functions normally. The advantage of making a base-case is to have a base that it is possible to turn back to if the copied versions of the base-case get ruined. The base-case is later copied to other cases to make it easier to change the parameters [33] [34].

Simulating KFX involves making a scenario file with a file ending ".scn". The scenario file will automatically be made when a KFX wizard scenario is being created by clicking the "create case files" button to the downright. This ".scn" file will have every input specified by the creator [34].

Together with the parameters defined in the fire and gas simulation wizard, there are parameters for RBM that have to be defined. To make sure that the simulations match the risk and barrier requirements to the installation, certain parameters must be specified [34].

The scenario file made from the base-case only contains the data to run one case. In almost every situation, it is wanted to run a lot of simulations where some of the parameters vary. Hence, in this case, where the wish is to vary the case for different leak rates, positions,

and directions and to create scenario files for every combination would be time-consuming. The directions for both leaks can be seen in Figure 5.1. Setting up the ".scn" file containing 72 cases is a highly time-consuming process. Luckily, there is a feature in KFX named power scan that allows the user to create a ".scn" file containing multiple cases in a much shorter time [33] [34].

Table 5.1: Parameter overview of all the directions the two leak rates will be simulated in.

Case	Leak Rate	Leak direction
1	0.1	xp
2	0.1	xn
3	0.1	yp
4	0.1	yn
5	0.1	zp
6	0.1	zn
7	1	xp
8	1	xn
9	1	yp
10	1	yn
11	1	zp
12	1	zn

For all simulations, the KFX wind boundary conditions were used on the sides of the calculation domain. On the wind inlet side KFX will apply a wind velocity and turbulence profile. On the outlet side and the top of the domain, a constant pressure boundary condition is used. For the bottom boundary, a solid boundary condition is used with the terrain roughness.

## 5.2 Making a base-case in KFX Wizard

The first step when making a case was to use the "Fire and Gas Cloud Simulation Wizard" tool to set up the first gas cloud simulation for the base-case.

The parameters used to set up the base-case for all geometries are shown in Table 5.2. The only parameters that will change are the leak rate and the leak location. The two leak rates will be simulated in all six directions.

Table 5.2: Constant parameters used for setting up the ISO container simulation in KFX

Pressure [barg]	Wind Direction	Wind speed	Temperature	Substance
350	West	3	11	H2

When the tank pressure and leak rate are specified in the Wizard, KFX will perform expansion calculations to establish the jet inlet velocity, jet temperature, and leak diameter, this is presented in Table 5.3 and 5.4. This expansion calculation is performed before the case files are generated and will be used as the jet inlet parameters in the simulations.

Table 5.3: Tank temperature, pressure and leak rate for the jet inlet calculated by KFX for the 0.1 kg/s leak rate

	Temperature [K]	Velocity [m/s]	Hole diameter [m]
Container	229.196	768.989	0.0024
Refueling station	229.196	768.989	0.0024
Process plant	229.196	768.989	0.0024

Table 5.4: Tank temperature, pressure and leak rate for the jet inlet calculated by KFX for the 1 kg/s leak rate

	Temperature [K]	Velocity [m/s]	Hole diameter [m]
Container	229.196	768.989	0.0076
Refueling station	229.196	768.989	0.0076
Process plant	229.196	768.989	0.0076

### 5.2.1 Powerscan- Creating multiple cases at once

When clicking the "create case files" in Figure 3.4, a scenario case file with the extension ".scn" is created. This file contains two rows when opening. The first row shows the column headings, while the second row shows the input data. The ".scn" file makes it effortless to make multiple cases quickly, without needing to go by the GUI Wizard. Since the base case is more or less the same for every simulation, all the parameters are also more or less the same. The scenario variations can be done by copying the scenario line in the text editor and changing only the parameter for the individual case. When working with an immense number of scenarios this is a very efficient way to make small changes to a case and automatically provide generations of scenario files with a proper calculation grid [33] [34]. Powerscan uses a grid generator named Meshmerize and the code from the GUI panel Fire and Gas cloud simulation wizard in KFX. A summary of the input data

from the ".scn" file can be seen in Table 5.5 and 5.6. Not all of the values have been modified, most of them are default values [33] [34].

Table 5.5: Parameters for the scenario file- Part 1. From [34]

Parameter	Unit	Description
Case_name	-	Path to location
Data_type	-	Release tab active
T_max	s\textasciicircum{3}	Maximum simulation time
Jet_position	-	Coordinates for hole location
m_step	-	Unknown
Jet_direction	-	Release direction
Res_temperature	C	Reservoir temperature
Jet_pressure	barg	Jet gauge pressure
Jet_flowrate	kg/s	-
Jet_gas_components	-	Released H2 vector
Jet_gas_composition	-	H2 mixture volumetric fraction
Gas_cloud_sim	-	Simulation type (0=fire, 1=gas dispersion)
Wind_angle	m/s	Clockwise angle from North
Wind_10	-	Wind speed at altitude 10 m
Wind_stability	-	Wind class (Pasquill)
Ambient_T	C	Ambient temperature
Wind_roughness	m	Ground roughness
Geometry_file	-	Path to geometry file
Geometry_min	-	Lower corner grid coordinates
Geometry_max	-	Upper corner grid coordinates
Vol_box_min	-	Lower corner coordinates for domain of interest
Vol_box_max	-	Upper corner coordinates for domain of interest
Stoppro	s	Stop simulation when the flammable cloud plateaus

Table 5.6: Parameters for the scenario file- Part 2. From [34].

Parameter	Unit	Description
Dt_rowcum	s	Intervals for saving cumulative gas cloud reports
Dt_volstop	s	Stop run criterion based on cloud size
Gridpoints	-	Grid points in calculation domain
Lockedplanes	-	Number of grid planes locked
Spray_file	-	Attached to the case
Jet_gas_massflow	-	
Jet gas time		
Grid_parameters	-	Data vector for controlling the grid generator
Block_parameters	-	Defining a volume with homogeneous grid
Sub_block	-	Data vector for defining the sub block
Pool_parameters	-	Input data vector for poolsimulation
Time_controls	-	Input data for controlling time step creation
History_points	-	Text file with coordinates for history data monitoring
Subsea_parameters	-	Data for controlling subsea releases
Rbm_parameters	-	Input data for rbm

Table 5.7: RBM parameters for the scenario file. From [34]

Position	Description	Unit	Base case
1	Segment name		'Segment_1'
2	Segment volume	m <sup>3</sup>	0.55
3	Blowdown pressure requirement	Pa	790,000
4	Blowdown time requirement	s	600
5	Blowdown activation time	s	-
6	Number of detectors initiating ESDS/BD	-	-
7	Max inflow segment from neighboring segments	0	-
8	Pressure conversion factor. From Pa to bar	1e-05	-
9	Immediate ignition probability	-	0.00235
10	ESDV closure time	s	-
11	Simulation time before start of leak	s	0
12	Blowdown calculations (0=no, 1=yes)	-	1
13 to 16	Unknown	-	-

The `rbm_parameters` include the transient calculations for the leak flow rate, together with the ESD and BD systems, as shown in Table 5.7. This parameter together with the ones in Table 5.5 and 5.6 will tell kfx about the base case when submitted [34].

The base case was created with the Fire and Gas cloud simulation wizard, but since 72 individual cases needed to be created, the base case was copied 71 more times. For each case, distinct names were assigned, each reflective of the specific parameters given in the case. Appendix B shows the naming system for a completed scenario file with the ".scn" ending.

### 5.3 Simulation of 40' ISO-container

For this thesis, three distinct geometries will be used to examine the model's performance as the complexity and scale of the geometry escalate. The smallest and least complex geometry is the 40' ISO-container.

The container is a standard 40 ft. ISO-container that is 2.4 meters wide, 2.6 meters high, and 12 meters long as shown in Figure 5.1 [39]. The geometry is provided by Safetec and has been used in Myrstad [28] master thesis from 2023.



Figure 5.1: Standard 40' ISO-container. Picture from [39]

The 3D model of a ISO container is given in Figure 5.2 The 3D geometry is made by writing the dimensions for the box with coordinates. The code can be seen in the appendix. As shown in the figure, there are 11 small circles in the geometry to visualize where the hydrogen tanks are located inside the container. There is also a small opening in the two long side walls, this is done for the sake of KFX to be able to simulate the leak.



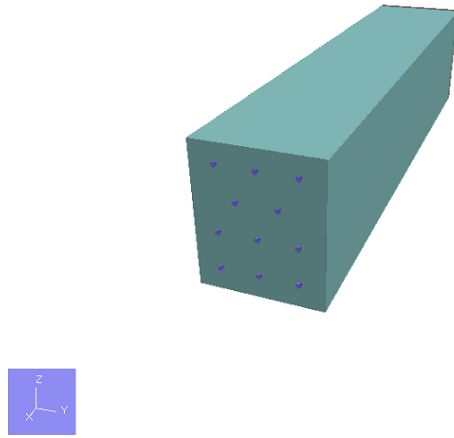


Figure 5.2: 3D geometry of the ISO-container used for the simulations

The inside of the container can be seen in Figure 5.3. The Figure has been cut 2 meters from the top to visualize how it looks from the inside.

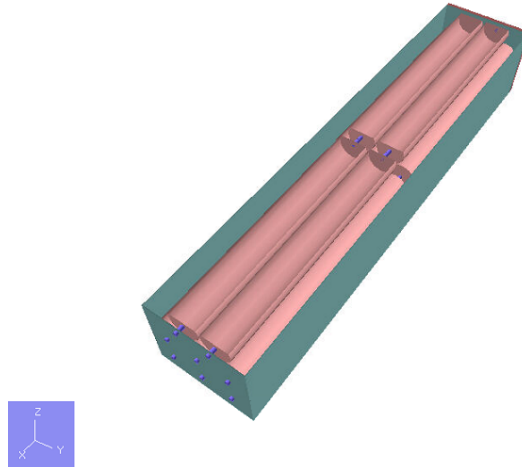


Figure 5.3: 3D geometry of the ISO-container used for the simulations where the top is cut off to see what it looks like inside

Four infrared point sensors (IR-detectors) was placed inside the container geometry. Together with these detectors, five ignitors was also placed in the geometry. These five ignitors was defined as presented in Table 5.8.

Table 5.8: SAFEN hydrogen ignition model parameters for Ex-rated equipment used in the XML file for every case

	Continuous [ $m^3$ ]	Discrete [ $m^3 \cdot sec^{-1}$ ]
Other	1.8E-06	1.2E-08
Electrical equipment	5.4E-06	1.5E-09
Rotating equipment	1.1E-05	1.5E-09
Electrostatic discharges	2.0E-05	4.0E-07

## 5.4 Simulation of hydrogen refueling station

The hydrogen refueling station slightly surpasses the size of the 40' ISO container. A three-dimensional representation of the station is depicted in Figure 5.4. The dimensions of the refueling station measure 20 meters in length and 13 meters in width, with a surrounding fence standing at a height of 5 meters, resulting in a fenced volume area of  $1300 m^3$ . While the figure displays a shop and a refueling dispenser, the area of interest remains the fenced area enclosing the process equipment that stores hydrogen. While Figure 5.5 shows the geometry as it is viewed in KFX view.

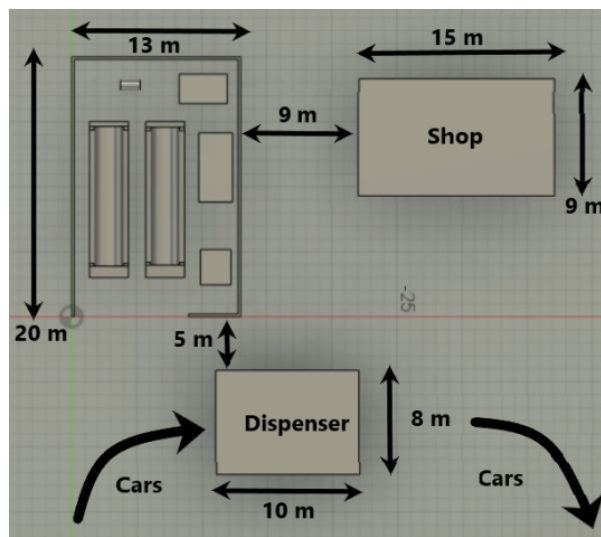


Figure 5.4: The figure shows the dimensions of the refueling station. However, the area of interest is the fenced area around the process equipment. From [28]

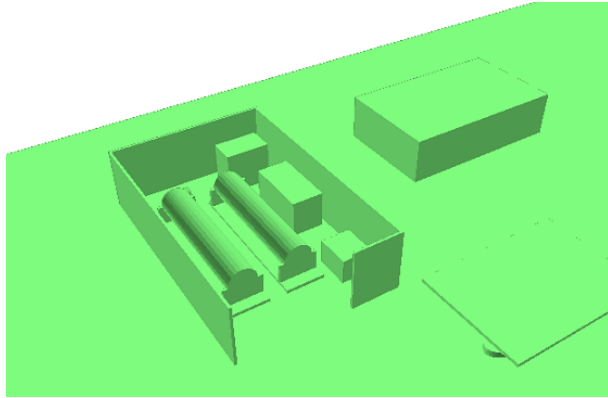


Figure 5.5: The figure shows the geometry for the refueling station from kfx view

10 IR detectors was positioned at an elevation of 2 meters above the floor. This was done to ensure uniform coverage across the entire process area. Together with these 10 IR detectors, the ignitors in Table 5.8 was also placed in the geometry.

## 5.5 Simulation of onshore process unit

The onshore process unit represents the largest geometry within this thesis, encompassing an area of approximately 80,000 gross cubic meters. This geometry contains the highest concentration of process equipment and is by this reason the most complex geometry.

As seen in Figure 5.6 The unit consists of 2 floors where all sides are open. There was placed a total of 200 detectors inside the process plant. These detectors are placed in two separate planes, each containing 100 detectors together with the ignitors in Table 5.8.

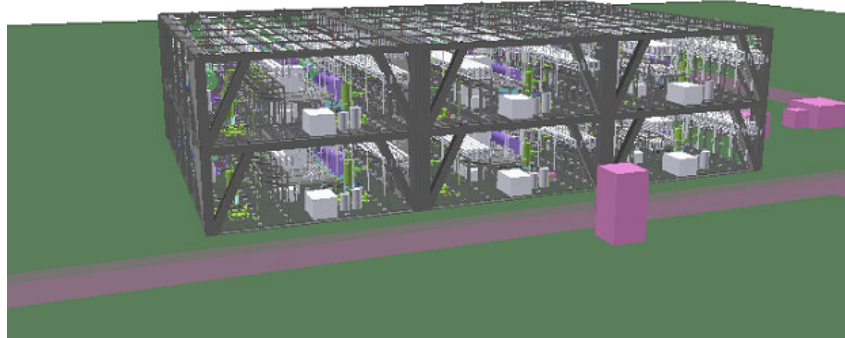


Figure 5.6: The figure shows the geometry of the process plant

For the first plane, the 100 detectors are positioned 1 meter above the ground, arranged in rows of 10 detectors per row. In the second plane, the detectors are placed 8 meters above the ground, arranged in the same pattern as in the first plane, with 10 detectors per row. The detectors were placed at 1 and 8 meters above ground to make sure that as few detectors as possible were placed inside the process equipment.

# 6 Results from 40' ISO-container

## 6.1 Hydrogen

### 6.1.1 Gas Dispersion

Figure 6.1 and 6.4 shows the amount of gas in the area of interest. If the area of interest were different, the release profile would look different.

Figure 6.2 presents the surface plot with 4 % resulting from a leak in the middle of the geometry with a leak rate of 0.1 kg/s in a downward release. Figure 6.3 illustrates the surface plot for a leak rate of 1 kg/s under the same conditions.

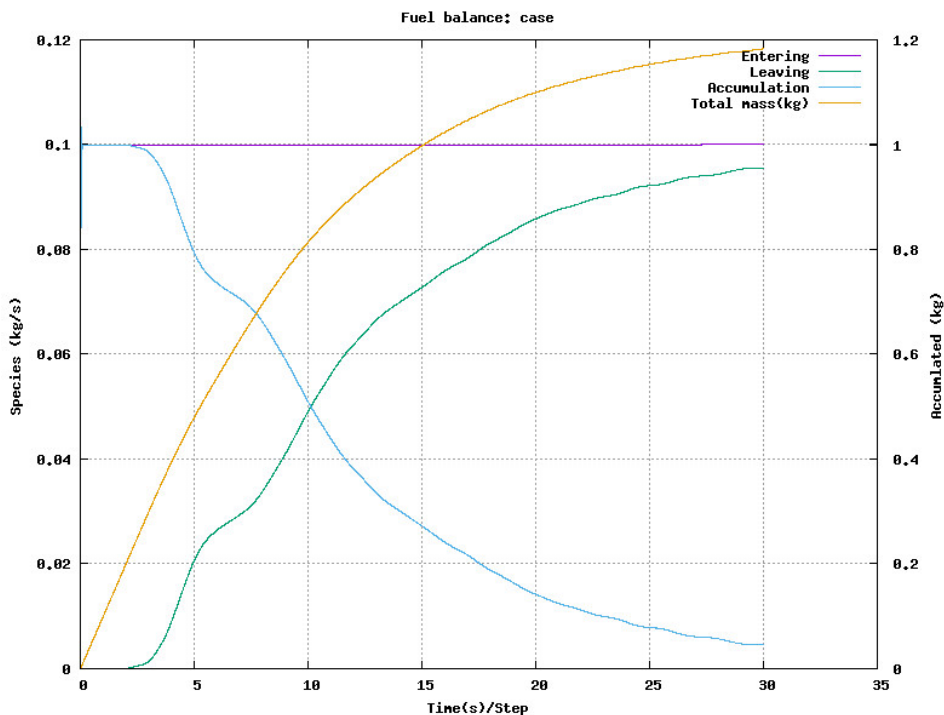


Figure 6.1: Release profile of 0.1 kg/s downward release where the location is in the middle of the container geometry

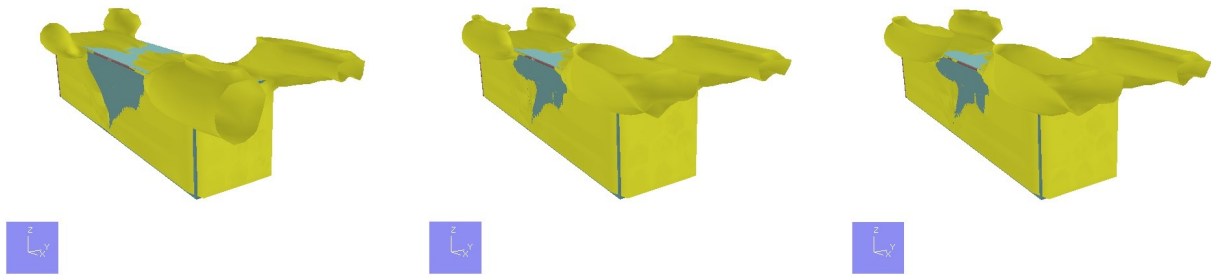


Figure 6.2: Surface plots of 4% H<sub>2</sub> concentration for 0.1 kg/s downward release at different time points: 10 seconds, 20 seconds, and 30 seconds where the leak locations are in the middle of the container geometry.

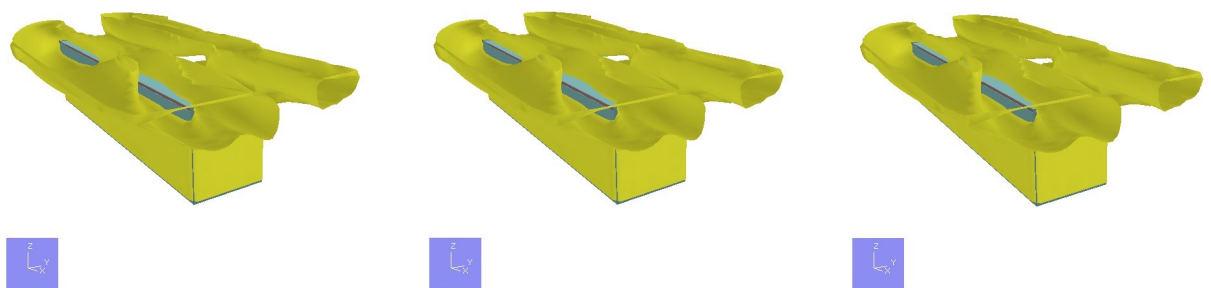


Figure 6.3: Surface plots of 4% H<sub>2</sub> concentration for 1 kg/s downward release at different time points: 10 seconds, 20 seconds, and 30 seconds where the leak locations are in the middle of the container geometry.

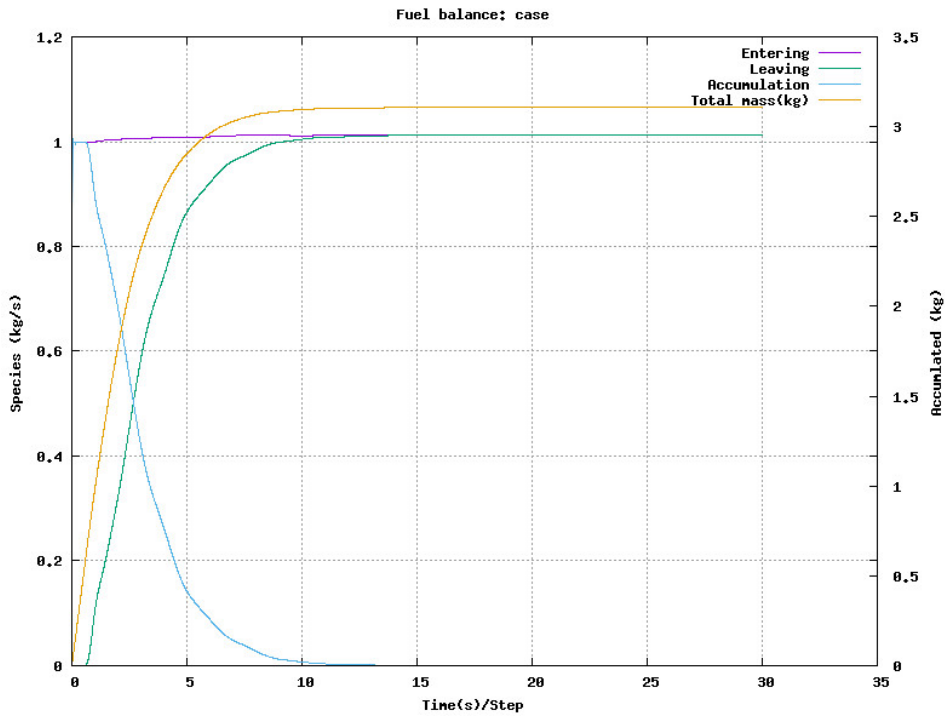


Figure 6.4: Release profile of 1 kg/s downward release where the location is in the middle of the container geometry

Figure 6.5 presents the surface plot with 4 % resulting from a leak in the middle of the container geometry with a leak rate of 0.1 kg/s in a downward release. Figure 6.6 illustrates the surface plot for a leak rate of 1 kg/s under the same conditions.

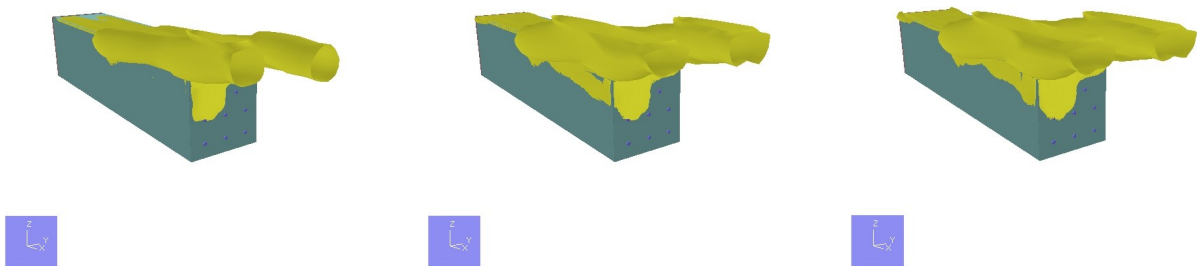


Figure 6.5: Surface plots of 4% H<sub>2</sub> concentration for 0.1 kg/s downward release at different time points: 10 seconds, 20 seconds, and 30 seconds where the leak locations are in the corner of the container geometry.

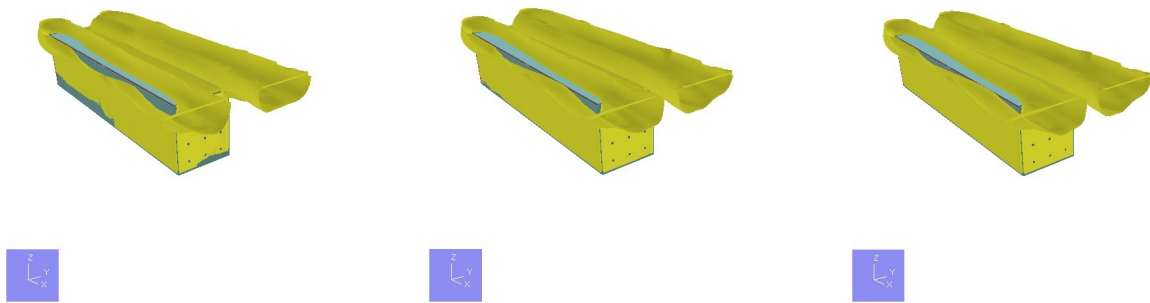


Figure 6.6: Surface plots of 4% H<sub>2</sub> concentration for 1 kg/s downward release at different time points: 10 seconds, 20 seconds, and 30 seconds where the leak locations are in the corner of the container geometry.

### 6.1.2 Flammable Cloud

Figure 6.7 and 6.8 present the stoichiometric equivalent cloud volume for the 0.1 kg/s leak rate and 1 kg/s leak rate.

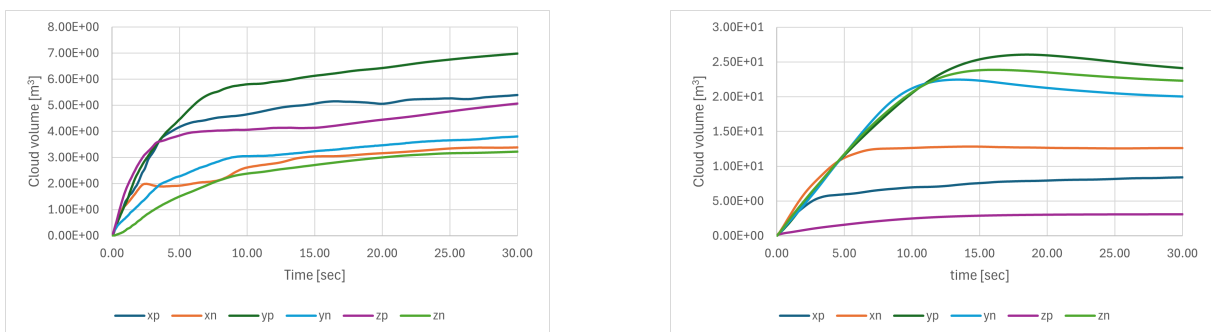


Figure 6.7: Stoichiometric equivalent cloud volume for corner (left) and middle (right) leak in all directions with leak rate 0.1kg/s for the container geometry.



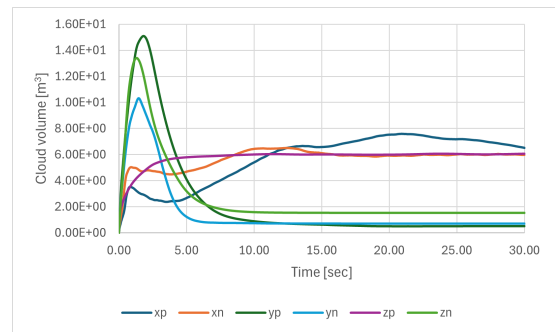
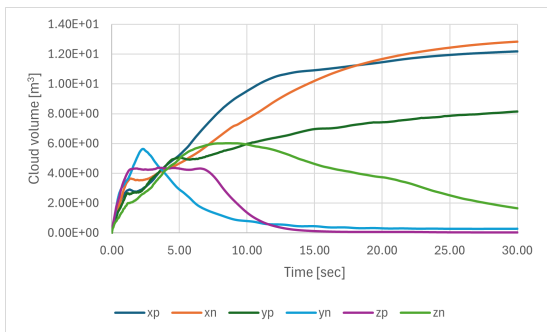


Figure 6.8: Stoichiometric equivalent cloud volume for corner (left) and middle (right) leak in all directions with leak rate 1 kg/s for the container geometry.

Figure 6.9 and 6.10 present the flammable cloud volume between the upper and lower flammability limit.

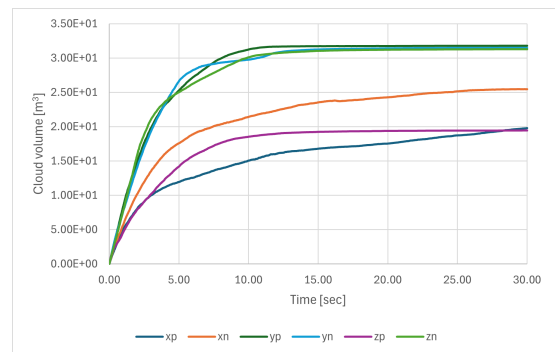
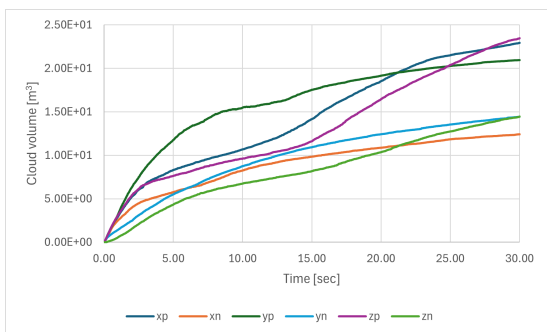


Figure 6.9: Flammable cloud volume between lower- and upper flammability limit for corner (left) and middle (right) leak in all directions with leak rate 0.1kg/s for the container geometry.

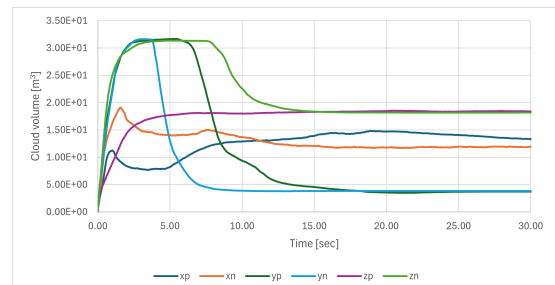
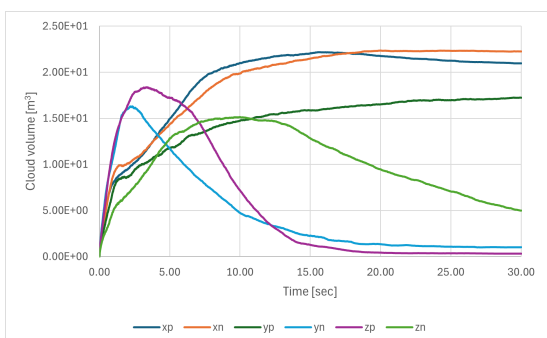


Figure 6.10: Flammable cloud volume between lower- and upper flammability limit for corner (left) and middle (right) leak in all directions with leak rate 1 kg/s for the container geometry.

### 6.1.3 Ignition Probability

Figure 6.11 presents the ignition probabilities for the 0.1 kg/s leak for both the middle and corner locations, and the 1.0 kg/s leak with both the locations at the start of the leak while Figure 6.12 presents the ignition probabilities at the end of the leak. Figure 6.13 shows the average ignition probability for the 0.1 kg/s leak and the 1.0 kg/s leak.

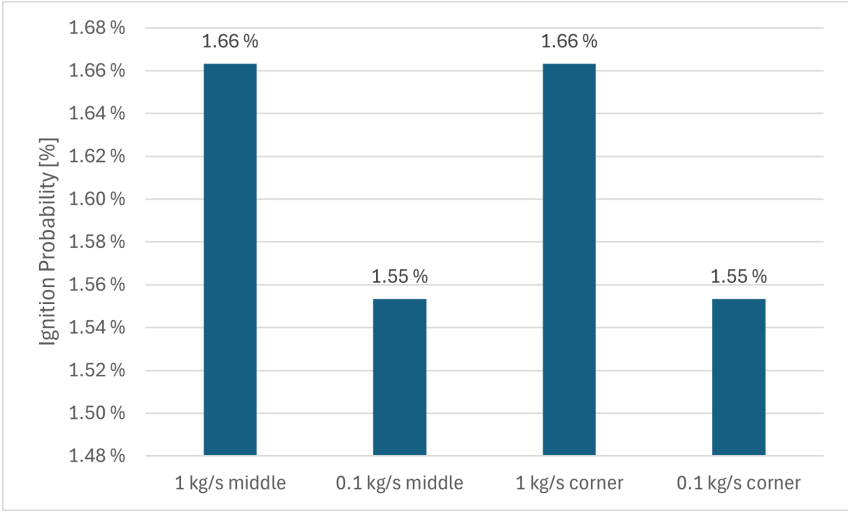


Figure 6.11: Ignition probability for the different leaks and their locations at the start of the leak (t=0)

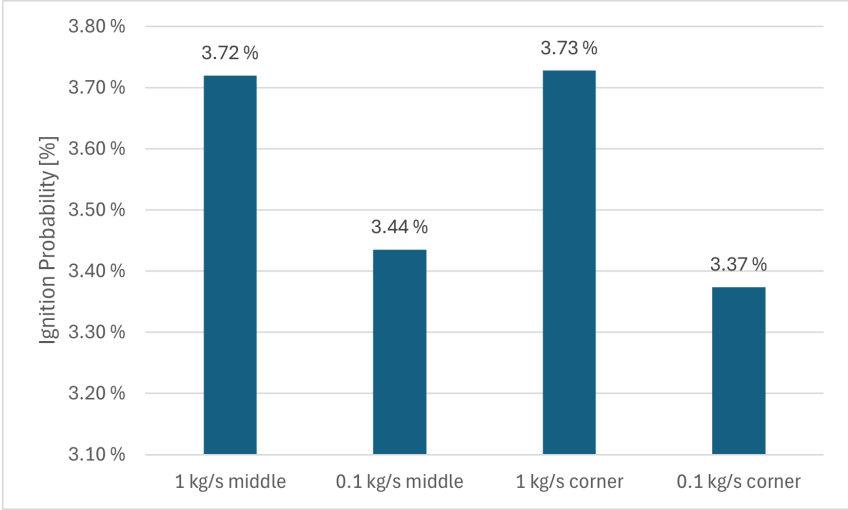


Figure 6.12: Ignition probability for the different leaks and their locations at the end of the leak for the container scenario.

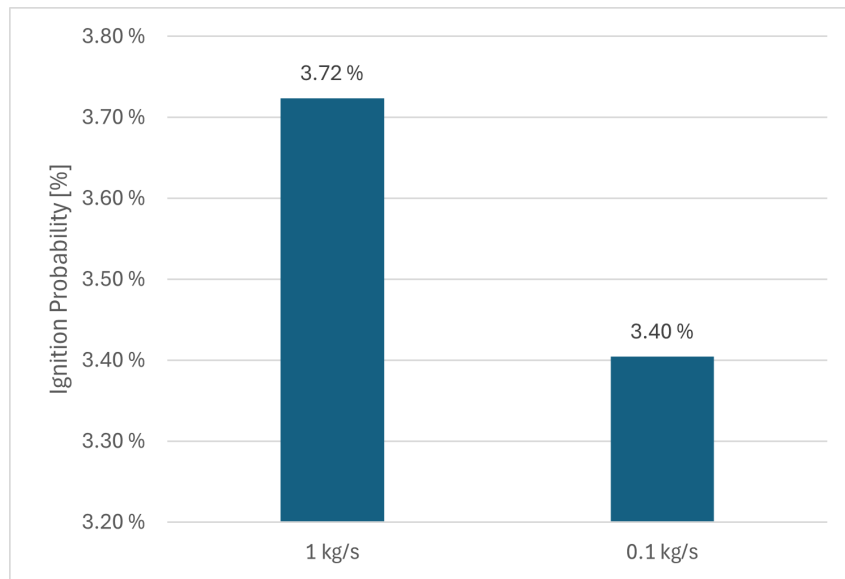


Figure 6.13: Average total ignition probability for the 1 kg/s leak and 0.1 kg/s for the container scenario.

Table 6.1 and 6.2 presents the ignition probability for the corner and middle leak on 1 kg/s. Where the continuous and discrete ignition probability is presented for the four ignitors.

Table 6.1: Total probability for the ignitors placed in the area of the container for the 0.1 kg/s leak.

		Total Probability	Continuous	Discrete
Middle 0.1 kg/s leak	Other generic	4.02E-05	2.49E-05	1.08E-05
	Electrical equipment	2.83E-05	2.70E-05	1.33E-06
	Rotating equipment	3.82E-04	3.18E-04	1.33E-06
	Electrostatic discharges	1.05E-03	6.92E-04	3.53E-04
Corner 0.1 kg/s leak	Other generic	2.31E-05	1.87E-05	4.41E-05
	Electrical equipment	1.79E-05	1.73E-05	5.40E-07
	Rotating equipment	2.40E-04	2.40E-04	5.40E-07
	Electrostatic discharges	5.80E-04	4.36E-04	1.44E-04

Table 6.2: Total probability for the ignitors placed in the area of the container for the 1 kg/s leak.

		Total Probability	Continuous	Discrete
Middle 1 kg/s leak	Other generic	3.38E-05	2.68E-05	7.00E-06
	Electrical equipment	2.39E-05	2.31E-05	8.56E-07
	Rotating equipment	4.66E-04	4.65E-04	8.56E-07
	Electrostatic discharges	1.07E-03	8.45E-04	2.28E-04
Corner 1 kg/s leak	Other generic	3.52E-05	2.88E-05	6.47E-06
	Electrical equipment	2.56E-05	2.48E-05	7.91E-07
	Rotating equipment	5.00E-04	4.99E-04	7.91E-07
	Electrostatic discharges	1.12E-03	9.08E-04	2.11E-04

### 6.1.4 Ignition Probability Contributors

Figure 6.14 shows a logarithmic representation of the contributors to the ignition probability.

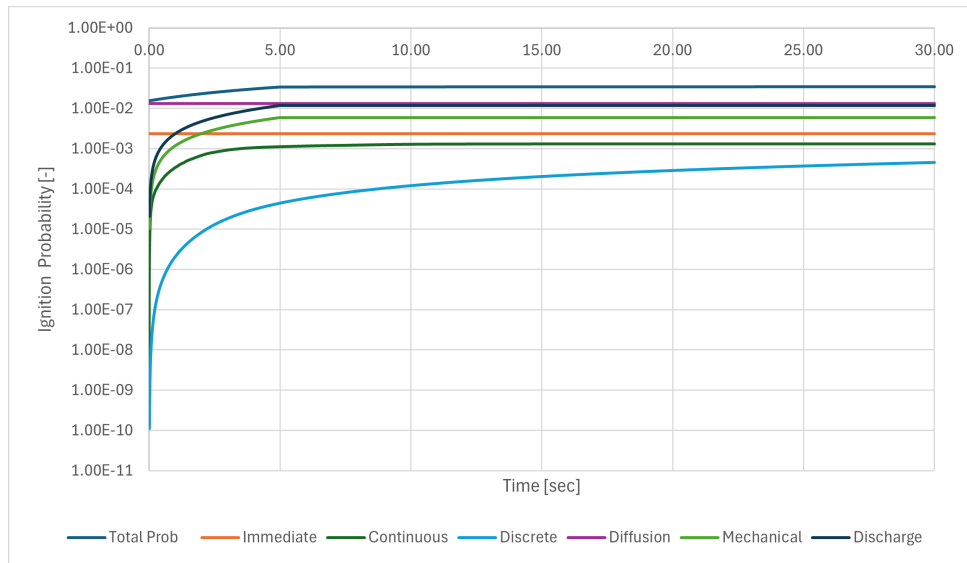


Figure 6.14: Logarithmic representation of the contributors that contribute to the total ignition probability for the container scenario.

Figure 6.15 shows what contributes to the ignition probability at the start of the leak, where all the leaks are presented. Figure 6.16 presents the contributors to the ignition probability at the end of the leak.

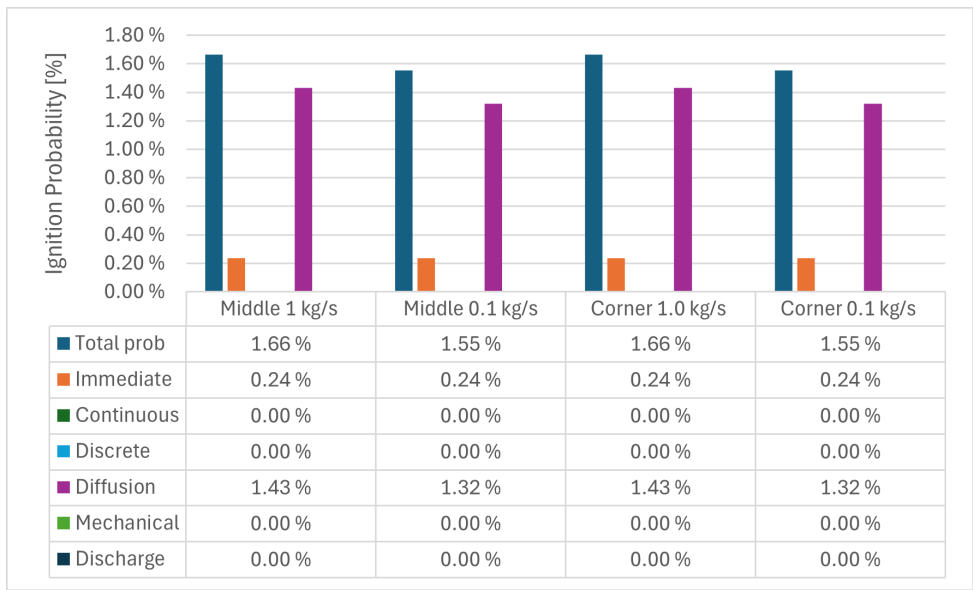


Figure 6.15: Contributors to the total ignition at the start of the leak for the container scenario.

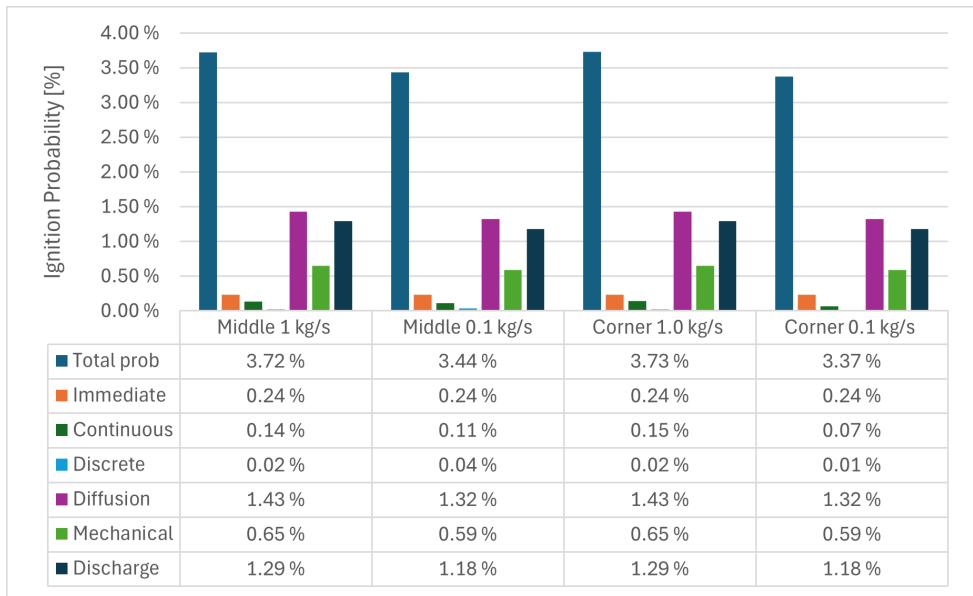


Figure 6.16: Contributors to the total ignition after the leak has exceeded in 30 sec for the container scenario.

Figure 6.17 and 6.18 presents the relationship between ignition probability and combustible volume. These plots allow for a clearer analysis of how the volume of the gas cloud influences ignition probability.

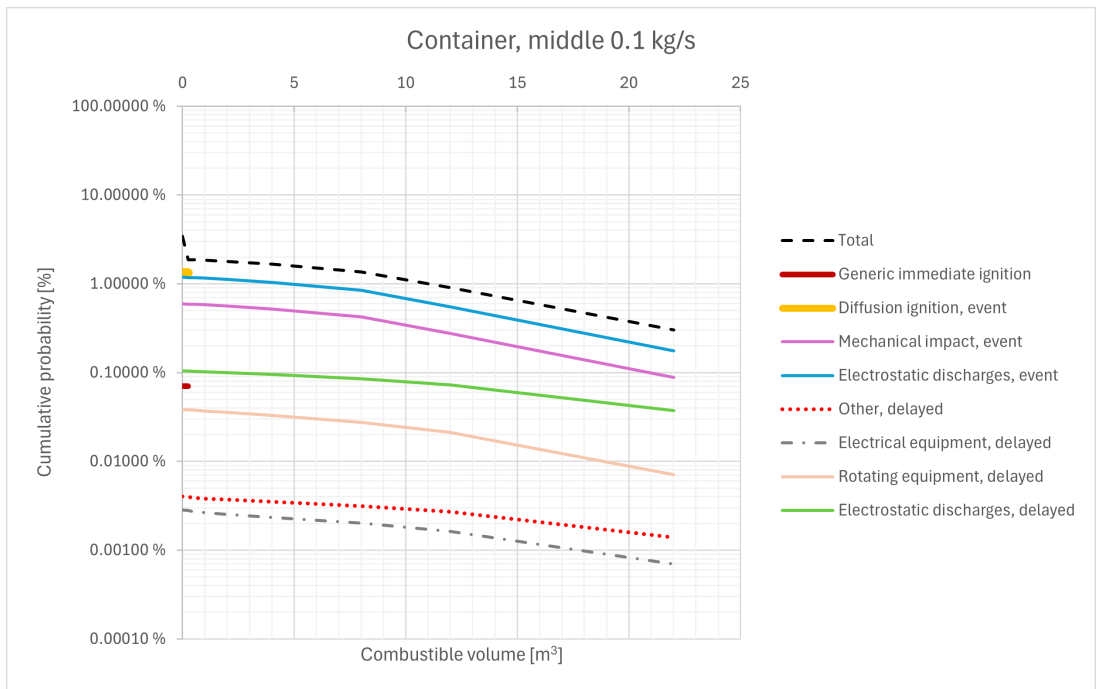


Figure 6.17: Contributors to the total ignition where the ignition probability is plotted against the cloud volume, for the middle leak with 0.1 kg/s leak rate.

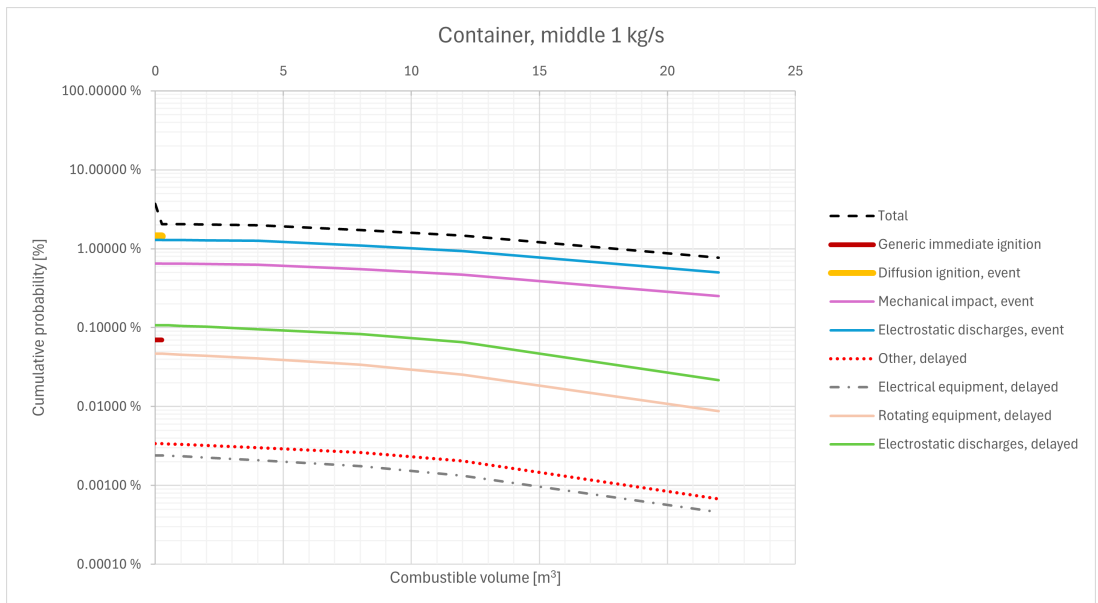


Figure 6.18: Contributors to the total ignition where the ignition probability is plotted against the cloud volume, for the middle leak with 1 kg/s leak rate.

### 6.1.5 Sensitivity

To check the grid sensitivity for the simulations for the container geometry all simulations were carried out with 100,000, 300,000, and 500,000 grid cells.

Figure 6.19 and 6.20 presents the grid sensitivity for the 0.1 kg/s and 1 kg/s hydrogen leak with their contributors.

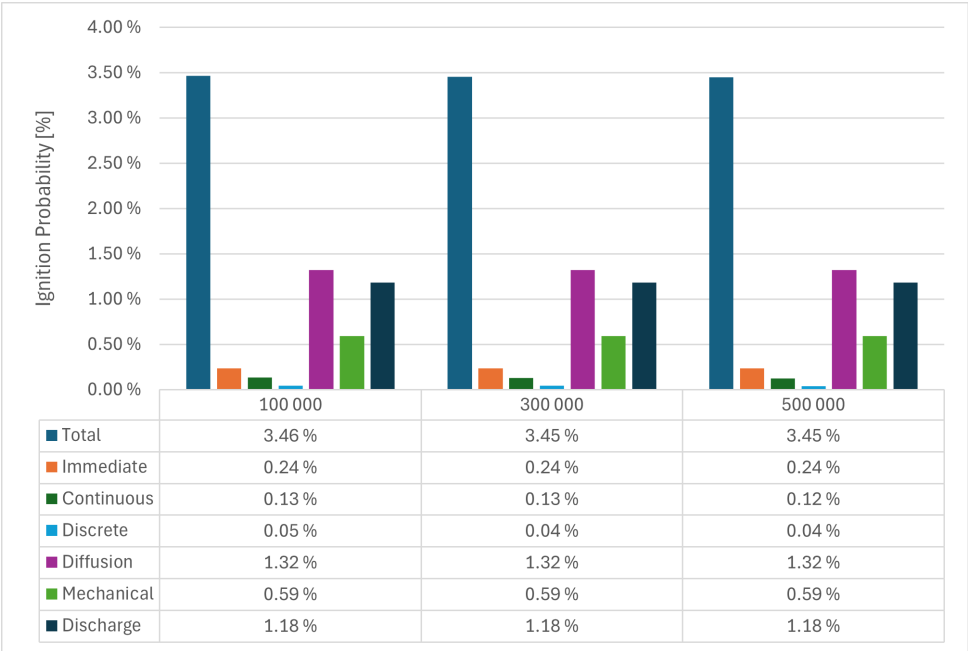


Figure 6.19: Grid sensitivity for the 0.1 kg/s leak with the different contributors

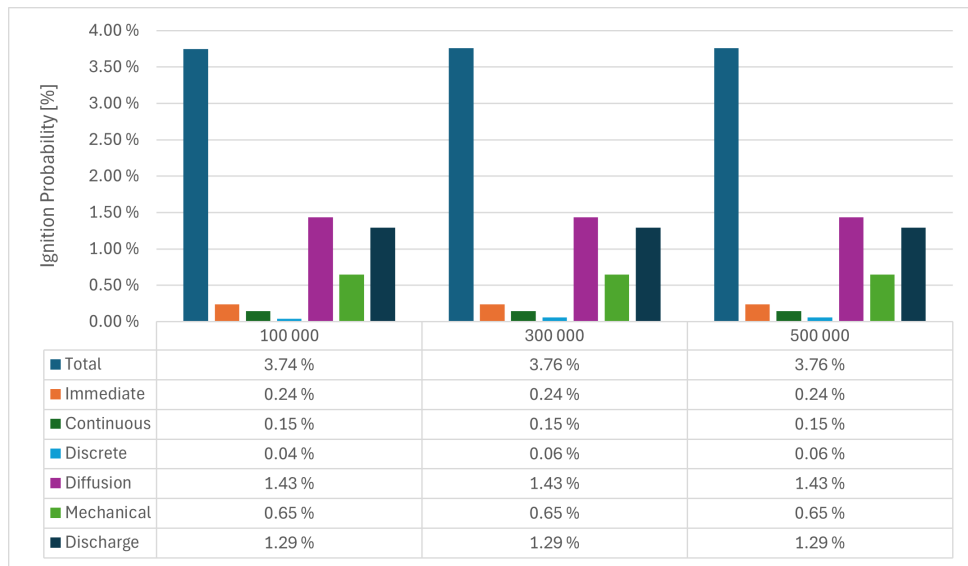


Figure 6.20: Grid sensitivity for the 1 kg/s leak with the different contributors

Figure 6.21 shows the flammable cloud volume for the 0.1 and 1 kg/s leak.

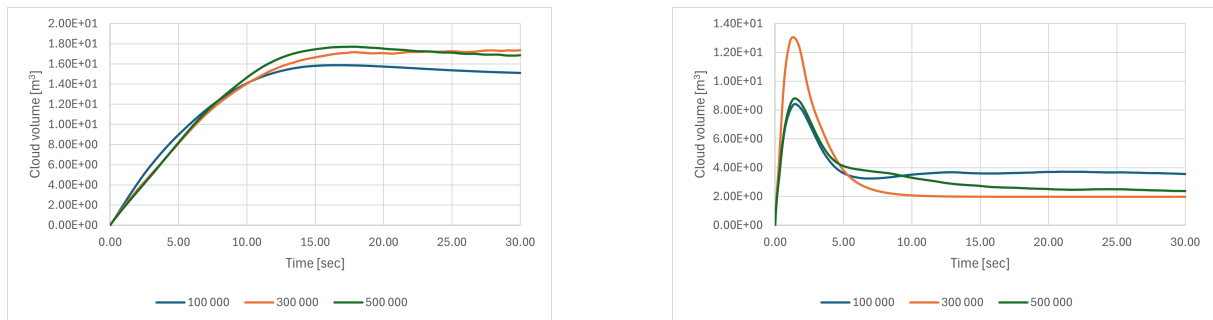


Figure 6.21: Flammable cloud volume for the 0.1 kg/s (left) and 1 kg/s (right) leaks

Figure 6.22 shows the cloud volume where the maximum speed and maximum expansion are considered for the 0.1 kg/s leak and the 1 kg/s leak.



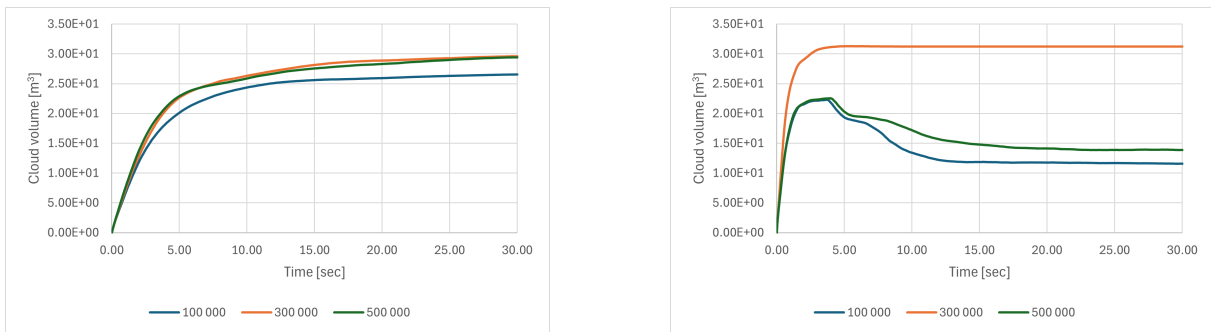


Figure 6.22: Flammable cloud volume between lower- and upper flammability limit for the 0.1 kg/s (left) and 1 kg/s (right) leaks

## 6.2 Methane

### 6.2.1 Methane

The gas cloud dispersion for a 1 kg/s methane leak downward release is shown in 6.23. The surface plot is done at 4% volumetric concentration.

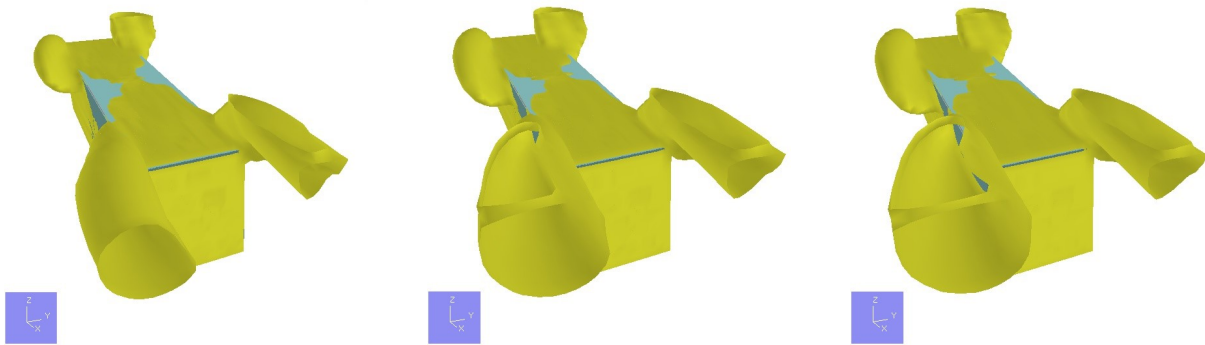


Figure 6.23: Surface plots of 4% methane concentration for 1 kg/s downward release at different time points: 10 seconds, 20 seconds, and 30 seconds where the leak locations are in the middle of the container geometry.

Figure 6.24 shows the volumetric cloud for the methane leak compared to hydrogen. While 6.25 shows the flammable cloud volume for both leak rates of methane and hydrogen. The figure to the right shows the ignition probability for different time steps. For the hydrogen ignition probability, it straightens out after about five seconds, this is mentioned in Chapter 2.8, and is just applied to hydrogen, not methane in the SAFEN model.

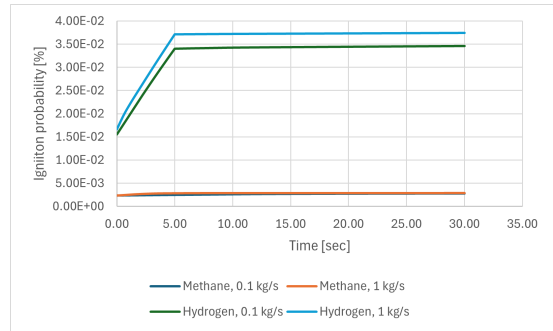
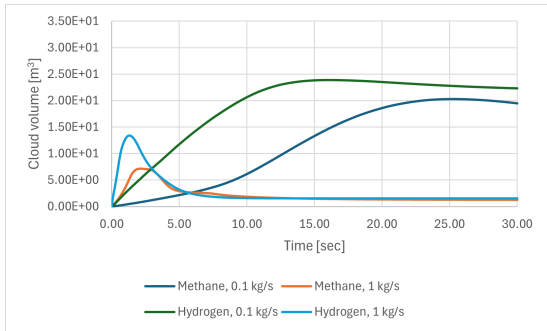


Figure 6.24: Stoichiometric equivalent cloud volume for both hydrogen and methane, compared to the ignition probability

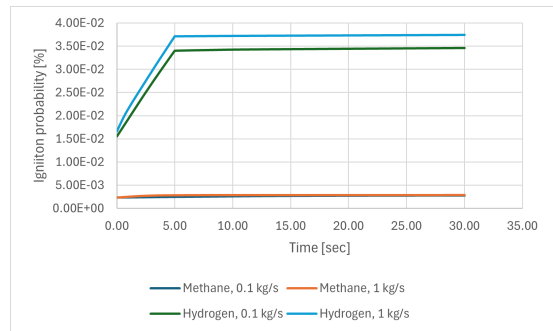
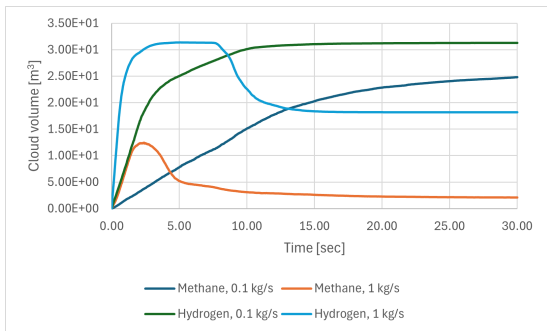


Figure 6.25: Flammable cloud volume between lower- and upper flammability limit for both methane and hydrogen compared to the ignition probability

Figure 6.26 presents the total ignition probability for methane compared to hydrogen as a histogram.

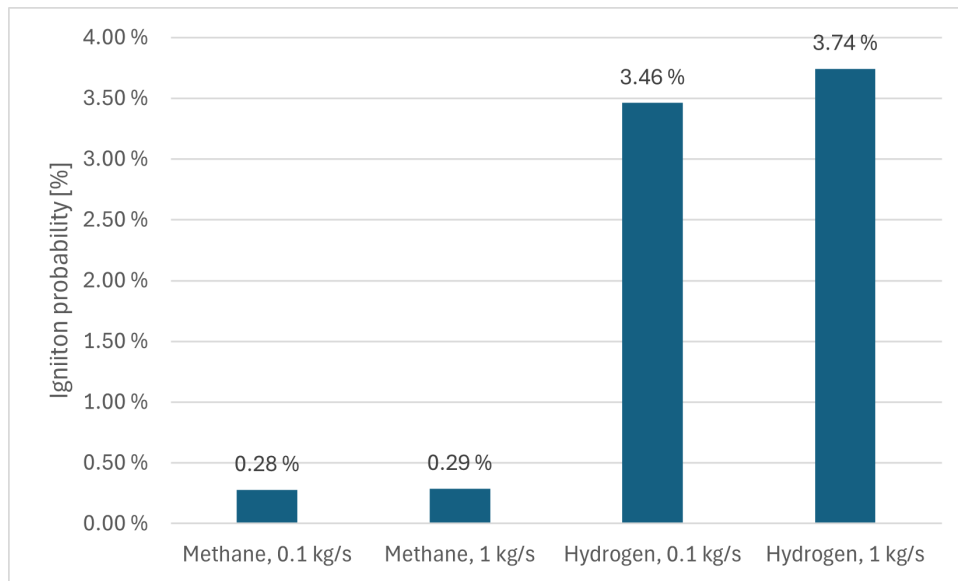


Figure 6.26: Average ignition probability at t=30 for methane and hydrogen



# 7 Result from Hydrogen Refueling Station

## 7.1 Hydrogen

### 7.1.1 Gas dispersion

The amount of gas in the domain and the transient leak of a cracked vessel can be seen in Figure 7.1 and 7.4 where the red line is the hydrogen entering the vessel, the green line is the hydrogen leaving the vessel, while the blue line is the accumulation. The pink line shows the total number of kilograms of gas in the calculation area and is read off on the right-hand y-axis.

Figure 7.2 and 7.5 show the 4% volumetric concentration cloud surface.

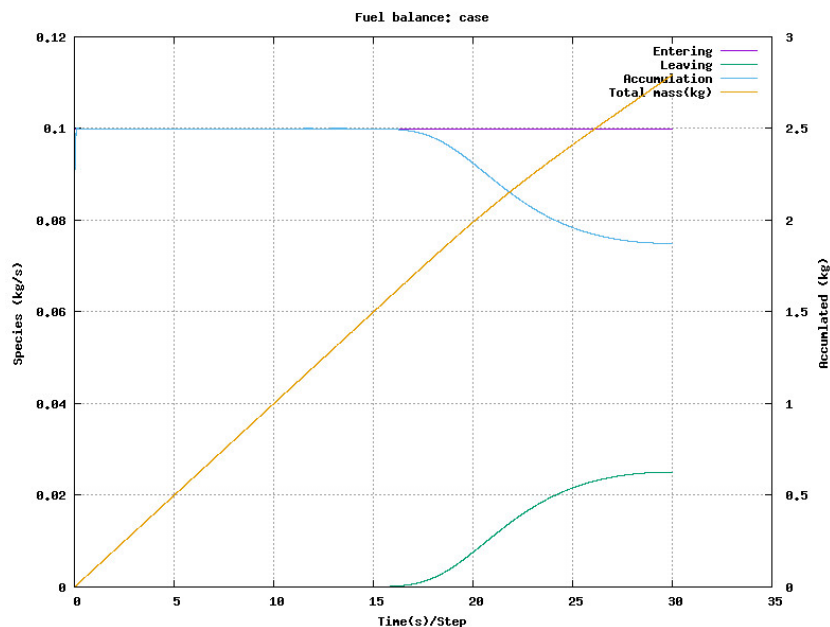


Figure 7.1: Release profile of 0.1 kg/s downward release where the location of the leak is in the middle of the refueling station geometry.

Figure 7.2 and 7.5 show the 4% volumetric concentration cloud surface for the middle leak, while Figure 7.3 and 7.6 shows the 0.1 kg/s leak and 1 kg/s leak when the leak is located in the corner of the geometry, at 10, 20 and 30 seconds.

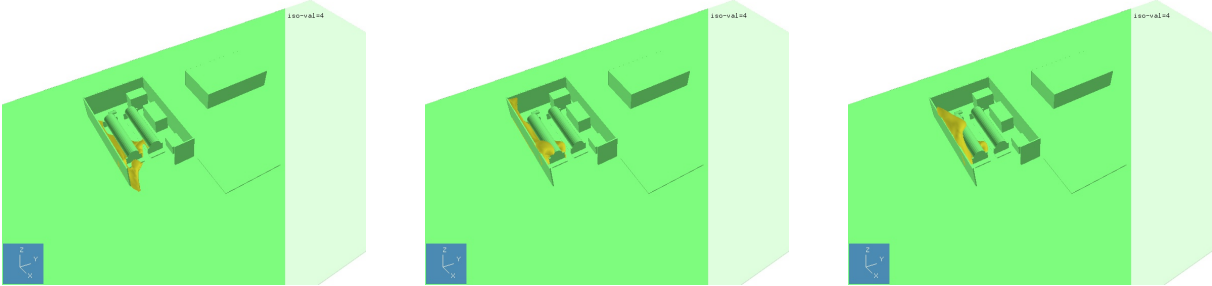


Figure 7.2: Surface plots of 4% H2 concentration for 0.1 kg/s downward release at different time points: 10 seconds, 20 seconds, and 30 seconds where the leak locations are in the middle of the refueling station geometry.

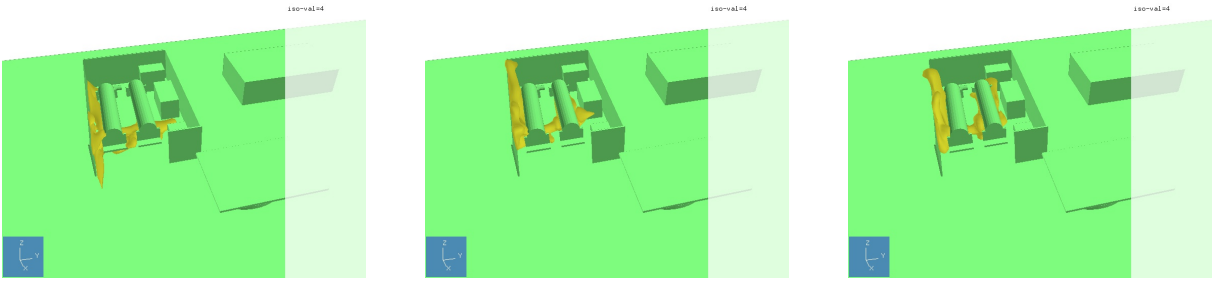


Figure 7.3: Surface plots of 4% H2 concentration for 0.1 kg/s downward release at different time points: 10 seconds, 20 seconds, and 30 seconds where the leak locations is in the corner of the refueling station geometry.

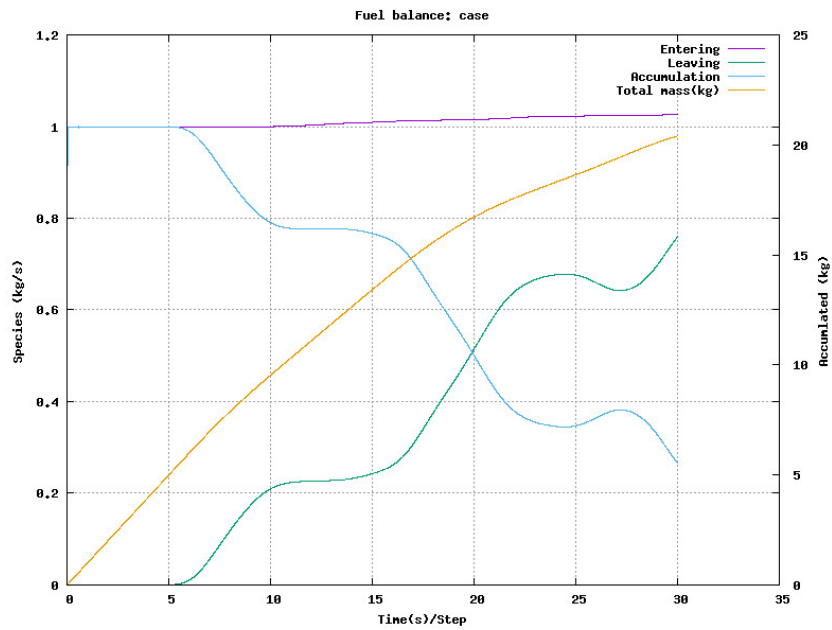


Figure 7.4: Release profile of 1 kg/s downward release where the location of the leak is in the middle of the refueling station geometry.

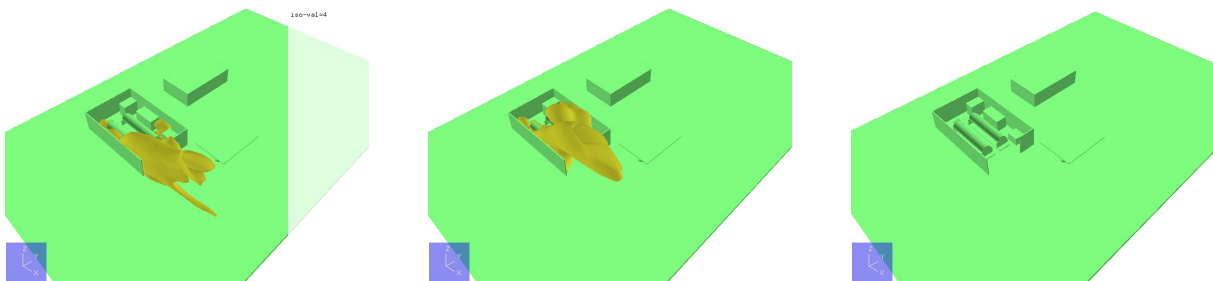


Figure 7.5: Surface plots of 4% H<sub>2</sub> concentration for 0.1 kg/s downward release at different time points: 10 seconds, 20 seconds, and 30 seconds where the leak locations is in the middle of the refueling station geometry.

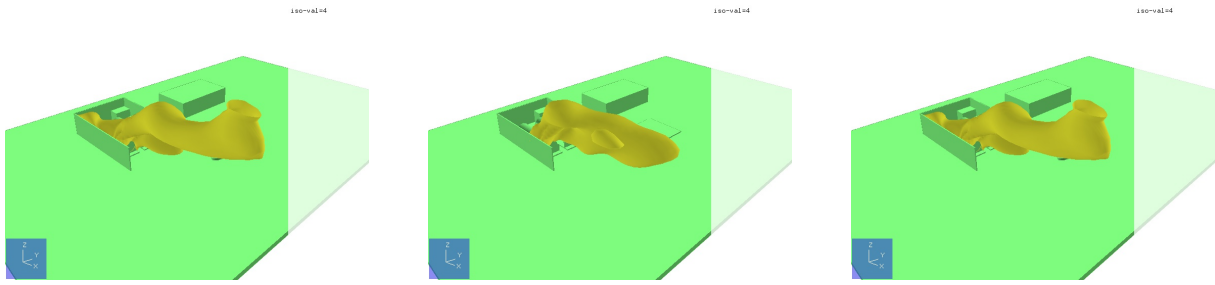


Figure 7.6: Surface plots of 4% H<sub>2</sub> concentration for 1 kg/s downward release at different time points: 10 seconds, 20 seconds, and 30 seconds where the leak locations is in the corner of the refueling station geometry.

Figure 7.7 presents the release cloud for different directions, all for 0.1 kg/s releases.

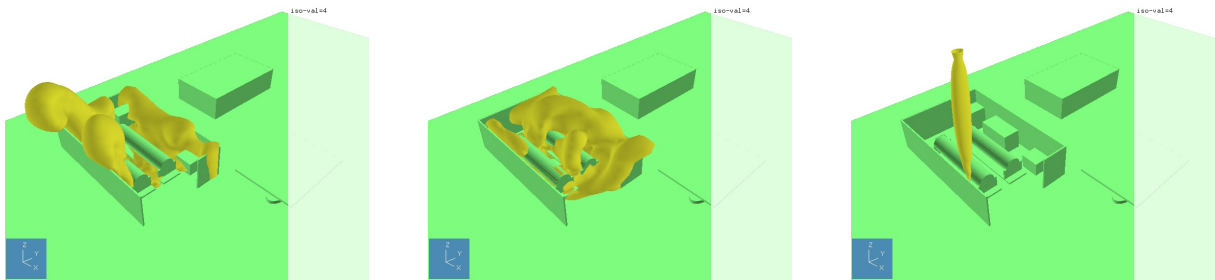


Figure 7.7: Surface plot of 4% H<sub>2</sub> concentration for 0.1 kg/s releases at 10 seconds in x, y and z direction.

### 7.1.2 Flammable cloud

Figure 7.8 and 7.9 present the cloud volume between the upper and lower explosion limit for the 0.1kg/s leak and 1kg/s leak for all six directions.

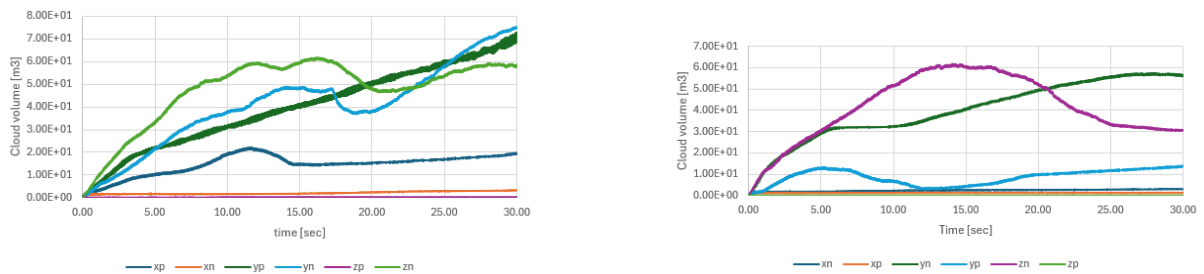


Figure 7.8: Flammable cloud volume for corner (left) and middle (right) leak in all directions with leak rate 0.1kg/s for the refueling station geometry.



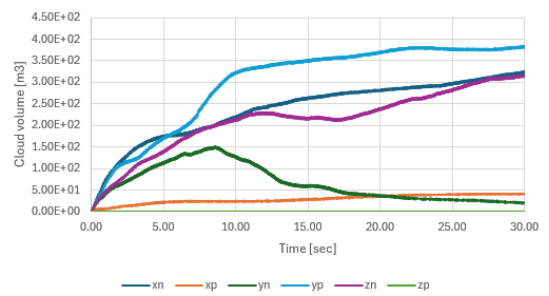
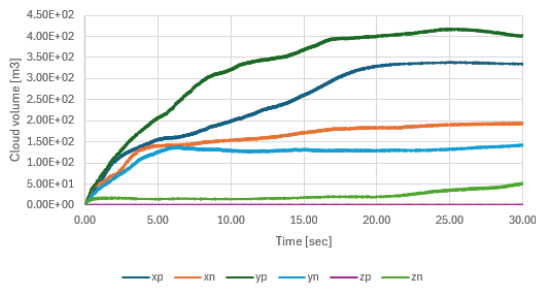


Figure 7.9: Flammable cloud volume for corner (left) and middle (right) leak in all directions with leak rate 1kg/s for the refueling station geometry.

Figure 7.10 and 7.11 presents the stoichiometric equivalent cloud volume for the 0.1 kg/s leak rate, and the 1 kg/s leak rate.

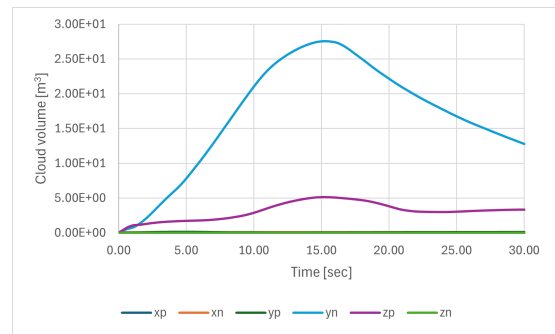
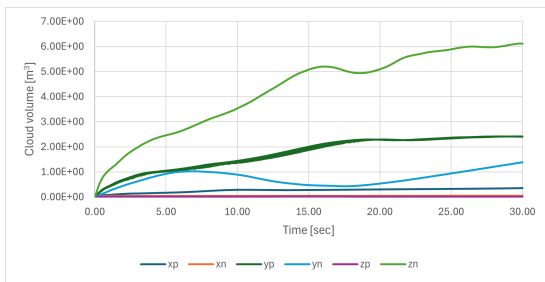


Figure 7.10: Stoichiometric equivalent cloud volume for corner (left) and middle (right) leak in all directions with leak rate 0.1 kg/s for the refueling station geometry.

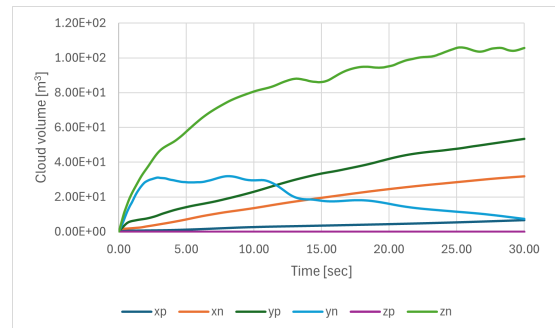
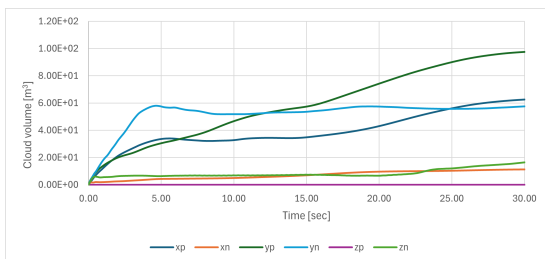


Figure 7.11: Stoichiometric equivalent cloud volume for corner (left) and middle (right) leak in all directions with leak rate 1 kg/s for refueling station geometry.

### 7.1.3 Ignition Probability

Figure 7.12 and 7.13 present the ignition probabilities for the 0.1 kg/s leak for both the middle and corner locations, and the 1.0 kg/s leak with both locations. Table 7.1 presents the total probability for the igniters in the area in interest for the 0.1 kg/s leak.

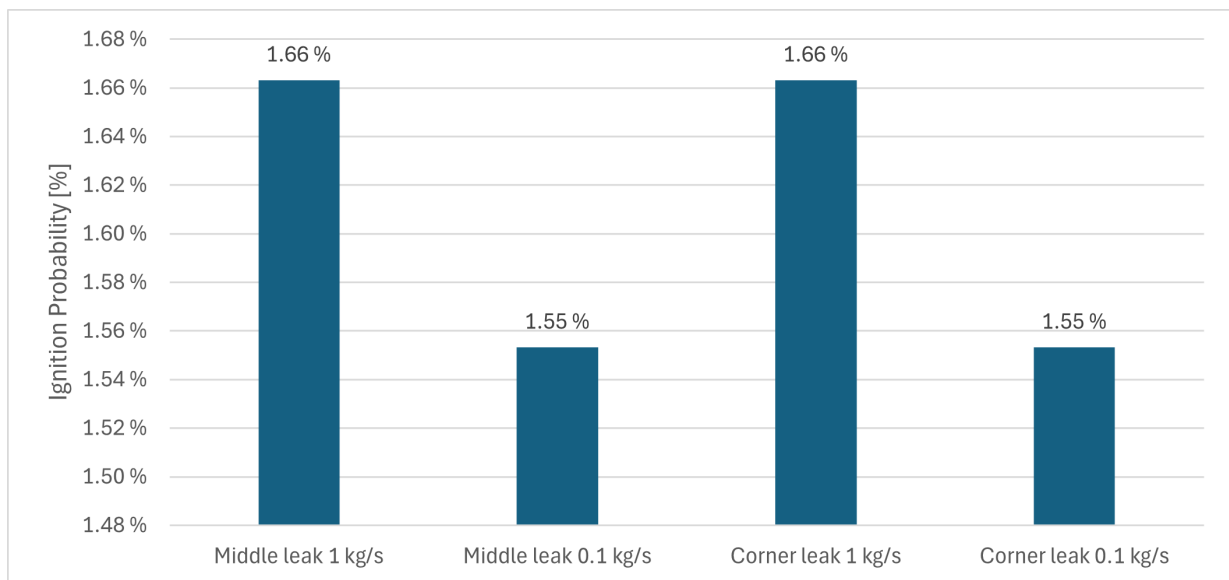


Figure 7.12: Average ignition probability for all leaks with their leak rate at the start of the leak ( $t=0$ ) for the refueling station geometry.

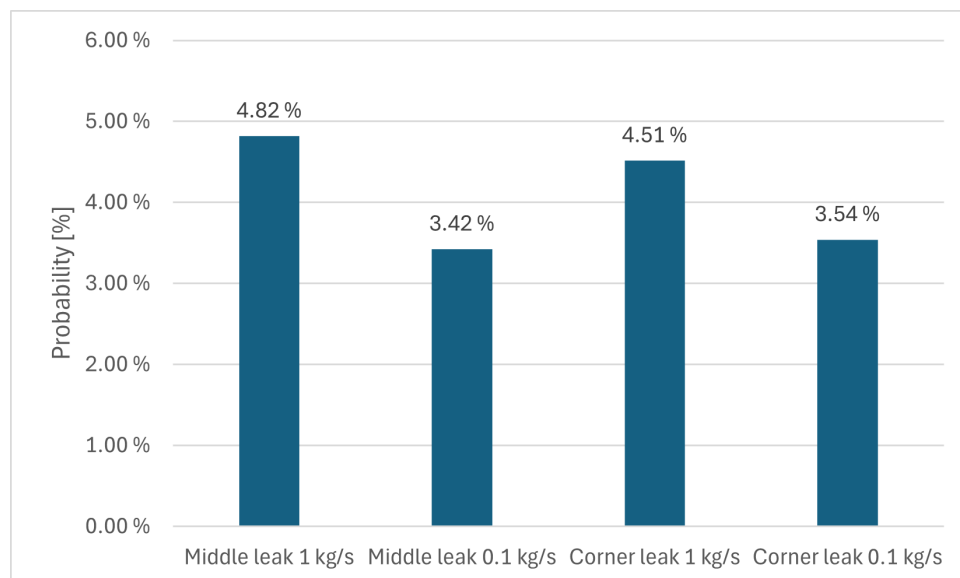


Figure 7.13: Average ignition probability for all leaks with their leak rate at the end of the leak for the refueling station geometry.

Figure 7.14 presents the average ignition probabilities for the two leak rates.

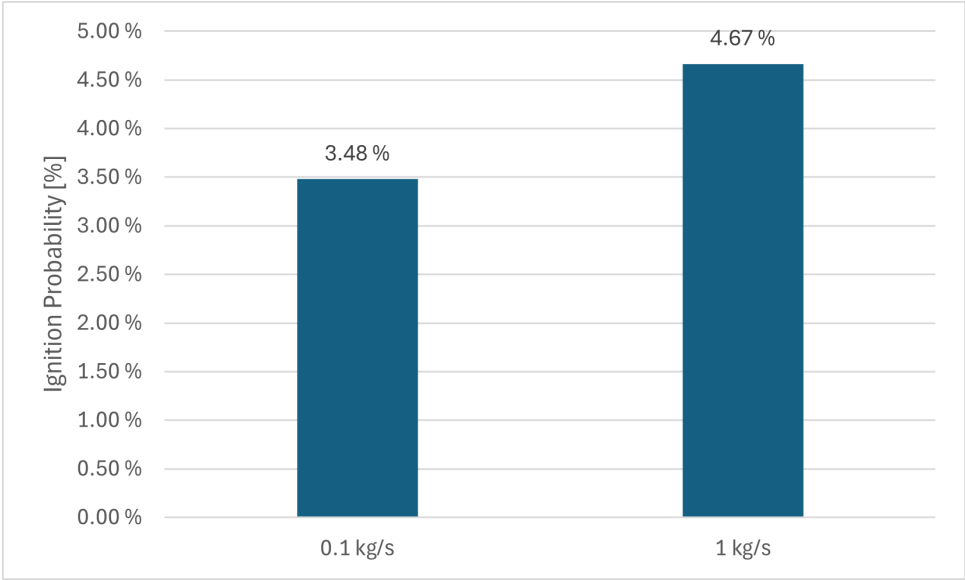


Figure 7.14: Average total ignition probability for the two leak rates for the refueling station geometry.

Table 7.1 and 7.2 presents the ignition probability for the corner and middle leak on 1 kg/s. Where the continuous and discrete ignition probability is presented for the four ignitors.

Table 7.1: Total probability for the ignitors placed in the area of the fueling station for the 0.1 kg/s leak.

		Total Probability	Continuous	Discrete
Middle 0.1 kg/s leak	Other generic	3.07E-05	2.49E-05	5.76E-06
	Electrical equipment	2.27E-05	2.20E-05	7.04E-07
	Rotating equipment	3.98E-04	3.97E-04	7.04E-07
	Electrostatic discharges	9.09E-04	7.22E-04	1.88E-04
Corner 0.1 kg/s leak	Other generic	2.13E-04	1.55E-04	5.85E-05
	Electrical equipment	1.40E-04	1.33E-04	7.15E-06
	Rotating equipment	2.71E-03	2.71E-03	7.15E-06
	Electrostatic discharges	6.81E-03	4.91E-03	1.90E-03

Table 7.2: Total probability for the ignitors placed in the area of the fueling station for the 1 kg/s leak.

		Total Probability	Continuous	Discrete
Middle 1 kg/s leak	Other generic	2.16E-04	1.64E-04	5.18E-05
	Electrical equipment	1.48E-04	1.41E-04	6.34E-06
	Rotating equipment	2.88E-03	2.87E-03	6.34E-06
	Electrostatic discharges	6.90E-03	5.21E-03	1.69E-03
Corner 1 kg/s leak	Other generic	2.13E-04	1.55E-04	5.85E-05
	Electrical equipment	1.40E-04	1.33E-04	7.15E-06
	Rotating equipment	2.71E-03	2.71E-03	7.15E-06
	Electrostatic discharges	6.81E-03	4.91E-03	1.90E-03

### 7.1.4 Ignition Probability Contributors

Figure 7.15 shows a logarithmic representation of the contributors to the ignition probability

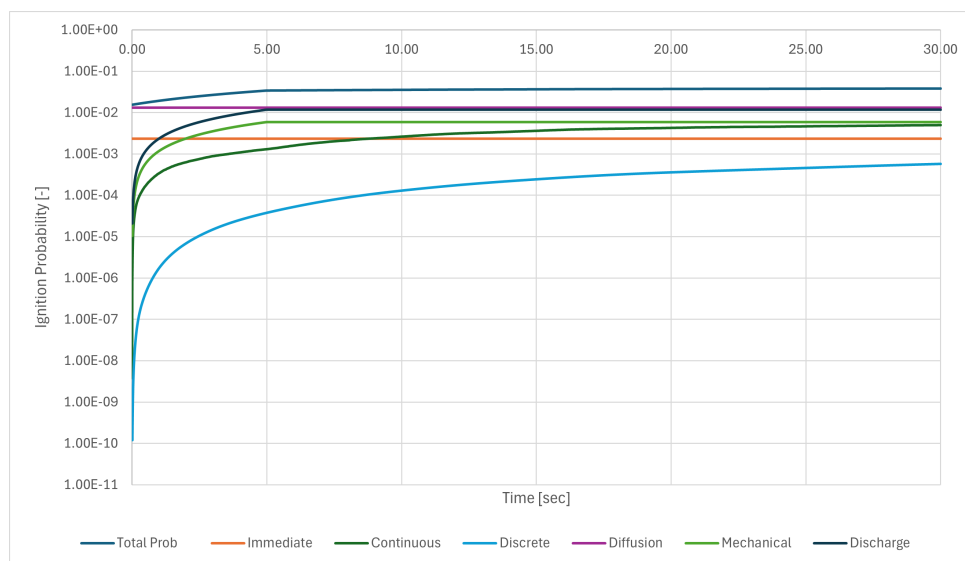


Figure 7.15: Logarithmic representation of the contributors that contribute to the total ignition probability for the refueling station geometry.

Figure 7.16 shows what contributes to the ignition probability at the start of the leak, where all the leaks are presented. Figure 7.17 presents the contributors to the ignition probability at the end of the leak.

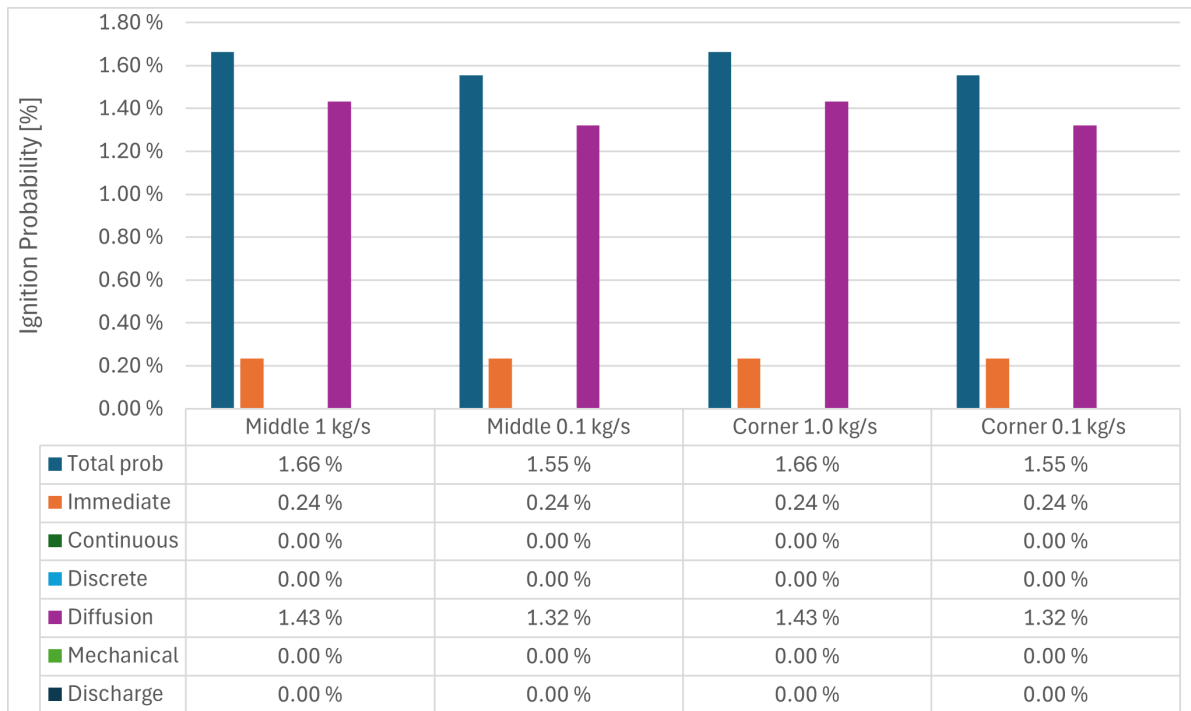


Figure 7.16: Contributors to the simulation at the start of the leak ( $t=0$ ) for the refueling station geometry.

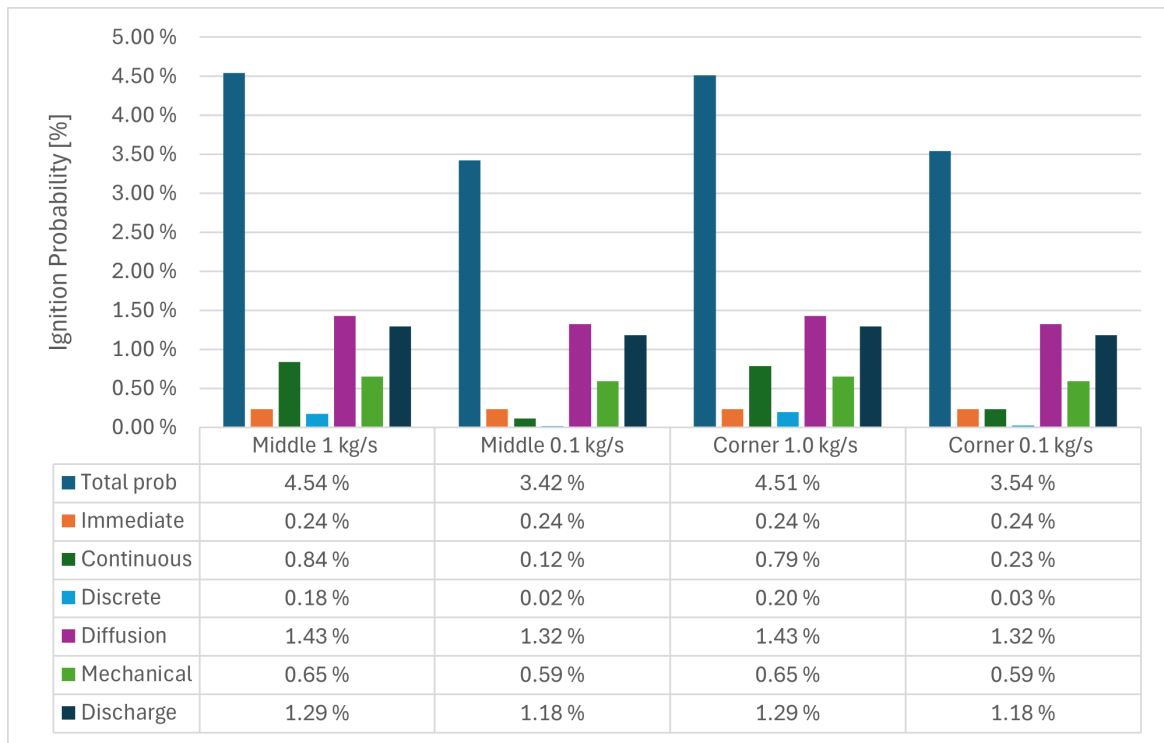


Figure 7.17: Contributors to the simulation at the end of the leak ( $t=30$ ) for the refueling station geometry.

## 7.1.5 Grid Sensitivity

For the grid sensitivity, all the cases were simulated with 100,000, 300,000, and 500,000 grid cells.

Figure 7.18 and 7.19 presents the grid sensitivity for the 0.1 kg/s and 1 kg/s hydrogen leak with their contributors.

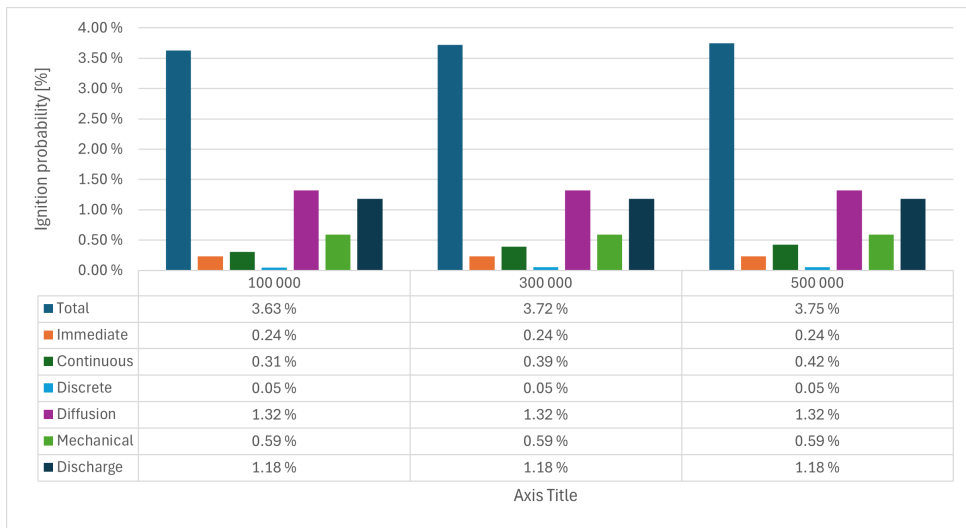


Figure 7.18: Grid sensitivity for the 0.1 kg/s leak with the different contributors.

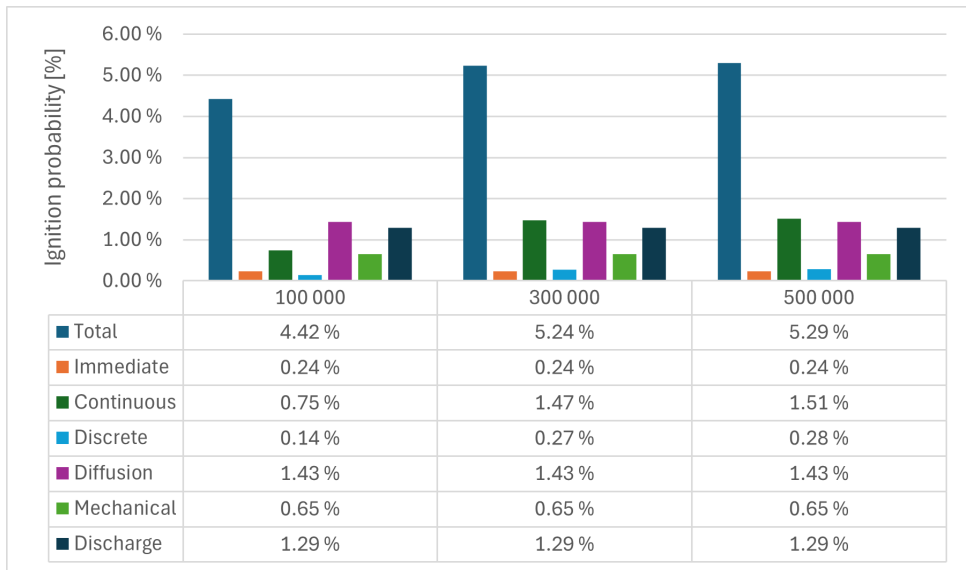


Figure 7.19: Grid sensitivity for the 1 kg/s leak with the different contributors.

Figure 7.20 shows the expansion-based weighted volume cloud for the 0.1 and 1 kg/s leak

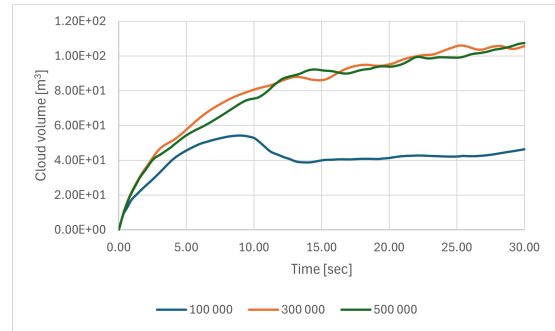
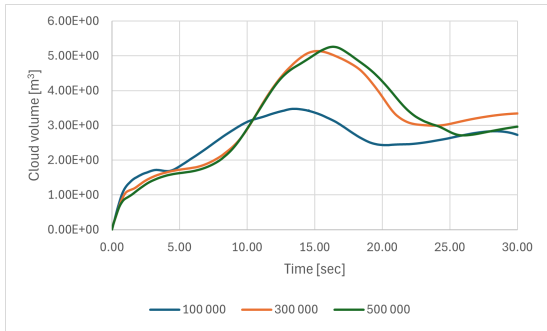


Figure 7.20: Stoichiometric equivalent cloud volume for the 0.1 kg/s (left) and 1 kg/s (right) leaks.

Figure 7.21 shows the cloud volume where the maximum speed and maximum expansion are considered for the 0.1 kg/s leak and the 1 kg/s leak.

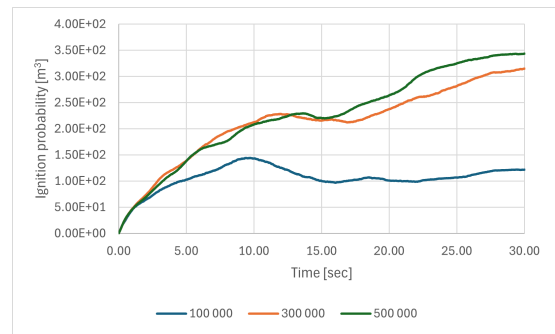
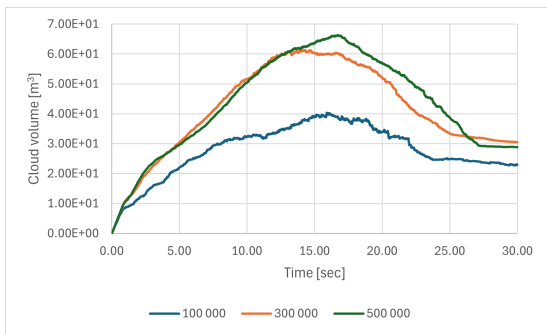


Figure 7.21: lammable cloud volume cloud for the 0.1 kg/s (left) and 1 kg/s (right) leaks.

## 7.2 Methane

### 7.2.1 Methane

The gas cloud dispersion for a 1.0 kg/s leak of CH<sub>4</sub> for a negative z-directions is presented in Figure 7.22



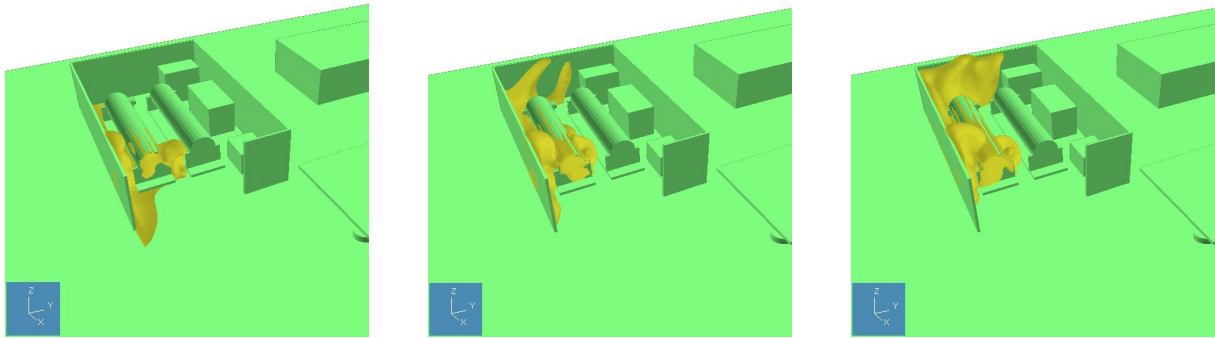


Figure 7.22: Surface plots of 4% CH<sub>4</sub> concentration for 1 kg/s downward release at different time points: 10 seconds, 20 seconds, and 30 seconds where the leak locations are in the middle of the geometry.

Figure 7.23 shows the stoichiometric equivalent cloud volume for the CH<sub>4</sub> leak with the 0.1 kg/s leak to the left and the 1.0 kg/s leak to the right. While 7.24 shows the gas cloud for the 0.1 and 1 kg/s methane leak.

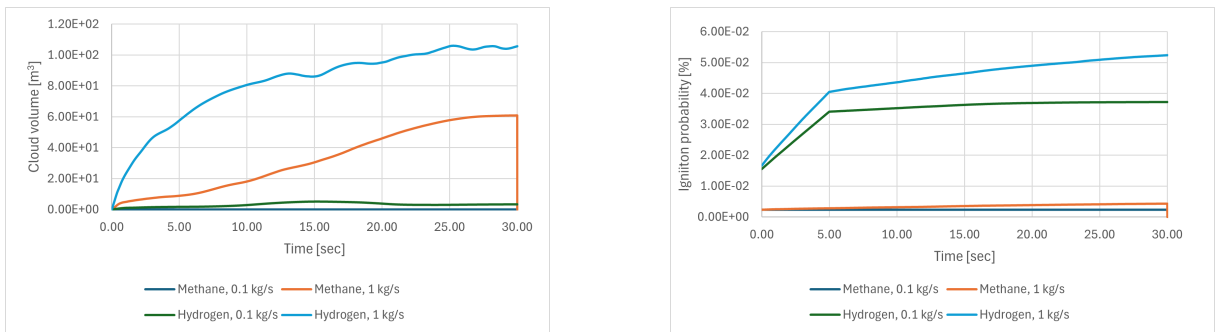


Figure 7.23: Stoichiometric equivalent cloud volume compared to the ignition probability for the hydrogen and methane comparison. The leak is done for the middle leak, in the negative z-direction for the refueling station geometry.

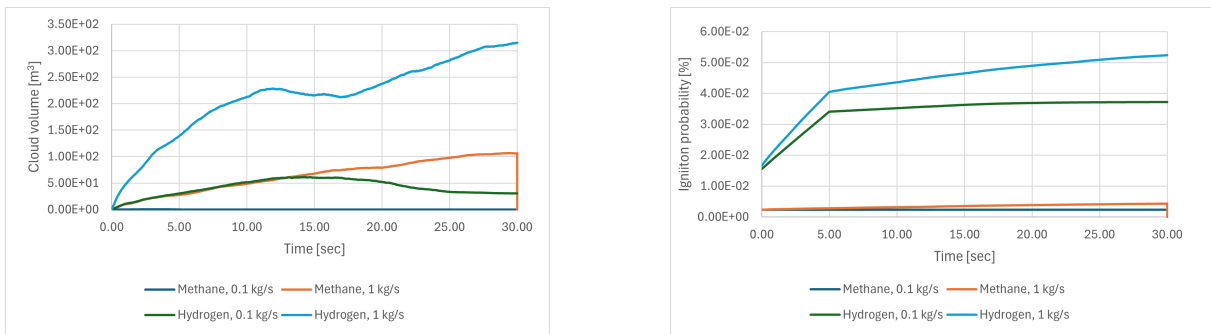


Figure 7.24: Flammable cloud volume for the middle leak, zn-direction, compared to the ignition probability for the hydrogen and methane comparison for the refueling station geometry.

The histogram in Figure 7.25 presents the ignition probabilities for the middle case with a leak rate in the negative z-direction, for both the 0.1 kg/s and 1 kg/s leak rates for methane and hydrogen.

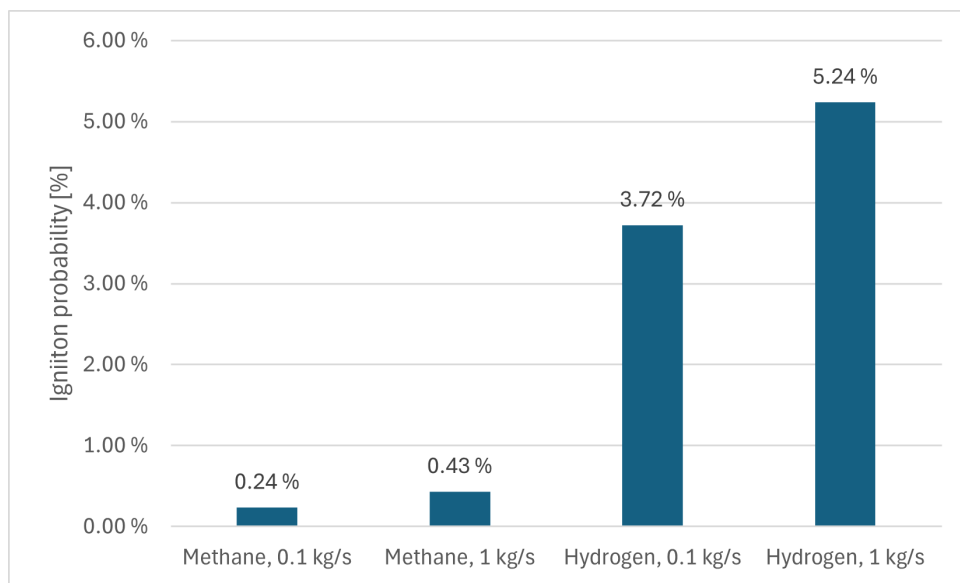


Figure 7.25: Histogram presenting the ignition probability for the methane leak, compared to the hydrogen leak for the refueling station geometry.

# 8 Process Plant

## 8.1 Hydrogen

### 8.1.1 Gas dispersion

Figure 8.1 and 8.4 shows the amount of gas in the area of interest. If the area of interest were different, the release profile would look different.

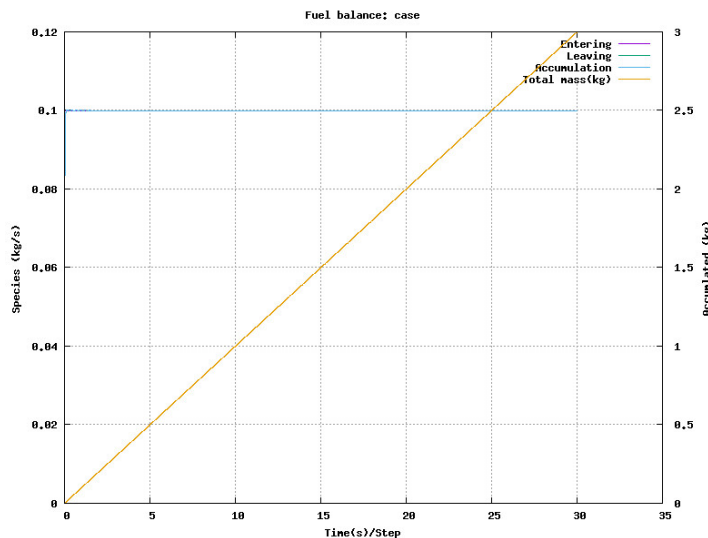


Figure 8.1: Release profile of 0.1 kg/s downward release where the location is in the middle of the geometry

Figure 8.2 presents the surface plot with 4 vol % resulting from a leak in the corner of the geometry with a leak rate of 0.1 kg/s in a downward release. Figure 8.3 illustrates the surface plot for a leak rate of 0.1 kg/s under the same conditions where the leak is located in the middle.

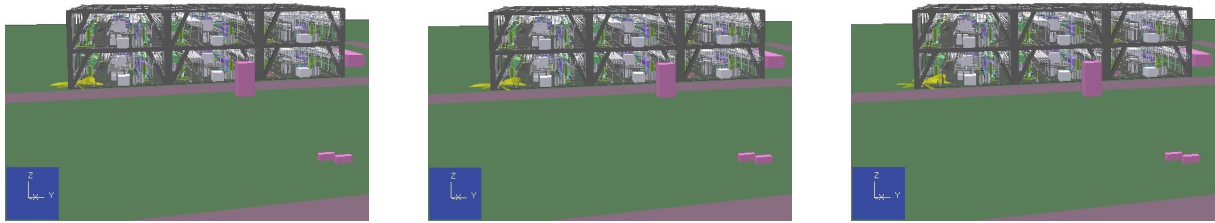


Figure 8.2: Surface plots of 4% H<sub>2</sub> concentration for 0.1 kg/s downward release at different time points: 10 seconds, 20 seconds, and 30 seconds where the leak locations are in the corner of the process plant geometry.

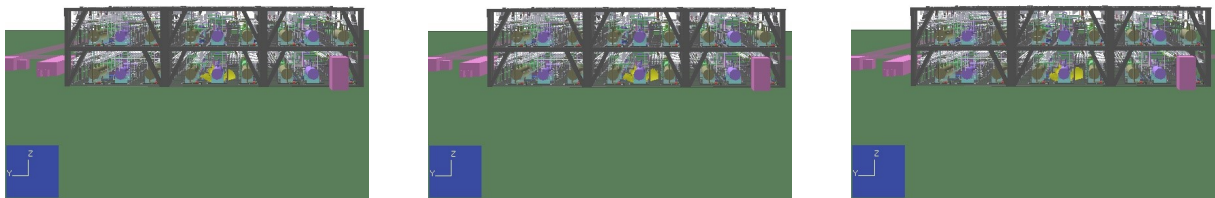


Figure 8.3: Surface plots of 4% H<sub>2</sub> concentration for 0.1 kg/s downward release at different time points: 10 seconds, 20 seconds, and 30 seconds where the leak locations are in the middle of the process plant geometry.

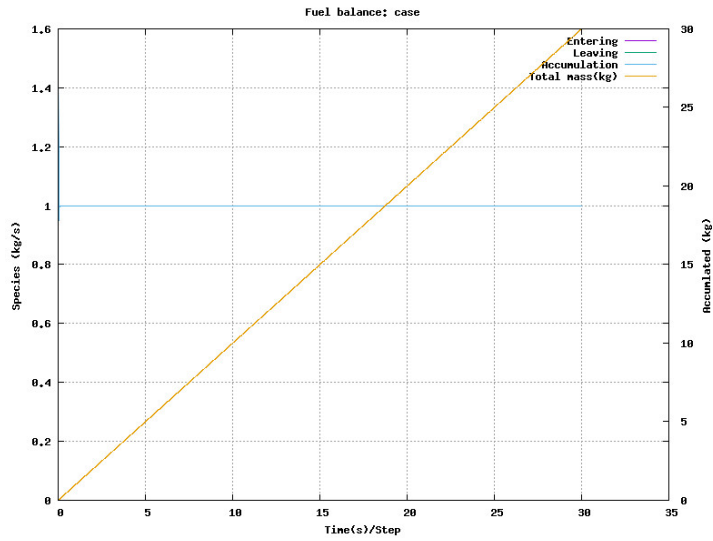


Figure 8.4: Release profile of 1 kg/s downward release where the location is in the middle of the geometry

Figure 8.5 presents the surface plot with 4 % resulting from a leak in the corner of the geometry with a leak rate of 1 kg/s in a downward release. Figure 8.6 illustrates the surface plot for the leak under the same conditions however, the leak is located in the middle of the geometry.

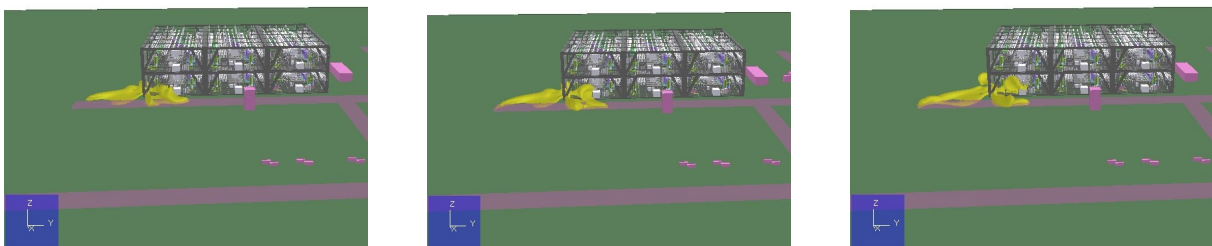


Figure 8.5: Surface plots of 4% H2 concentration for 0.1 kg/s downward release at different time points: 10 seconds, 20 seconds, and 30 seconds where the leak locations are in the corner of the process plant geometry.

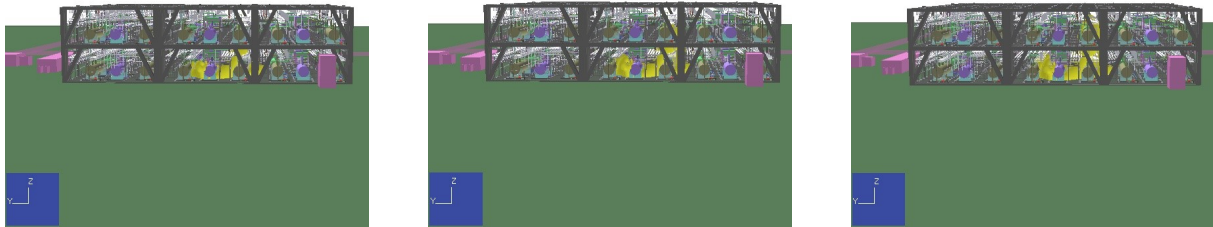


Figure 8.6: Surface plots of 4% H<sub>2</sub> concentration for 0.1 kg/s downward release at different time points: 10 seconds, 20 seconds, and 30 seconds where the leak locations are in the corner of the process plant geometry.

### 8.1.2 Flammable Cloud

Figure 8.7 and 8.8 present the flammable cloud volume between the upper and lower explosion limit for the 0.1kg/s leak and 1kg/s leak for all six directions.

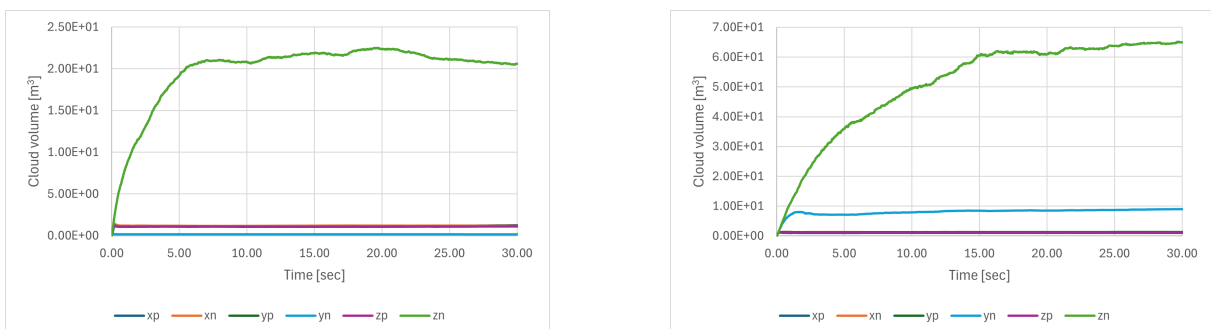


Figure 8.7: Flammable cloud volume for corner (left) and middle (right) leak in all directions with leak rate 0.1kg/s for the process plant geometry.

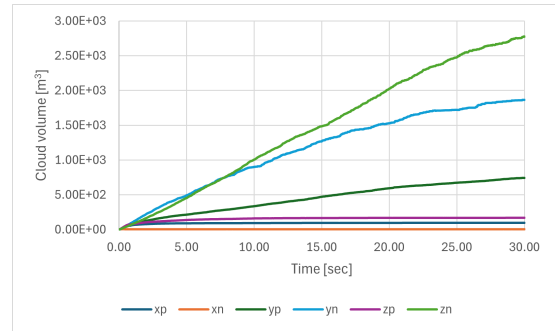
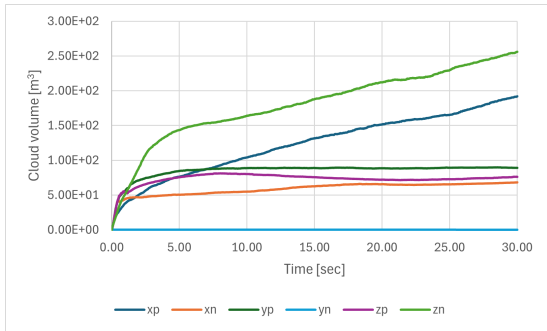


Figure 8.8: Flammable cloud volume cloud for corner (left) and middle (right) leak in all directions with leak rate 1 kg/s for the process plant geometry.

Figure 8.9 and 8.10 presents the stoichiometric equivalent cloud volume for the 0.1 kg/s leak and the 1 kg/s leak in all six directions.

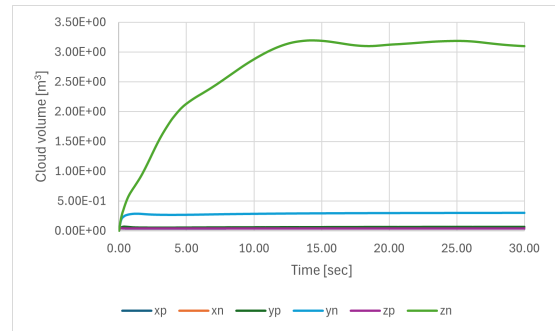
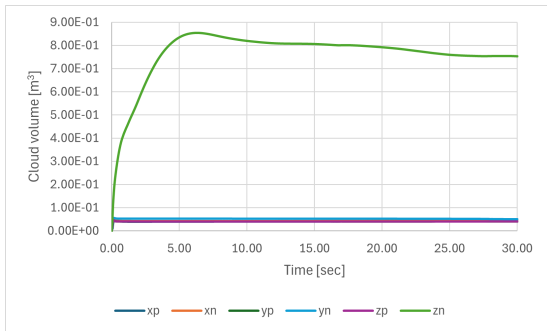


Figure 8.9: Stoichiometric equivalent cloud volume for corner (left) and middle (right) leak in all directions with leak rate 0.1kg/s for the process plant geometry.

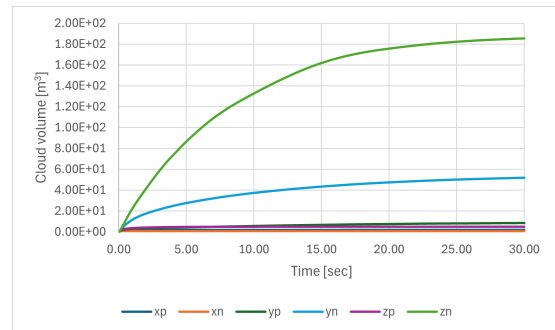
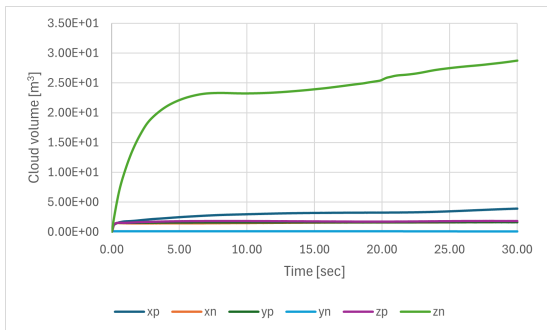


Figure 8.10: Stoichiometric equivalent cloud volume for corner (left) and middle (right) leak in all directions with leak rate 1kg/s for the process plant geometry.

### 8.1.3 Ignition Probability

Figure 8.11 shows the average ignition probability for the 0.1 kg/s leak and the 1.0 kg/s leak Figure 8.12 presents the ignition probabilities for the 0.1 kg/s leak for both the middle and corner locations, and the 1.0 kg/s leak for both locations, while Figure 8.13 present the average ignition probabilities for the two leak rates.

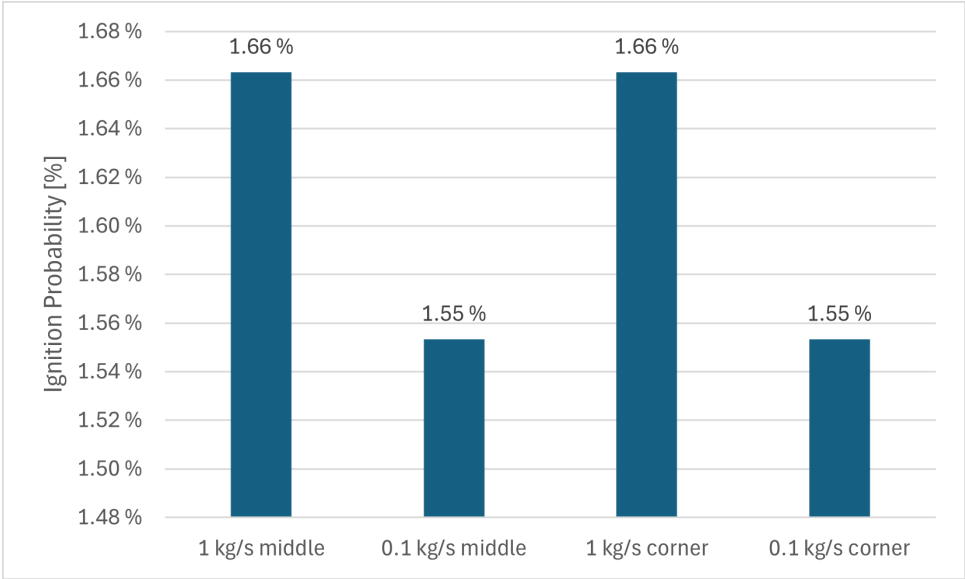


Figure 8.11: Average ignition probability for the 1 kg/s leak and 0.1 kg/s for the start of the leak.

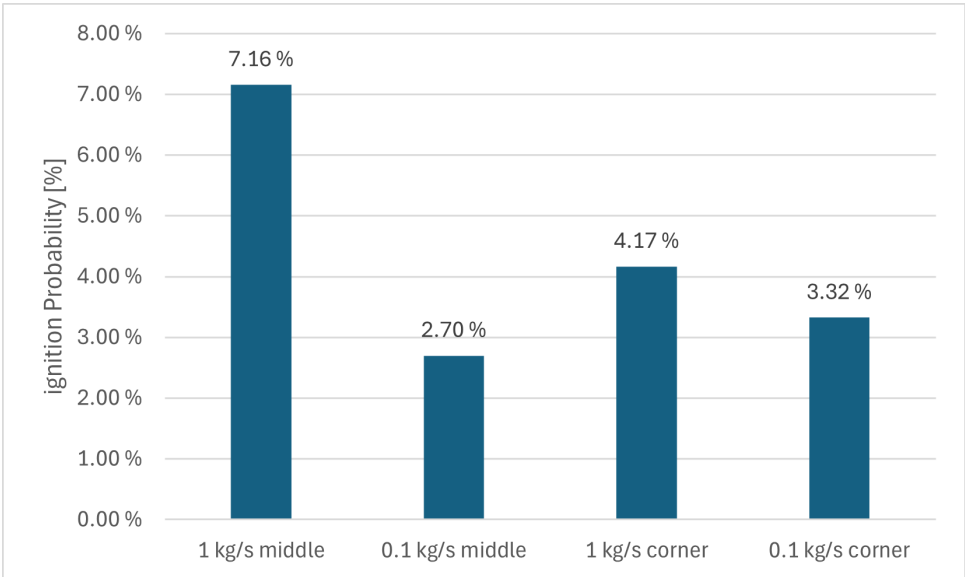


Figure 8.12: Ignition probability for the different leaks and their locations after 30 sec.



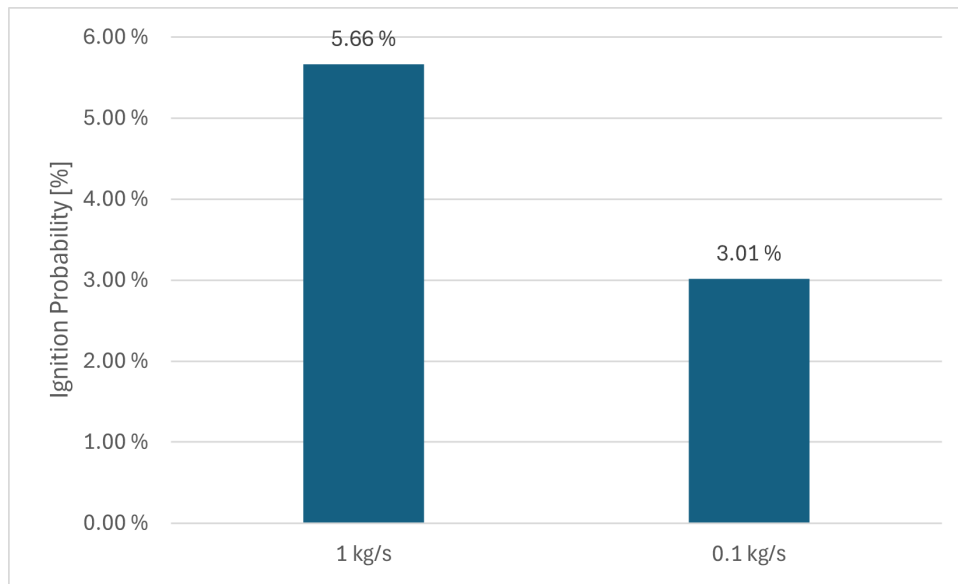


Figure 8.13: Average ignition probability for the 1 kg/s leak and 0.1 kg/s

Table 8.1 and 8.2 presents the ignition probability for the corner and middle leak on 1 kg/s. Where the continuous and discrete ignition probability is presented for the four ignitors.

Table 8.1: Total probability for the ignitors placed in the area of the process plant for the 0.1 kg/s leak.

		Total Probability	Continuous	Discrete
Middle 0.1 kg/s leak	Other generic	1-73E-05	1-32E-05	4.10E-06
	Electrical equipment	1.22E-05	1.17E-05	5.02E-07
	Rotating equipment	1.99E-04	1.99E-04	5.02E-07
	Electrostatic discharges	4.95E-04	3.61E-04	1.34E-04
Corner 0.1 kg/s leak	Other generic	9.22E-06	7.65E-06	1.57E-06
	Electrical equipment	7.18E-06	6.99E-06	1.92E-07
	Rotating equipment	9.88E-05	9.86E-05	1.92E-07
	Electrostatic discharges	2.31E-04	1.79E-04	5.12E-05

Table 8.2: Total probability for the ignitors placed in the area of the process plant for the 1 kg/s leak.

		Total Probability	Continuous	Discrete
Middle 1 kg/s leak	Other generic	9.11E-04	6.91E-04	2.20E-04
	Electrical equipment	6.22E-04	5.95E-04	2.69E-05
	Rotating equipment	1.20E-02	1.20E-02	2.69E-05
	Electrostatic discharges	2.86E-02	2.15E-02	7.13E-03
Corner 1 kg/s leak	Other generic	1.33E-04	1.00E-04	3.28E-05
	Electrical equipment	9.03E-05	8.62E-05	4.01E-06
	Rotating equipment	1.76E-03	1.75E-03	4.01E-06
	Electrostatic discharges	4.26E-03	3.19E-03	1.07E-03

### 8.1.4 Ignition Probability Contributors

Figure 8.14 shows a logarithmic representation of the contributors to the total ignition probability.

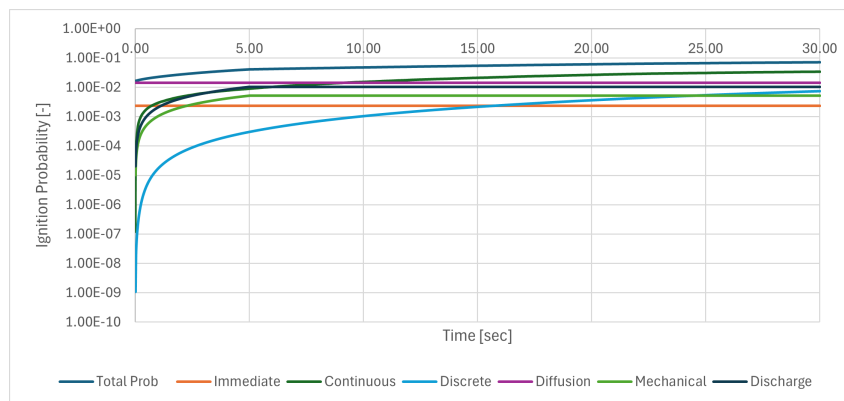


Figure 8.14: Logarithmic representation of the contributors that contribute to the total ignition probability for the process plant geometry.

Figure 8.15 shows what contributes to the ignition probability at the start of the leak, where all the leaks are presented. Figure 8.16 presents the contributors to the ignition probability at the end of the leak.

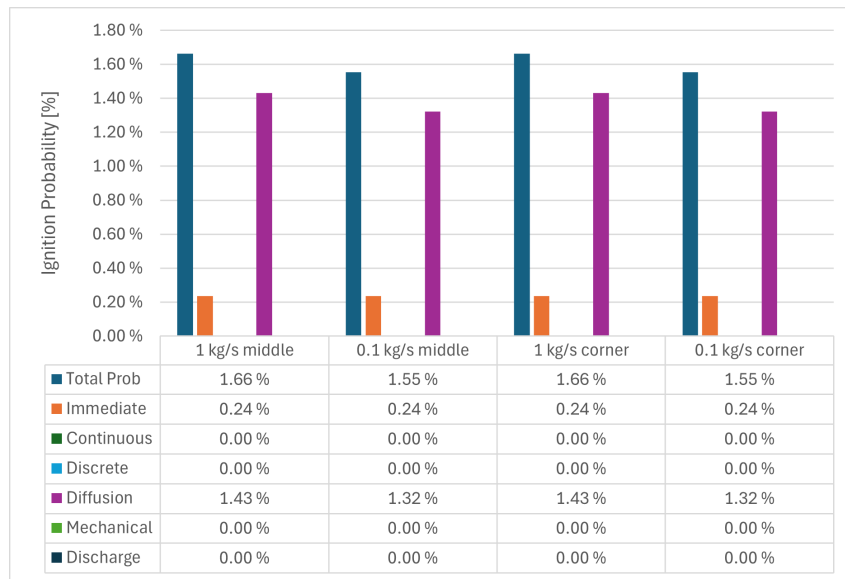


Figure 8.15: Contributors to the total ignition at the start of the leak for the process plant geometry.

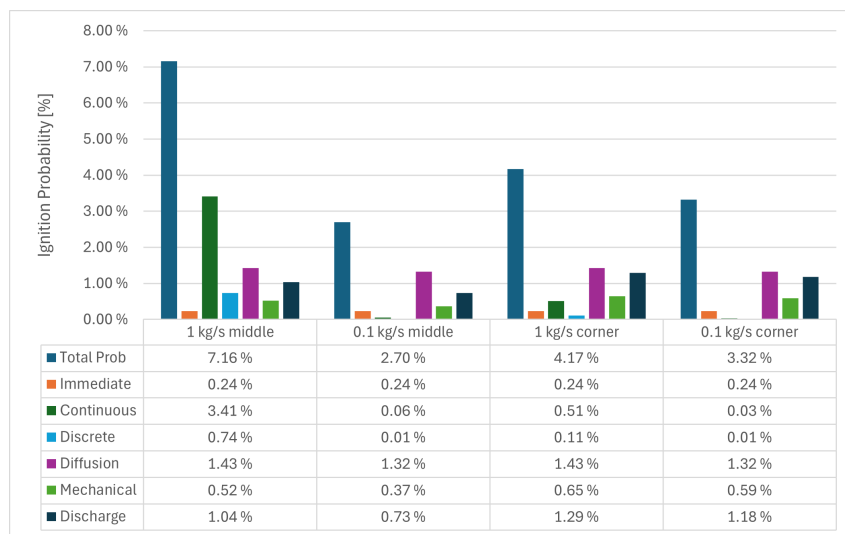


Figure 8.16: Contributors to the total ignition after the leak has exceeded in 30 sec

Figure 8.17 and 8.18 presents the relationship between ignition probability and combustible volume. These plots allow for a clearer analysis of how the volume of the gas cloud influences ignition probability.

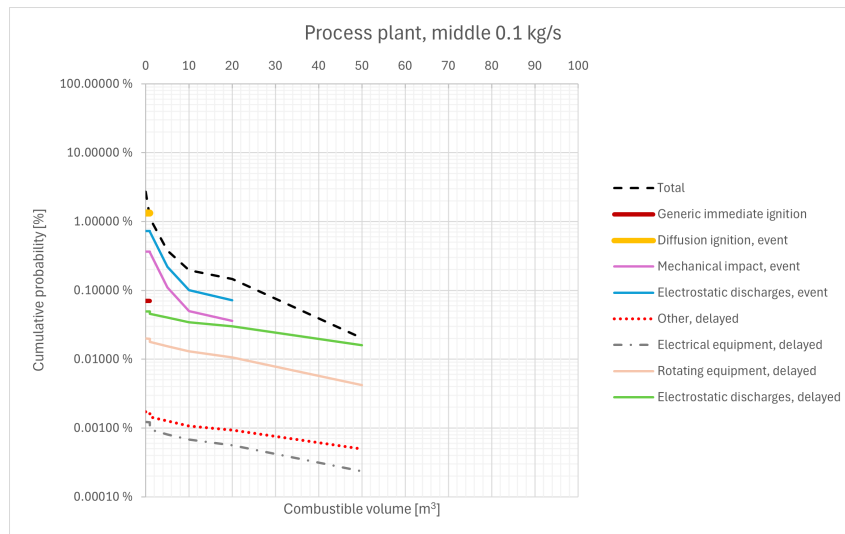


Figure 8.17: Contributors to the total ignition probability where the ignition probability is plotted against the cloud volume, for the middle leak with 0.1 kg/s leak rate for the process plant geometry.



Figure 8.18: Contributors to the total ignition probability where the ignition probability is plotted against the cloud volume, for the middle leak with 1 kg/s leak rate for the process plant geometry.

### 8.1.5 Grid sensitivity

For the process plant, the grid sensitivity was simulated with 100 000, 300 000, 500 000 and 800 000 grid cells. Figure 8.19 and 8.20 presents the grid sensitivity for the 0.1 kg/s and 1 kg/s hydrogen leak with their contributors at the end of the simulation.

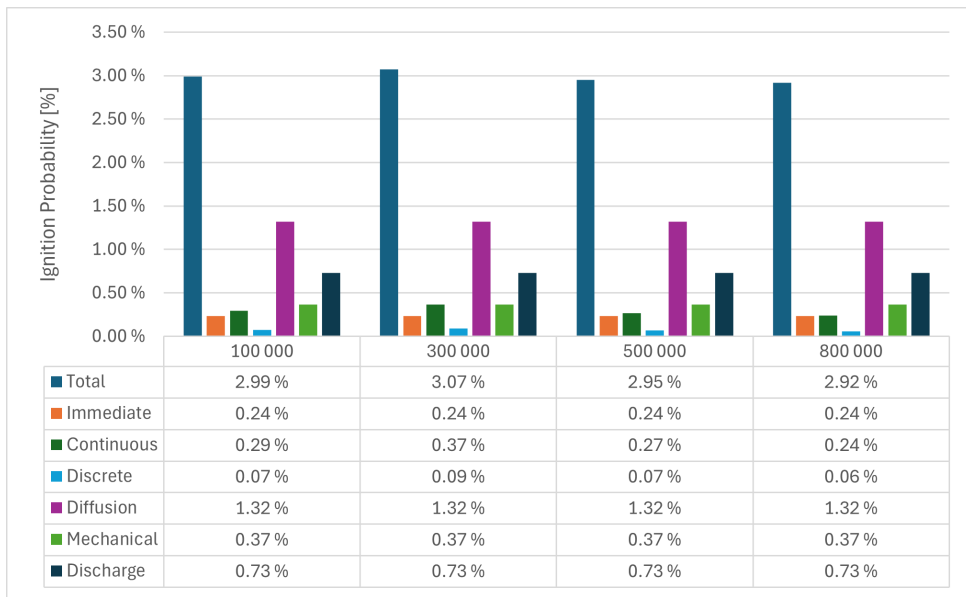


Figure 8.19: Grid sensitivity for the 0.1 kg/s leak with the different contributors.

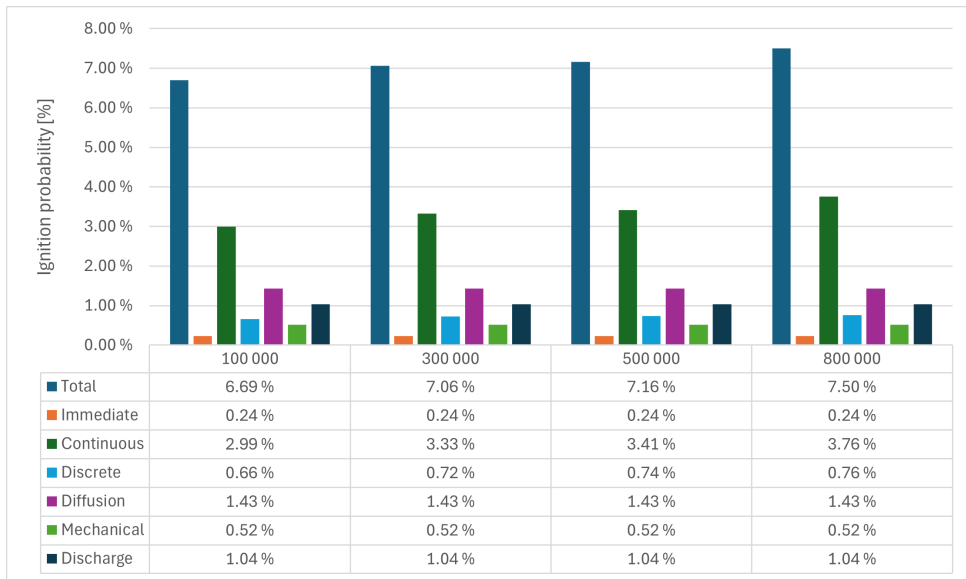


Figure 8.20: Grid sensitivity for the 1 kg/s leak with the different contributors.

Figure 8.21 shows the expansion-based weighted volume cloud for the 0.1 and 1 kg/s leak.

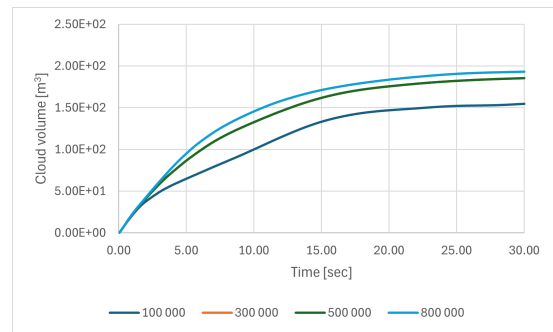
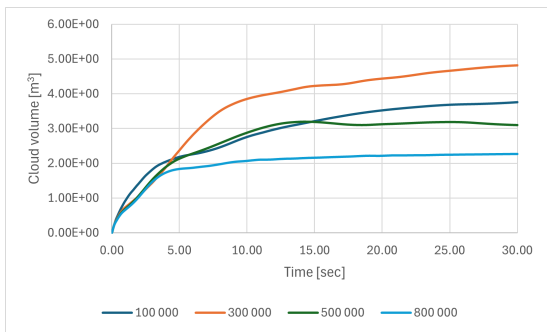


Figure 8.21: Stoichiometric equivalent cloud volume cloud for the 0.1 kg/s (left) and 1 kg/s (right) leaks.

Figure 8.22 shows the cloud volume where the maximum speed and maximum expansion are considered for the 0.1 kg/s leak and the 1 kg/s leak.

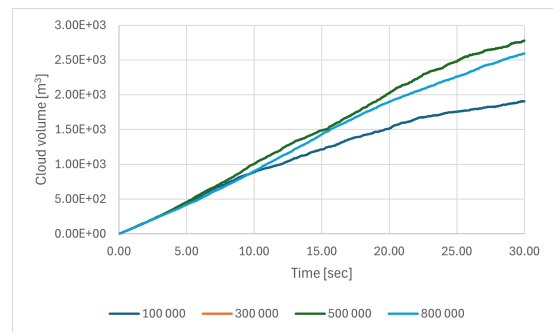
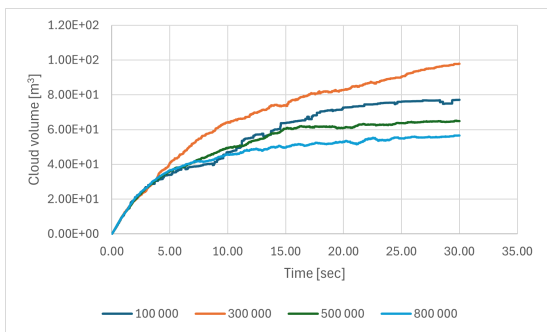


Figure 8.22: Flammable cloud volume for the 0.1 kg/s (left) and 1 kg/s (right) leaks.

## 8.2 Methane leak compared with hydrogen leak

### 8.2.1 Methane

The gas cloud dispersion for a 1 kg/s methane leak downward release is shown in Figure 8.23. The surface plot is done at 4% volumetric concentration. To visualize the leak better, Figure 8.24 shows the process plant where the geometry is cut to see the leak better.

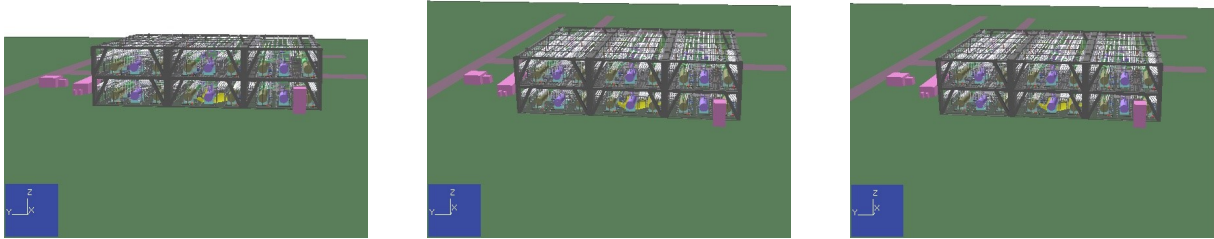


Figure 8.23: Surface plots of 4% CH<sub>4</sub> concentration for 1 kg/s downward release at different time points: 10 seconds, 20 seconds, and 30 seconds where the leak locations are in the middle of the geometry.

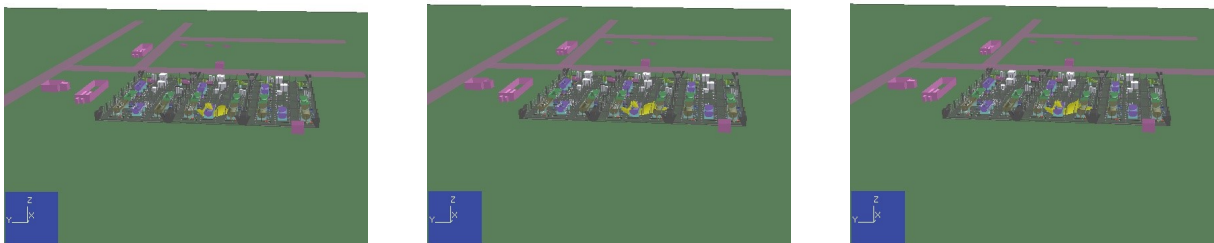


Figure 8.24: Surface plots where the process plant is cut after 3 meters to present the 4% CH<sub>4</sub> concentration for 1 kg/s downward release at different time points: 10 seconds, 20 seconds, and 30 seconds where the leak locations are in the middle of the geometry.

Figure 8.25 presents the stoichiometric equivalent cloud volume for the methane and hydrogen leak. While Figure 8.26 presents the gas flammable gas cloud for methane and hydrogen, together with the ignition probability profile

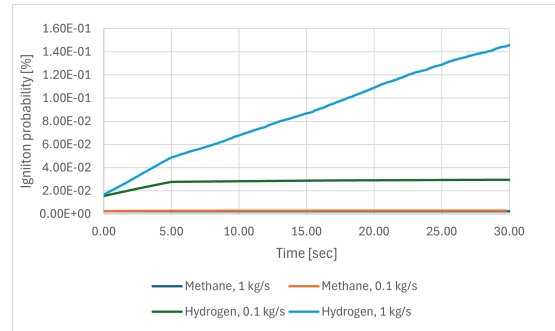
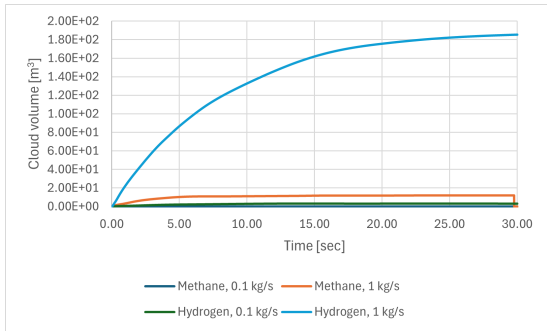


Figure 8.25: Stoichiometric equivalent cloud volume for both hydrogen and methane, compared to the ignition probability

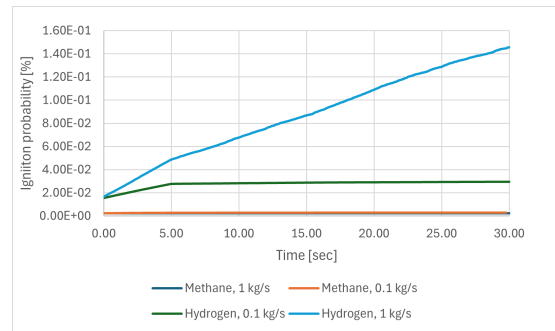
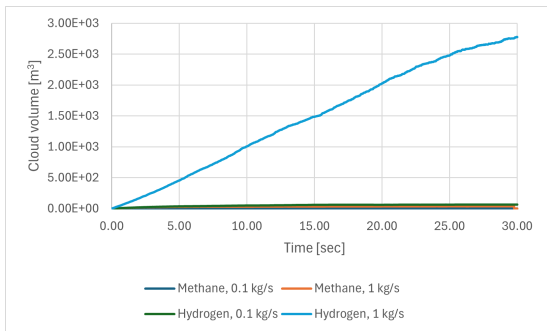


Figure 8.26: Flammable cloud volume between lower- and upper flammability limit for both methane and hydrogen compared to the ignition probability

Figure 8.27 present the total ignition probably for methane and hydrogen as a histogram for the middle leak location.



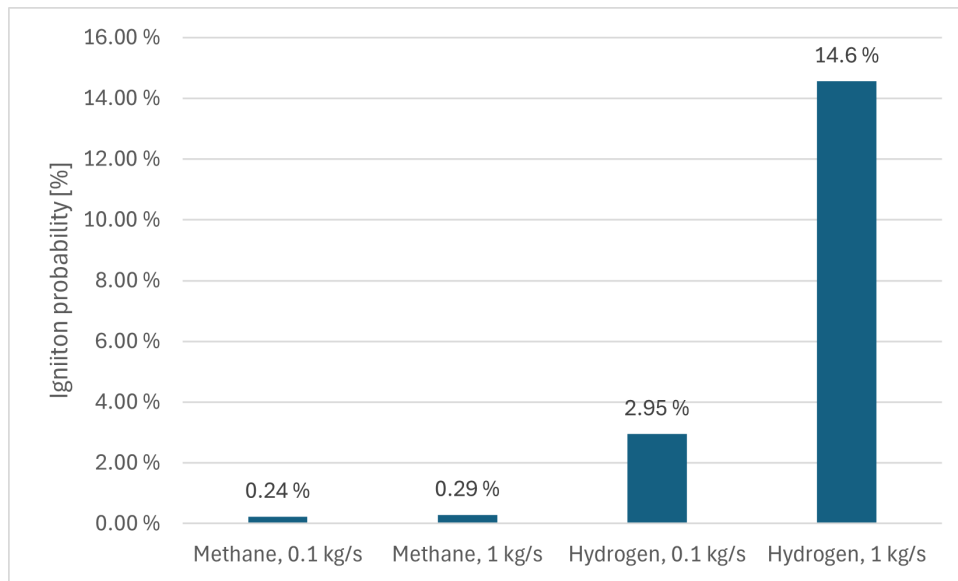


Figure 8.27: Average total ignition probability for methane and hydrogen

## 8.3 Comparison with HYEX and DNV model

### 8.3.1 DSB

Figure 8.28 compares the recommended total ignition probability for hydrogen leaks from the DSB article to the total ignition probabilities for the three geometries. The plot gives a visual understanding of ignition probabilities for hydrogen jet release and how they are predicted by the HYEX model and the DNV model from 2007 used in HyRAM. While Figure 8.28 presents the specific scenarios for the container, refueling station, and process plant is annotated on the graphs.

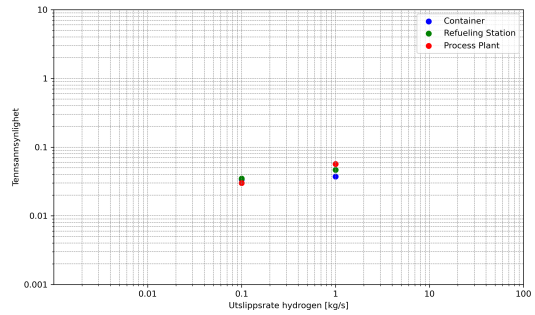
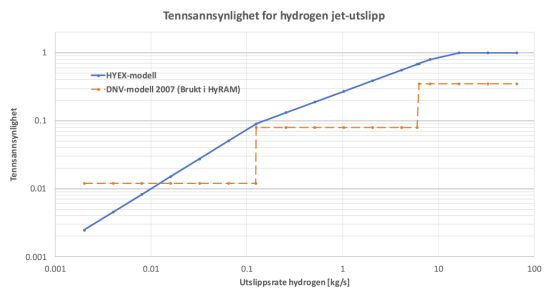


Figure 8.28: Comparison of DSB’s figure about Recommended total ignition probability for hydrogen leaks for the HYEX and DNV model compared to the ignition probability for the three geometries in this thesis

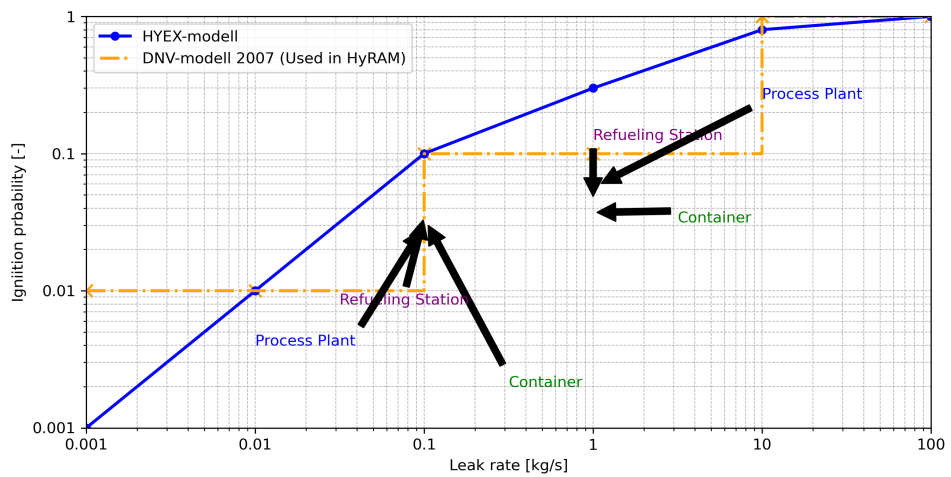


Figure 8.29: Visual representation indicating the ignition probabilities for the three geometries based on the DNV model and HYEX model from [19]

## 9 Discussion

This thesis focuses on testing the SAFEN ignition probability model and validating the implementation of the model in KFX-RBM. Simulations with the updated version of KFX-RBM were conducted for three different geometries to examine how the ignition probability varies with geometric complexity.

First, a simple test case was made where it was possible to validate the results from KFX-RBM by comparing them with hand calculations, see Chapter 4. Simulations with KFX-RBM was then performed for three realistic facilities that differ in size. Grid sensitivity simulations was also performed for all geometries. The simulations were simulated with hydrogen and methane to compare the differences in the ignition probability between hydrogen and a common hydrocarbon.

### 9.1 Total ignition probability (after 30 sec)

All simulations were run for 30 seconds, and at this point, the total ignition probability was extracted. For large geometries, such as the process plant, the gas cloud's size, and the ignition's probability may continue to grow if the release continues. However, 30 seconds was selected for all cases to make it easy to compare results.

A summary of the the total ignition probabilities for the geometries are presented in Table 9.1.

Table 9.1: Total ignition probability for the container, hydrogen refueling station, and process plant. Values averaged for all release directions.

	0.1 kg/s	1.0 kg/s
Container	3.40 %	3.72 %
Refueling station	3.48 %	4.67 %
Process plant	3.01 %	5.66 %

The data presents that all the geometries have an increase in ignition probability with higher hydrogen release rates. The container shows a similar ignition probability for the 0.1 kg/s leak and the 1 kg/s leak.

For the refueling station, the difference in ignition probability between the two leak rates is more significant than for the container. The process plant shows the highest difference, making it more sensitive to an increase in release rate, since it goes from 3.01 % to 5.66 %.

All the calculated ignition probabilities are within the expected range for the SAFEN model which is below 10 % [8].

Keep in mind that these ignition probabilities are averaged values from different leak locations and directions.

### 9.1.1 Variation regarding rate

As shown in Table 9.1, the 0.1 kg/s leak rate exhibits a similar probability for all geometries. However, for the 1.0 kg/s leak rate, the process plant has a significantly higher ignition probability than the other two geometries.

The container shows that at 30 seconds the ignition probability for the two different rates is quite similar, with 3.40 % and 3.72 %. The reason for this is that the volume inside the container is limited and congested. A significant part of the container volume is quickly filled with gas above the upper flammability limit even for the lower release rate.

The refueling station has about the same ignition probability for the 0.1 kg/s case as the container. However, for the 1.0 kg/s case, the ignition probability is significantly higher since it shows an increase from 3.48 % to 4.67 %. For the refueling station, the larger release rate results in a larger flammable volume and a higher ignition probability.

The process plant presents the highest difference in ignition probability between the 0.1 kg/s and 1 kg/s. The 0.1 kg/s release has a total ignition probability of 3.01 % which is lower than both the container and refueling station. The 1 kg/s has a total ignition probability of 5.66 %. This is higher than the container and refueling station. In contrast to the other geometries, the process plant has no closed walls towards the surroundings. This means that some of the gas can more easily escape the facility and the cloud inside the process plant will become smaller for some release directions. For other combinations of leak rates and locations, the total gas volume inside the process plant may become larger. This is further discussed in section 9.1.4 and 9.1.3

In a cloud with a larger volume, the presence of equipment units and components is greater than in a smaller cloud. For a smaller geometry, there might be approximately 10 electrical equipment units capable of energy generation that may ignite a hydrogen cloud. For bigger geometries, the presence of electrical equipment units may surpass several thousand, thereby amplifying the probability of equipment failure, which can lead to ignition.

## 9.1.2 Contributors

After the simulations have reached 30 seconds, the biggest contributors to the total ignition probability are the discharge ignition probability, the diffusion ignition probability and the mechanical ignition probability.

The electrostatic discharge ignition probability (denoted discharge in the figures), as mentioned in section 2.8.4, is the ignition caused by electrostatic discharges such as spark discharges, brush discharges, and corona discharges. The phenomena scale with the leak rate. As the leak increases, more hydrogen molecules are released into the environment making the ignition probability for electrostatic discharges exacerbate.

When the diffusion ignition probability is high, it implies that hydrogen has to be released rapidly into a confined space with air or oxygen. As illustrated in Figure 6.14 for the container, the diffusion ignition significantly contributes to the total ignition probability.

The mechanical ignition probability is the third biggest contributor to the total ignition probability. As presented in Figure 6.16 the mechanical ignition probability is the same for the same leakage and this suggests that it only depends on rate.

The three lowest contributors are the immediate, continuous, and discrete ignition probabilities. The immediate ignition probability is the ignition probability that there will be an immediate ignition, so after 30 seconds, this probability will be very small. The same goes for the continuous ignition probability, which covers the ignition mechanisms that are present continuously and ignite the atmosphere when it is initially exposed. Lastly, the discrete ignition probability an effective ignition source only at a specific moment in time.

Figure 6.17 and 6.18 shows the total ignition probability as a function of cloud size for the middle leak in the container for the two leak rates. It can be seen that for the 1 kg/s rate the ignition probability for large clouds (e.g. 20 m<sup>3</sup>) is significantly higher than for a cloud of the same size from the 0.1 kg/s rate. significant difference between the 0.1 kg/s leak rate and the 1.0 kg/s leak rate. This is because the cloud volume grows much faster. The "event" category consists of the mechanical impact (event) and the electrostatic discharges (event), and it proves that these are more important when the leak rate is bigger, and the cloud volume is bigger. It is important to note that higher ignition probability for a larger cloud also implies a higher probability for larger blast pressures. Similar plots for the process plant are shown in Figure 8.17 and 8.18. However, as the cloud volume differs significantly for the two leak rates it is more difficult to see the same effect from the plots.

### 9.1.3 Leak Direction

The size of the gas cloud is for most cases highly influenced by the direction of the hydrogen leak within the designated area of study. As presented in Chapter 7.1.1 for the hydrogen refueling station, it is possible to see how well the fences around the process equipment contain the gas. In the case of ignition, the fence may hinder the gas and blast wave from moving outside of the hydrogen refueling station, making most of the blast move upwards and not to the sides. As seen in the geometry (Figure 5.5), there is an opening in front where trucks can access the equipment to deliver the hydrogen. A large amount of hydrogen will be released through this opening. This will most likely not be the case in a real-life scenario. An area like this would not face the area where cars are refilled.

As depicted in Figure 6.8 for the container, the volumetric extent of the cloud from the 1 kg/s hydrogen leak in the middle of the geometry is significantly higher for the positive y-direction leak. However, the positive x and z directions have both a small cloud volume.

There are substantial variations in the volumetric extent of the cloud resulting from a 1 kg/s hydrogen leak at the middle for the different leak directions for the container. For the negative y-direction, the leak exhibits an increase in the cloud volume, whereas both the positive x- and z-directions form a smaller cloud volume. For all six directions, the cloud continues to increase in size until 30 seconds have passed. However, in the case of the corner leak, in Figure 6.8 the maximal cloud volume is observed in the positive and negative x-directions.

From Figure 6.7 the flammable gas cloud volume differs in different directions. However, due to the limited size of the container, the flammable gas cloud volume is also limited.

For the process plant, the hydrogen cloud is significantly larger in the negative z-direction for both the 0.1 kg/s leak (see Figure 8.9) and the 1 kg/s leak (see Figure 8.10).

One particularly notable thing is that the refueling station doesn't have any overhead structures like a roof, so it would be likely that the gas cloud would only continue to grow in the upward direction (positive z). For the x and y directions, the cloud would be less significant since there is a wall stopping the cloud formation. Unlike the fueling station, which lacks any overhead structure but has surrounding walls, the process plant is entirely open. It contains no walls or structures around it. This means that there won't be anything stopping the hydrogen cloud from expanding outside the process plant. However for the container, which is an almost entirely enclosed structure, the hydrogen cloud will stop expanding upon reaching the walls.

### 9.1.4 Location

For the container, the ignition probability shows minimal changes based on the leakage location. As seen in Figure 6.12 there is no significant difference in the ignition probability for the container. This also applies to the refueling station, where the ignition probability for the two leak locations is about the same. This can be seen in Figure 7.17 where all the ignition probabilities are about the same. This can be because of effective safety measures in the geometry of the refueling station.

While for the process plant, Figure 8.16, the ignition probability is significantly higher for the 1 kg/s middle leak, than any other leaks. The 1 kg/s corner leak has about half as big an ignition probability as the 1 kg/s middle leak. For the 0.1 kg/s leaks the difference is smaller but the corner leak has a higher ignition probability than the middle leak. This variation indicates that the leak location has a substantial impact on the ignition probability. This can be because of differences in the placement of equipment or potential ignition sources. For the high leak rate at the corner, it is more likely that the gas escapes outside the facility and thereby reduces the ignition probability inside the plant.

## 9.2 Total ignition probability (at 0 seconds)

At the very start of the simulations, the ignition probabilities exhibit substantial differences compared to what is observed after 30 seconds. The ignition probability immediately after the onset of the leak provides insight into the likelihood of a direct fire occurring. This information is important for determining what safety measures that should be used.

The ignition probabilities for the geometries at the start of the leak are presented in Table 9.2. The table suggests that the ignition probability remains constant for all geometries. This implies that the model depends on the assumption that the initial conditions, such as the hydrogen concentration are uniform for all geometries. However, the real-world scenario will most likely have a varying ignition probability due to the influence of geometry. This model is only a simplified version of a real-world scenario. Keep in mind that the ignition probability is an averaged number for all leak directions as well as leak locations.

Table 9.2: Summary of the total ignition probability for the container, hydrogen refueling station, and process plant at  $t=0$ . Values averaged for all release directions.

	0.1 kg/s	1 kg/s
Container	1.66 %	1.55 %
Refueling station	1.66 %	1.55 %
Process plant	1.66 %	1.55 %

### 9.2.1 Variation regarding rate

As shown in Table 9.2, the 0.1 kg/s and the 1 kg/s have the same ignition probability for all three geometries. This is because the ignition probabilities are picked from right upon the start of the leak, where the cloud has not had time to form.

The size of the gas cloud is influenced by the ignition probability in the selected area of study. A larger gas cloud will expand the volume of flammable gas, which will increase the likelihood of encountering ignition sources and produce an ideal atmosphere for combustion. At  $t=0$ , where the gas cloud is still small, which makes the ignition probability low. This is due to the low amount of flammable gas available. This reduces the possibility of a combustion occurring.

### 9.2.2 Contributors

At the start of the leak, the dominant contributors for all cases are the probability of diffusion ignition (`prob_diff`) and the immediate ignition probability (`prob_I`), for the refueling station this can be seen in Figure 7.16. In this figure, all other contributors are zero, except for the immediate ignition probability and diffusion ignition probability.

As mentioned in sub-chapter 2.8, the immediate ignition probability refers to the likelihood of ignition happening before the formation of the flammable gas cloud. Since these contributors assessed to the very start of the leak, there has been no time for a gas cloud to form.

As seen in Figure 7.16 the diffusion ignition probability is 1.43 % for both the middle 1 kg/s leak and corner 1 kg/s leak. For the middle and corner 0.1 kg/s leak, the diffusion ignition probability is 1.32 %. The diffusion ignition probability is only dependent on the hole diameter and pressure.

This results in the fact that the immediate ignition probability and the diffusion ignition probability are the primary factors influencing the ignition probability at the initial stage of the hydrogen leak.

### 9.2.3 Direction

At the very start of the hydrogen leak ( $t=0$ ), the gas cloud has not started to form. As mentioned in Chapter 2.8, the immediate ignition probability occurs before the flammable cloud has started to form and there is no difference in ignition probability at  $t = 0$  for various directions. It is, however, interesting to look at how the leak direction affects the ignition probability for the very beginning of the leak.



For the container geometry, the middle 0.1 kg/s leak in the negative x-direction appears to result in the largest gas cloud volume at the initial start of the leak, as presented in Figure 6.7. While for the corner 0.1 kg/s leak the positive z-direction seems to result in the largest cloud at the initial start of the leak. For the 1 kg/s leak rate, the negative x-direction seems to give the largest gas cloud for the corner leak, while the positive y-direction appears as if to give the largest cloud for the middle leak (Figure 6.8).

For the refueling station, the largest gas cloud appears to be in the negative z-direction for the 0.1 kg/s corner leak, while the largest occurs in the negative y-direction for the middle leak, see Figure 7.10. For the 1 kg/s leak, the largest leaks are in negative y-direction for the corner leak, and negative z-direction for the middle leak, see Figure 7.11.

For the process plant the negative z-direction seems to give the largest gas cloud for all leaks and their leak rates, see Figure 8.9 and 8.10

This phenomenon can be explained similarly to the discussion in Section 9.1.3, where it was explained that the fueling station has fences that prevent the cloud from forming in the x- and y-direction. While the container scenario features a fully enclosed structure, which restricts the gas dispersion. While the process plant has a completely open geometry that allows the gas cloud to disperse in all directions.

### 9.3 Total ignition between 1-5 seconds

In the SAFEN ignition model, two of the ignition probability contributors are associated with the initial phase of the leak. This ignition is generated by mechanical and electrostatic sources. It is assumed that the onset of the leak can generate mechanical impact leading to hot surfaces of burning particles and electrostatic discharges due to potential differences, as described in section 2.8

Table 9.3 presents the ignition probabilities for the three geometries at 5 seconds.

Table 9.3: Total ignition probability for the container, hydrogen refueling station, and process plant at 5 seconds. Values averaged for all release directions.

	0.1 kg/s	1 kg/s
Container	3.68 %	3.35 %
Refueling station	3.27 %	3.69 %
Process plant	2.99 %	3.99 %

### 9.3.1 Contributors

For most real-life leak scenarios the release rate will be highest at the start of the leak. This is due because of the pressure, and as time passes, the pressure goes down together with the leakage. Meanwhile, with electrostatic discharges and mechanical generates sources, as presented in Figure 7.15 and 6.14, they stabilize after about 5 seconds. The reasoning behind this is that the SAFEN model suggest that these three only will happen in the first 5 seconds, and the probability of them occurring after 5 seconds are relatively small.

This is correlated with the start of the leak, so the model says that electrostatic discharges and mechanical should be uniformly distributed over the first 5 seconds. However, this decision has uncertainty, and other choices may give a different outcome. This characteristic can be seen in the model results.

## 9.4 Comparison of Ignition Probability Models

The Norwegian Directorate for Civil Protection (DSB) has a article named "Guidelines for quantitative risk analysis of facilities handling hazardous substances" (see Section 2.7.2) where Figure 2.1 presents the recommended total ignition probability for hydrogen leaks.

The plot in Figure 8.28, illustrates the ignition probability for hydrogen jet releases, comparing the HYEX model and the DNV model from 2007 that has been used in HyRAM.

For the container scenario, the release rate of 0.1 kg/s, the ignition probability is 3.4 % which aligns closely with the DNV model, however, it is slightly lower than the 10 % ignition probability after the first step. For the release rate of 1 kg/s, the ignition probability is around 3.72 % which makes it in line with the DNV model, while it also fits within the increase trend of the HYEX model.

The refueling station scenario shows that for the 0.1 kg/s leak rate, the ignition probability is 3.48 %. This is the position between the first and second steps of the DNV model. For the 1.0 kg/s leak, the ignition probability is annotated at 4.67 %, which also falls into the DNV model 10 % step.

For the process plant scenario at 0.1 kg/s, the ignition probability is annotated at 3.01 %. This is slightly lower than the container and refueling station scenario, however, it is still above the first step for the DNV model. The 1.0 kg/s leak rate has a probability of 5.66 %. This fits with the 10 % step in the DNV model.

The ignition probability for the three scenarios matches the HYEX and DNV model's predictions. They are higher for the first step in the DNV model, however they are lower

than the second step. This implies a gradual increase in risk does not necessarily fit with the step changes in the DNV model. However, for the HYEX model where there is a smooth increase of the ignition risk, it seems to be more accurate when reflecting the ignition probabilities for these scenarios, rather than the step function in the DNV model.

## 9.5 Grid sensitivity

In this section, the grid sensitivity analysis will be employed to determine the appropriate number of grid cells for this type of simulation. All the geometries have been simulated with 100,000, 300,000, and 500,000 grid cells, however, the process plant has also been simulated with 800,000 grid cells.

For the container (See Figure 6.19 and 6.20) there was a very light variation of the total ignition probability, for both the 0.1 kg/s leak, and for the 1 kg/s leak. However, the 300 and 500,000 grid cells gave both 3.45 % for the 0.1 kg/s leak, while 100,000 cells gave 3.46 % ignition probability, which is a small difference. This also applied to the 1 kg/s leak. The size of the cloud volume is slightly higher for the 300,000 grid cell, for the 1 kg/s leak rate in Figure 7.20 and 7.21

For the refueling station, there was no significant difference in ignition probability for the 0.1 kg/s leak, the 500,000 grid cells had a slightly higher ignition probability at 3.75 %, compared to 3.63% for the 100,000 grid cells. However, for the 1 kg/s leak, the ignition probability was 4.42% for the 100,000 grid cells and 5.29% for the 500,000 grid cells. Figures 7.20 and 7.21 illustrate that the cloud volume for the 100,000 grid cells is lower than that of the other two cases, while the cloud volumes for the 300,000 and 500,000 grid cells are similar.

The process plant (see Figures 8.19 and 8.20) shows that for the 0.1 kg/s leak, the ignition probability increases to 3.07% for the 300,000 grid cell simulation, decreases to 2.95% for the 500,000 grid cell simulation, and further decreases to 2.82% for the 800,000 grid cell simulation. For the 1 kg/s leak rate, the probabilities are fairly consistent across simulations, with the 800,000 grid cell simulation having a slightly higher ignition probability at 7.50%, compared to 7.16% for the 500,000 grid cell simulation. The size of the gas cloud presented in Figure 8.21 and Figure 8.22, shows that the difference in cloud volume is not significant for most cases. However, the 300,00 grid cells for the 0.1 kg/s release have a slightly bigger volume than the other grid cells, while the 800,000 grid cells show a smaller gas cloud volume, in Figure 8.21.

Keep in mind that this grid analysis has only been conducted for the middle leak, not the corner leak. The difference in grid cells for all the cases is small for both the 0.1 kg/s and 1 kg/s release. For the 800,000 and 300,000 grid cells in the process plant, there

was a difference in the cloud volume. For this thesis, the shorter simulation time was prioritized over the improved precision that the 800,000 grid cells would have given. This approach was applied for all the cases since there was no significant difference in ignition probability.

Overall, the ignition probability results are quite insensitive to the grid size. The reason for this may be that the smallest grids are sufficiently large to resolve the gas dispersion. This finding is probably also due to the ignition probabilities being calculated from averaged values and are thus less sensitive to coarse grids. This is an important finding because when KFX-RBM is used for quantitative risk analyses for large facilities a large number of simulations is required and using a "coarse" grid will be time-saving.

## 9.6 Methane leak compared to hydrogen leak

For the comparison between hydrogen and methane, the middle leak location was chosen together with a release direction in the negative z-direction.

For all geometries, the ignition probability for hydrogen was significantly higher than for methane. This is as expected. This can be seen in the summary table in Figure

Table 9.4: Summary of the ignition probability for methane and hydrogen, for the middle leak in the negative z-direction. All these are mentioned in Chapter 6.2.1, 7.2.1 and 8.2.1

	CH4, 0.1 kg/s	CH4, 1 kg/s	H2, 0.1 kg/s	H2, 1 kg/s
Container	0.28 %	0.29 %	3.46 %	3.74 %
Refueling station	0.24 %	0.43 %	3.72 %	5.24 %
Process plant	0.37 %	0.29 %	2.95 %	14.6 %

As presented in Figure 6.24, both the hydrogen and methane leaks at a rate of 1 kg/s demonstrate a rapid increase in cloud volume inside the container, followed by a decrease in cloud size. This happens because a substantial amount of the flammable gas accumulates inside the container quickly, but the volume decreases as the hydrogen concentration exceeds UFL.

In contrast, with a leak rate of 0.1 kg/s, it takes a longer time to reach a flammable gas concentration before it becomes too "rich". This indicates that a smaller leak possibly can be more hazardous than a larger leak since a significant leak rapidly will displace all air in the container, leading to a gas concentration that is too rich to ignite.

As presented in Table 9.4, the ignition probability for hydrogen is much higher than what it is for methane. The ignition probability for methane is 0.82 % for the 1 kg/s leak rate, while for hydrogen the ignition probability for the same case is 5.24 %.

For both the refueling station (Figure 7.23 and 7.24) and the process plant geometry, see Figure 8.25 and 8.26 the 1 kg/s hydrogen leak accumulates the biggest cloud volume. This is attributed to hydrogen's broader flammability range, which spans from 4-75 % Methane, however, has a flammability range from 5.3-14 % which is more narrow than hydrogen. The wider flammability range of hydrogen increases its ability to ignition.



# 10 Conclusion and further work

## 10.1 Conclusion

The objective of this master's thesis was to look into the performance and efficiency of the SAFEN model and how it performs concerning larger-scale geometries and more detailed models. The SAFEN model in KFX-RBM has also been checked.

First, a validation check of the implementation of the SAFEN ignition probability model in KFX-RBM as performed. This was an iterative process where DNV updated the model in KFX-RBM based on the results from the validation. This resulted in a new version of KFX-RBM which is fully aligned with the SAFEN ignition probability model for hydrogen.

The updated KFX-RBM tool was used to investigate three geometries: one 40' iso container, one hydrogen refueling station, and one process plant. The simulations were carried out with two different leak rates, 0.1 kg/s and 1 kg/s, as well as with different leak locations, to see if the ignition probability changed much. The simulation of the 40' iso container resulted in an ignition probability of 3.40 % for the 0.1 kg/s leak rate and 3.72 % for the 1 kg/s leak rate. For the hydrogen refueling station, the 0.1 kg/s leak rate gave an ignition probability of 3.48 %, while the 1 kg/s leak rate gave a 4.67 % ignition probability. Finally, the process plant gave an ignition probability of 3.01 % for the 0.1 kg/s leakage and 5.66 % for the 1 kg/s leakage.

For the 40' ISO container, the increase in ignition probability from the 0.1 kg/s leakage to the 1 kg/s leakage indicated a stable risk profile. The volume of the gas cloud is not large because the enclosed geometry quickly fills up with a combustible mixture. On the other hand, the hydrogen refueling station and the process plant showed a larger increase in ignition probability for the 1 kg/s leakage compared to the 0.1 kg/s leakage. This can be because the geometries are more complex. All the geometries show that the biggest contributors to the total hydrogen ignition probability are diffusion ignition, electrostatic discharge, and mechanical ignition mechanisms.

Together with the different leak rates, the different leak locations demonstrated that the location of the leak within a geometry could influence the ignition probability, proving the importance of considering multiple leak locations during a risk analysis. Additionally, the volume of the gas cloud created after a leak has been shown to have a significant impact

on the ignition probability. Larger gas clouds raise the total ignition probability since the likelihood of equipment coming into contact with the cloud is much higher. Together with the different leak rates, the different leak locations demonstrated that the location of the leak within a geometry could influence the ignition probability, proving the importance of considering multiple leak locations during a risk analysis. Additionally, the volume of the gas cloud created after a leak has been shown to have a significant impact on the ignition probability. Larger gas clouds increase the total ignition probability since the likelihood of equipment coming into contact with the cloud is much higher. These results show the importance of using a 3-dimensional simulation tool which takes into account the effect of geometry on the gas dispersion when performing quantitative risk assessments.

Hydrogen was also compared to the hydrocarbon methane. The simulation shows that the ignition probability for hydrogen is significantly higher than for methane. This is as expected. Additionally, the volume of the hydrogen cloud is much larger than the volume of the methane cloud.

This thesis contributes to the knowledge of hydrogen ignition probability in various geometries and leak scenarios, offering important new information for improving safety precautions when handling hydrogen. The results show the importance of conducting a thorough risk assessment and putting extensive safety plans into effect in order to handle the challenges that come with handling hydrogen.

## 10.2 Further work

To further enhance the SAFEN model for estimating hydrogen ignition probabilities, several things could be further investigated.

- Transient release analysis: Make scenarios with a transient hydrogen release to better understand how a hydrogen leak behaves over time. This will give usefully insight into the variations in the ignition probability under more realistic conditions.
- Comprehensive documentation of KFX-RBM: To continue using KFX-RBM, there needs to be more detailed documentation of the program. This should include definitions and explanations of the ignition probability log (ignprob.log) to ensure better and more understandable results
- Test with different geometries and release rates. This should be done to understand how different geometries and leak rates affect the ignition probability.
- Mixtures of other substances. The ignition probability model should investigate how mixtures of different substances affect the ignition probability. Especially, in environments where multiple chemicals are present.



# Bibliography

- [1] United Nations, *Population*, <https://www.un.org/en/global-issues/population>, Accessed: 2024-02-23.
- [2] I. Mohammadfam and E. Zarei, 'Safety risk modeling and major accidents analysis of hydrogen and natural gas releases: A comprehensive risk analysis framework,' *International Journal of Hydrogen Energy*, vol. 40, no. 39, pp. 13 653–13 663, Oct. 2015, ISSN: 0360-3199. DOI: 10.1016/j.ijhydene.2015.07.117. [Online]. Available: <https://www.sciencedirect.com/science/article/pii/S0360319915019205>.
- [3] A. Züttel, 'Hydrogen storage methods,' *Naturwissenschaften*, vol. 91, no. 4, pp. 157–172, Apr. 2004, ISSN: 1432-1904. DOI: 10.1007/s00114-004-0516-x. [Online]. Available: <https://doi.org/10.1007/s00114-004-0516-x>.
- [4] J. A. Løkke, *The Kjørbo Incident*. [Online]. Available: <https://www.sintef.no/globalassets/sintef-industri/arrangement/sh2ift/learnings-from-thekjoerbo-incident-nel.pdf>.
- [5] D. A. Crawl and Y.-D. Jo, 'The hazards and risks of hydrogen,' *Journal of Loss Prevention in the Process Industries*, vol. 20, no. 2, pp. 158–164, 2007. DOI: 10.1016/j.jlp.2007.02.002. [Online]. Available: <https://doi.org/10.1016/j.jlp.2007.02.002>.
- [6] J. X. Wen and et al., 'Statistics, lessons learned and recommendations from analysis of hiad 2.0 database,' *International Journal of Hydrogen Energy*, vol. 47, no. 38, pp. 17 082–17 096, 2022. DOI: 10.1016/j.ijhydene.2022.03.170. [Online]. Available: <https://doi.org/10.1016/j.ijhydene.2022.03.170>.
- [7] K. M. Groth and E. S. Hecht, 'Hyrax: A methodology and toolkit for quantitative risk assessment of hydrogen systems,' *International Journal of Hydrogen Energy*, vol. 42, no. 11, pp. 7485–7493, 2017. DOI: 10.1016/j.ijhydene.2016.07.002. [Online]. Available: <https://doi.org/10.1016/j.ijhydene.2016.07.002>.
- [8] I. Fossan, K. van Wingerden, Ø. Knudsen, J. Wiklund and A. V. Gaathaug, 'The safen ignition probability model for hydrogen,' 2024.
- [9] N. I. Badea, 'Hydrogen as energy sources—basic concepts,' *Energies*, vol. 14, no. 18, p. 5783, 2021. DOI: 10.3390/en14185783. [Online]. Available: <https://doi.org/10.3390/en14185783>.

- [10] N. Yang, J. Deng, C. Wang, Z. Bai and J. Qu, ‘High pressure hydrogen leakage diffusion: Research progress,’ *International Journal of Hydrogen Energy*, vol. 50, pp. 1029–1046, 2024. DOI: 10.1016/j.ijhydene.2023.08.221. [Online]. Available: <https://doi.org/10.1016/j.ijhydene.2023.08.221>.
- [11] N. A. A. Rusman and M. Dahari, ‘A review on the current progress of metal hydrides material for solid-state hydrogen storage applications,’ *International Journal of Hydrogen Energy*, vol. 41, no. 28, pp. 12 108–12 126, 2016. DOI: 10.1016/j.ijhydene.2016.05.244. [Online]. Available: <https://doi.org/10.1016/j.ijhydene.2016.05.244>.
- [12] F. Yang and et al., ‘Review on hydrogen safety issues: Incident statistics, hydrogen diffusion, and detonation process,’ *International Journal of Hydrogen Energy*, vol. 46, no. 61, pp. 31 467–31 488, 2021. DOI: 10.1016/j.ijhydene.2021.07.005. [Online]. Available: <https://doi.org/10.1016/j.ijhydene.2021.07.005>.
- [13] E. Kim, J. Park, J. H. Cho and I. Moon, ‘Simulation of hydrogen leak and explosion for the safety design of hydrogen fueling station in Korea,’ *International Journal of Hydrogen Energy*, vol. 38, no. 3, pp. 1737–1743, 2013, ISSN: 0360-3199. DOI: <https://doi.org/10.1016/j.ijhydene.2012.08.079>. [Online]. Available: <https://www.sciencedirect.com/science/article/pii/S0360319912018812>.
- [14] S. B. Dorofeev, V. P. Sidorov, A. E. Dvoinishnikov and W. Breitung, ‘Deflagration to detonation transition in large confined volume of lean hydrogen-air mixtures,’ *Combustion and Flame*, vol. 104, no. 1, pp. 95–110, 1996. DOI: 10.1016/0010-2180(95)00113-1. [Online]. Available: [https://doi.org/10.1016/0010-2180\(95\)00113-1](https://doi.org/10.1016/0010-2180(95)00113-1).
- [15] Q. Hu, X. Zhang and H. Hao, ‘A review of hydrogen-air cloud explosions: The fundamentals, overpressure prediction methods, and influencing factors,’ *International Journal of Hydrogen Energy*, vol. 48, no. 36, pp. 13 705–13 730, 2023. DOI: 10.1016/j.ijhydene.2022.11.302. [Online]. Available: <https://doi.org/10.1016/j.ijhydene.2022.11.302>.
- [16] A. R. Soman and G. K. Sundararaj, *Consequence assessment of vapour cloud explosion involving hydrogen release*, 2012. [Online]. Available: <https://api.semanticscholar.org/CorpusID:15511119>.
- [17] D. R. Malik, W. B. Lowry, E. Vivanco and J. K. Thomas, ‘Very lean hydrogen vapor cloud explosion testing,’ *Process Safety Progress*, vol. 42, no. 2, pp. 242–251, 2023. DOI: 10.1002/prs.12459.
- [18] National Fire Protection Association, *Explosions vs. deflagrations vs. detonations*, <https://www.nfpa.org/news-blogs-and-articles/blogs/2023/03/27/explosions-vs-deflagrations-vs-detonations>, Accessed: 2024-05-27, 2023.
- [19] Joar Dalheim and A. Risan, ‘Guidelines for quantitative risk analysis of facilities handling hazardous substances,’ The Norwegian Directorate for Civil Protection (DSB), Tech. Rep. PRJ11100262033/R1, Nov. 2021. (visited on 22/01/2024).

- [20] M. R. Swain, P. A. Filoso and M. N. Swain, ‘Ignition of lean hydrogen–air mixtures,’ *International Journal of Hydrogen Energy*, vol. 30, no. 13, pp. 1447–1455, 2005. DOI: 10.1016/j.ijhydene.2004.10.017.
- [21] P. A. M. U. de Haag, B. J. M. Ale and J. G. Post, ‘T10-1 - the ‘purple book’: Guideline for quantitative risk assessment in the netherlands,’ in *Loss Prevention and Safety Promotion in the Process Industries*, H. J. Pasma, O. Fredholm and A. Jacobsson, Eds. Amsterdam: Elsevier Science B.V., 2001, pp. 1429–1438. DOI: 10.1016/B978-044450699-3/50053-7. [Online]. Available: <https://doi.org/10.1016/B978-044450699-3/50053-7>.
- [22] J.-E. Vinnem and W. Røed, *Offshore Risk Assessment Vol. 1: Principles, Modelling and Applications of QRA*, 4. utgave. Springer London Ltd, 2019, ISBN: 9781447174431.
- [23] J.-E. Vinnem and W. Røed, *Offshore Risk Assessment Vol. 2: Principles, Modelling and Applications of QRA*, Engelsk, 4. utgave. Springer London Ltd, 2020, Publisert: 2020-09-20, ISBN: 9781447174509.
- [24] Risktec, ‘Quantitative risk assessment across major hazard industries,’ *Risktec Solutions*, 2024, Accessed: 2024-05-25. [Online]. Available: <https://www.risktec.tuv.com/wp-content/uploads/2019/05/SCS-2019-QRA-Role-in-a-Safety-Case.pdf>.
- [25] B. D. Ehrhart, E. S. Hecht and B. B. Schroeder, *Hydrogen plus other alternative fuels risk assessment models (hgram+): Version 5.1 technical reference manual*, Accessed: March 4, 2024, Sandia National Laboratories, 2023. [Online]. Available: <http://hgram.sandia.gov/>.
- [26] A. V. Tchouvelev, R. T. Hay and P. Bénard, ‘Comparative risk estimation of compressed hydrogen and cng refuelling options,’ 2008. [Online]. Available: <https://api.semanticscholar.org/CorpusID:46985060>.
- [27] I. Fossan, K. van Wingerden and J. Wiklund, ‘St-17462-4 wp5 appendix c safen ignition model for hydroge,’ Tech. Rep 17462.
- [28] H. E. Myrstad, ‘Ignition probability of hydrogen facilities,’ M.S. thesis, Norwegian University of Science and Technology, Trondheim, 2023. [Online]. Available: <https://ntnuopen.ntnu.no/ntnu-xmlui/bitstream/handle/11250/3094260/no.ntnu%3ainspera%3a142434234%3a34543275.pdf?sequence=1&isAllowed=y>.
- [29] I. Fossan, ‘Modelling of ignition sources on land-based oil and gas facilities,’ Tech. Rep. ST-16542-1.
- [30] I. Fossan and A. Sæbø, ‘Modelling of ignition sources on offshore oil and gas facilities - MISOF,’ Tech. Rep 107566.
- [31] D. Bjerketvedt and A. Mjaavatten, ‘Hydrogen-air explosion in an ammonia plant,’ in *Proceedings of the International Conference on Hydrogen Safety*, Conference Paper, 2005. [Online]. Available: [http://www.hydrogen.energy.gov/pdfs/safety\\_biblio/ichs2005/papers/100096.pdf](http://www.hydrogen.energy.gov/pdfs/safety_biblio/ichs2005/papers/100096.pdf).

- [32] DNV, *Cfd simulation - kameleon fireex - kfx*, Accessed: 2024-05-25, 2024. [Online]. Available: <https://www.dnv.co.kr/services/cfd-simulation-kameleon-fireex-kfx-110598/>.
- [33] B. Grimsmo, N. Lilleheie, K. Rian *et al.*, *KFX - User Manual*, 2017.
- [34] S. Govindarajan, ‘Quantitative risk assessment of the performance of barriers controlling fire and explosion risk,’ M.S. thesis, Norwegian University of Science and Technology (NTNU), 2020. [Online]. Available: <https://ntnuopen.ntnu.no/ntnu-xmlui/handle/11250/2656760>.
- [35] C. Jang, S. Choi and B. J.B, ‘Cfd modeling and fire damage analysis of jet fire on hydrogen pipeline in a pipe rack structure,’ *International Journal of Hydrogen Energy*, vol. 40, pp. 15 760–15 772, 2015. DOI: 10.1016/j.ijhydene.2015.09.070. [Online]. Available: <https://doi.org/10.1016/j.ijhydene.2015.09.070>.
- [36] B. Magnussen and B. Hjertager, ‘On mathematical modeling of turbulent combustion with special emphasis on soot formation and combustion,’ *Symposium (International) on Combustion*, vol. 16, pp. 719–729, Dec. 1977. DOI: 10.1016/S0082-0784(77)80366-4.
- [37] H. K. Versteeg and W. Malalasekera, *An Introduction to Computational Fluid Dynamics: The Finite Volume Method*. Pearson Education Limited, 2007.
- [38] S. Impoco, ‘Probabilistic analysis of the performance of barriers controlling the ignition of combustible gas in gas turbine air intakes,’ M.S. thesis, Università di Bologna, 2019.
- [39] P. Space. ‘40ft x 8ft one-trip shipping container (blue).’ (), [Online]. Available: <https://www.portablespace.co.uk/product/40ft-x-8ft-one-trip-shipping-container-blue> (visited on 07/03/2024).
- [40] M. West, A. Al-Douri, K. Hartmann, W. Buttner and K. M. Groth, ‘Critical review and analysis of hydrogen safety data collection tools,’ *International Journal of Hydrogen Energy*, vol. 47, no. 40, pp. 17 845–17 858, 2022, ISSN: 0360-3199. DOI: <https://doi.org/10.1016/j.ijhydene.2022.03.244>. [Online]. Available: <https://www.sciencedirect.com/science/article/pii/S0360319922013945>.
- [41] B. D. Ehrhart, E. Hecht and K. Groth, ‘Hydrogen risk assessment models (hram) (v.3.1) (technical reference manual),’ May 2021. DOI: 10.2172/1784842. [Online]. Available: <https://www.osti.gov/biblio/1784842>.
- [42] M. Koyama, E. Akiyama, Y.-K. Lee, D. Raabe and K. Tsuzaki, ‘Overview of hydrogen embrittlement in high-Mn steels,’ *International Journal of Hydrogen Energy*, vol. 42, no. 17, pp. 12 706–12 723, 2017. DOI: 10.1016/j.ijhydene.2017.02.214. [Online]. Available: <https://doi.org/10.1016/j.ijhydene.2017.02.214>.

# **Appendix A**

## **xml file for container simulations**

```

<?xml version = "1.0" encoding="UTF-8" standalone="no" ?>
<kfxScript>
<GUI protection="No" />
<!--
  This is a command shedule file automatically generated by [Quick run setup] in
  the
  "KFX Fire & gas cloud simulation wizard".
  You may want to edit this file in a text editor. To avoid unintentional
  overwrite
  from GUI after your own editing set:
  <GUI Protection="Yes" >
  in the third line of this .xml file
-->
  <atStartAndRestart>
    <runParameters TFIL="10" TMAX="300" MSTEP="900000" />
    <xmlInclude xmlFile="blowdown.xml" />
    <RBM>
      <Detector id="1" name="Detector_1" type="Infrared point sensor" x0="-
11.66" y0="0.38" z0="1.75" processing_time="1" response_time="5"
trigger_matter="H2" trigger_point_low="0.01" trigger_point_high="0.02"
angle="0." />
      <Detector id="2" name="Detector_2" type="Infrared point sensor" x0="-
11.66" y0="2.25" z0="1.75" processing_time="1" response_time="5"
trigger_matter="H2" trigger_point_low="0.01" trigger_point_high="0.02"
angle="0." />
      <Detector id="3" name="Detector_3" type="Infrared point sensor" x0="-0.8"
y0="0.2" z0="1.75" processing_time="1" response_time="5" trigger_matter="H2"
trigger_point_low="0.01" trigger_point_high="0.02" angle="0." />
      <Detector id="4" name="Detector_4" type="Infrared point sensor" x0="-0.8"
y0="2.21" z0="1.75" processing_time="1" response_time="5" trigger_matter="H2"
trigger_point_low="0.01" trigger_point_high="0.02" angle="0." />
      <Detector id="5" name="Detector_5" type="Infrared point sensor" x0="-
4.82" y0="0.85" z0="2.76" processing_time="1" response_time="5"
trigger_matter="H2" trigger_point_low="0.01" trigger_point_high="0.02"
angle="0." />
      <Ignitor id="1" name="IGS_1" type="Other generic [Ex]" ProbType="EV"
x0="-12" y0="0" z0="0" x1="0" y1="2.45" z1="2.5" cont_expec="6.27073e-07"
t_hot="20" discr_expec="1.22647e-08" piso="0" />
      <Ignitor id="2" name="IGS_2" type="Electrical equipment, generic [Ex]"
ProbType="EV" x0="-12" y0="0" z0="0" x1="0" y1="2.45" z1="2.5" cont_expec="5.4e-
07" t_hot="100" discr_expec="1.5e-09" piso="0" />
      <Ignitor id="3" name="IGS_3" type="Rotating equipment, generic [Ex]"
ProbType="EV" x0="-12" y0="0" z0="0" x1="0" y1="2.45" z1="2.5" cont_expec="1.1e-
05" t_hot="100" discr_expec="1.5e-09" piso="0" />
      <Ignitor id="4" name="IGS_4" type="Other generic [Ex]" ProbType="EV"
x0="-12" y0="0" z0="0" x1="0" y1="2.45" z1="2.5" cont_expec="2.0e-05"
t_hot="100" discr_expec="4.0e-07" piso="0" />
    </RBM>
  </atStartAndRestart>
  <atFixedTimeInterval dt="1" begin="0" end="5">
    <save type="field" macro="s">
      <file name="$c_std_$t.r3d" counter="4" />
    </save>
    <save type="field" macro="rbm">
      <file name="$c_rbm_$t.r3d" counter="4" />
    </save>
  </atFixedTimeInterval>
  <atFixedTimeInterval dt="10" begin="10" end="1e+30">
    <save type="field" macro="s">
      <file name="$c_std_$t.r3d" counter="4" />
    </save>
    <save type="field" macro="rbm">
      <file name="$c_rbm_$t.r3d" counter="4" />
    </save>
  </atFixedTimeInterval>

```

```
</atFixedTimeInterval>  
<atAllTimeSteps>  
  <runParameters TFIL="30" TMAX="30" />  
</atAllTimeSteps>  
<atExit>  
</atExit>  
</kfxScript>
```





# Appendix B

## Figures showing the container scn file

#Case_name	data_type	tmax	jet_position	mstep	jet_direction	res_temperature	jet_pressure	jet_flowrate	jet_diameter	transient_jet	jet_gas_components	jet_gas_composition
./cont_01kgps_gr100_corner_new_xp/case'	'Jet_release_data'	1e+30	(-3.472,0.53417,1.50835)	900000	(1,0,0)	11	350	0.1	0			
./cont_01kgps_gr100_corner_new_xm/case'	'Jet_release_data'	1e+30	(-3.472,0.53417,1.50835)	900000	(-1,0,0)	11	350	0.1	0			
./cont_01kgps_gr100_corner_new_yp/case'	'Jet_release_data'	1e+30	(-3.472,0.53417,1.50835)	900000	(0,1,0)	11	350	0.1	0			
./cont_01kgps_gr100_corner_new_yn/case'	'Jet_release_data'	1e+30	(-3.472,0.53417,1.50835)	900000	(0,-1,0)	11	350	0.1	0			
./cont_01kgps_gr100_corner_new_zp/case'	'Jet_release_data'	1e+30	(-3.472,0.53417,1.50835)	900000	(0,0,1)	11	350	0.1	0			
./cont_01kgps_gr100_corner_new_zn/case'	'Jet_release_data'	1e+30	(-3.472,0.53417,1.50835)	900000	(0,0,-1)	11	350	0.1	0			

Figure B.1: Figure shows a picture of the .scn file for the container geometry- part 1

liquid_composition	gas_cloud_sim	wind_angle	wind_10	wind_stability	wind_Z0	ambient_T	wind_roughness	geometry_file	geometry_min	geometry_max	vol_box_min
'N/A'	('C0')	(100)	()		1	270	3	'neutral'	0	11	0.0002
'N/A'	('C0')	(100)	()		1	270	3	'neutral'	0	11	0.0002
'N/A'	('C0')	(100)	()		1	270	3	'neutral'	0	11	0.0002
'N/A'	('C0')	(100)	()		1	270	3	'neutral'	0	11	0.0002
'N/A'	('C0')	(100)	()		1	270	3	'neutral'	0	11	0.0002
'N/A'	('C0')	(100)	()		1	270	3	'neutral'	0	11	0.0002

Figure B.2: Figure shows a picture of the .scn file for the container geometry- part 2

vol_box_min	vol_box_max	stoppro	dt_roucum	dt_volstop	gridpoints	lockedplanes	spray_file	jet_gas_massflow	jet_gas_time	grid_parameters	block_parameters	sub_block	pool_parameters	time_controls	history_points
0.0002	./proj/P10475_RA/STUDENTS/2024/Signe/Geometri1/container_07_origo_v2.kfx'	(-15,-3,0)	(3,7,4)	(-12,0,0)	(0.2,2.45,2.9)	1	0.1	10000	100000	2	'N/A'				
0.0002	./proj/P10475_RA/STUDENTS/2024/Signe/Geometri1/container_07_origo_v2.kfx'	(-15,-3,0)	(3,7,4)	(-12,0,0)	(0.2,2.45,2.9)	1	0.1	10000	100000	2	'N/A'				
0.0002	./proj/P10475_RA/STUDENTS/2024/Signe/Geometri1/container_07_origo_v2.kfx'	(-15,-3,0)	(3,7,4)	(-12,0,0)	(0.2,2.45,2.9)	1	0.1	10000	100000	2	'N/A'				
0.0002	./proj/P10475_RA/STUDENTS/2024/Signe/Geometri1/container_07_origo_v2.kfx'	(-15,-3,0)	(3,7,4)	(-12,0,0)	(0.2,2.45,2.9)	1	0.1	10000	100000	2	'N/A'				
0.0002	./proj/P10475_RA/STUDENTS/2024/Signe/Geometri1/container_07_origo_v2.kfx'	(-15,-3,0)	(3,7,4)	(-12,0,0)	(0.2,2.45,2.9)	1	0.1	10000	100000	2	'N/A'				

Figure B.3: Figure shows a picture of the .scn file for the container geometry- part 3

subsea_parameters	rhm	xmlspray	expanded_parameters	vistemp_parameters
()	()	('Grow', 'N/A', 0, 1, 0, 0)	(0, 0, 0, 10, 10, 10, 9999, 9999, 9999)	(1, 4000, 1000, 0, 0, 0, 0, 0) ('Rectangle', 0.01, 0.005, 373, 288, 0, 1, 0, 0) (1, 1e+30, 10, 0, 0, 0, 0) 'N/A'
()	()	('Grow', 'N/A', 0, 1, 0, 0)	(0, 0, 0, 10, 10, 10, 9999, 9999, 9999)	(1, 4000, 1000, 0, 0, 0, 0, 0) ('Rectangle', 0.01, 0.005, 373, 288, 0, 1, 0, 0) (1, 1e+30, 10, 0, 0, 0, 0) 'N/A'
()	()	('Grow', 'N/A', 0, 1, 0, 0)	(0, 0, 0, 10, 10, 10, 9999, 9999, 9999)	(1, 4000, 1000, 0, 0, 0, 0, 0) ('Rectangle', 0.01, 0.005, 373, 288, 0, 1, 0, 0) (1, 1e+30, 10, 0, 0, 0, 0) 'N/A'
()	()	('Grow', 'N/A', 0, 1, 0, 0)	(0, 0, 0, 10, 10, 10, 9999, 9999, 9999)	(1, 4000, 1000, 0, 0, 0, 0, 0) ('Rectangle', 0.01, 0.005, 373, 288, 0, 1, 0, 0) (1, 1e+30, 10, 0, 0, 0, 0) 'N/A'
()	()	('Grow', 'N/A', 0, 1, 0, 0)	(0, 0, 0, 10, 10, 10, 9999, 9999, 9999)	(1, 4000, 1000, 0, 0, 0, 0, 0) ('Rectangle', 0.01, 0.005, 373, 288, 0, 1, 0, 0) (1, 1e+30, 10, 0, 0, 0, 0) 'N/A'

Figure B.4: Figure shows a picture of the .scn file for the container geometry- part 4

('Gauss', 1, 1, 3, 0, 0, 0, 'N/A', 'N/A')	('Segment_1', 1000, 3.21e+07, 1000, 0, 0, 1, 1e-05, 0.00235, 0, 0, 1, 0, 0, 0, 0)	(0.0005, 0.001, 0.0005, 0.5, 0, 0, 0, 0)	(0.768, 989, -43.804, 0, 0.0423816, 1, 0, 0, 0, 0, 0)	('DEFAULT', 0, 0, 0, 0, 0, 0)
('Gauss', 1, 1, 3, 0, 0, 0, 'N/A', 'N/A')	('Segment_1', 1000, 3.21e+07, 1000, 0, 0, 1, 1e-05, 0.00235, 0, 0, 1, 0, 0, 0, 0)	(0.0005, 0.001, 0.0005, 0.5, 0, 0, 0, 0)	(0.768, 989, -43.804, 0, 0.0423816, 1, 0, 0, 0, 0, 0)	('DEFAULT', 0, 0, 0, 0, 0, 0)
('Gauss', 1, 1, 3, 0, 0, 0, 'N/A', 'N/A')	('Segment_1', 1000, 3.21e+07, 1000, 0, 0, 1, 1e-05, 0.00235, 0, 0, 1, 0, 0, 0, 0)	(0.0005, 0.001, 0.0005, 0.5, 0, 0, 0, 0)	(0.768, 989, -43.804, 0, 0.0423816, 1, 0, 0, 0, 0, 0)	('DEFAULT', 0, 0, 0, 0, 0, 0)
('Gauss', 1, 1, 3, 0, 0, 0, 'N/A', 'N/A')	('Segment_1', 1000, 3.21e+07, 1000, 0, 0, 1, 1e-05, 0.00235, 0, 0, 1, 0, 0, 0, 0)	(0.0005, 0.001, 0.0005, 0.5, 0, 0, 0, 0)	(0.768, 989, -43.804, 0, 0.0423816, 1, 0, 0, 0, 0, 0)	('DEFAULT', 0, 0, 0, 0, 0, 0)
('Gauss', 1, 1, 3, 0, 0, 0, 'N/A', 'N/A')	('Segment_1', 1000, 3.21e+07, 1000, 0, 0, 1, 1e-05, 0.00235, 0, 0, 1, 0, 0, 0, 0)	(0.0005, 0.001, 0.0005, 0.5, 0, 0, 0, 0)	(0.768, 989, -43.804, 0, 0.0423816, 1, 0, 0, 0, 0, 0)	('DEFAULT', 0, 0, 0, 0, 0, 0)

Figure B.5: Figure shows a picture of the .scn file for the container geometry- part 5





# Appendix C

## Figures showing the ignition probability log for container scenario

time	DetIndex	VolEqStC1	VolUe12Le1	Prob	Prob_I	Prob_C	Prob_D	Prob_001
0.0000E+00	1000000	0.0000E+00	0.0000E+00	2.3500E-03	2.3500E-03	3.3710E-10	0.0000E+00	1.7374E-11
5.0000E-03	2000000	5.9971E-04	1.4090E-03	2.3500E-03	2.3500E-03	1.9891E-08	1.0747E-13	1.0253E-09
1.0000E-02	2000000	2.7595E-03	5.2068E-03	2.3501E-03	2.3500E-03	8.4638E-08	5.0493E-13	4.3625E-09
1.5000E-02	2000000	4.1426E-03	1.1137E-02	2.3502E-03	2.3500E-03	2.2081E-07	1.3548E-12	1.1382E-08
2.0000E-02	2000000	2.6731E-03	1.2491E-02	2.3503E-03	2.3500E-03	3.4407E-07	2.3083E-12	1.9250E-08
2.5000E-02	2000000	2.5241E-03	9.3771E-03	2.3504E-03	2.3500E-03	3.8771E-07	3.0238E-12	2.5203E-08
3.0000E-02	2000000	4.1467E-03	1.2151E-02	2.3504E-03	2.3500E-03	4.4243E-07	3.9512E-12	3.3049E-08
3.5000E-02	2000000	6.1495E-03	1.5214E-02	2.3506E-03	2.3500E-03	5.5782E-07	5.1125E-12	4.3063E-08
4.0000E-02	2000000	7.6345E-03	1.7170E-02	2.3507E-03	2.3500E-03	6.9482E-07	6.4230E-12	5.4646E-08
4.5000E-02	2000000	8.8508E-03	1.9206E-02	2.3508E-03	2.3500E-03	8.3724E-07	7.8888E-12	6.7968E-08
5.0000E-02	2000000	1.0357E-02	2.1094E-02	2.3510E-03	2.3500E-03	9.6673E-07	9.4987E-12	8.2916E-08
5.5000E-02	2000000	1.1907E-02	2.5272E-02	2.3511E-03	2.3500E-03	1.0830E-06	1.1428E-11	1.0052E-07
6.0000E-02	2000000	1.5465E-02	2.9530E-02	2.3512E-03	2.3500E-03	1.1952E-06	1.3681E-11	1.2051E-07
6.5000E-02	2000000	1.7496E-02	3.3729E-02	2.3513E-03	2.3500E-03	1.3091E-06	1.6256E-11	1.4322E-07
7.0000E-02	2000000	1.9966E-02	3.8707E-02	2.3514E-03	2.3500E-03	1.4392E-06	1.9210E-11	1.6911E-07
7.5000E-02	2000000	2.1017E-02	4.0707E-02	2.3515E-03	2.3500E-03	1.5389E-06	2.2317E-11	1.9629E-07
8.0000E-02	2000000	2.1541E-02	4.5657E-02	2.3517E-03	2.3500E-03	1.6817E-06	2.5804E-11	2.2674E-07
8.5000E-02	2000000	2.3574E-02	5.1040E-02	2.3518E-03	2.3500E-03	1.8238E-06	2.9726E-11	2.6060E-07
9.0000E-02	2000000	2.5337E-02	5.2754E-02	2.3519E-03	2.3500E-03	1.9458E-06	3.3830E-11	2.9594E-07
9.5000E-02	2000000	2.6722E-02	5.6669E-02	2.3521E-03	2.3500E-03	2.0858E-06	3.8316E-11	3.3432E-07
1.0000E-01	2000000	2.7406E-02	5.8167E-02	2.3522E-03	2.3500E-03	2.2203E-06	4.3160E-11	3.7568E-07
1.0500E-01	2000000	2.8169E-02	6.2835E-02	2.3524E-03	2.3500E-03	2.4024E-06	4.8558E-11	4.2117E-07
1.1000E-01	2000000	2.9291E-02	6.6735E-02	2.3526E-03	2.3500E-03	2.5726E-06	5.4432E-11	4.6669E-07
1.1500E-01	2000000	3.0470E-02	7.0272E-02	2.3527E-03	2.3500E-03	2.7436E-06	6.0850E-11	5.1119E-07
1.2000E-01	2000000	3.1491E-02	7.2437E-02	2.3529E-03	2.3500E-03	2.8785E-06	6.7606E-11	5.5262E-07
1.2500E-01	2000000	3.2464E-02	7.5287E-02	2.3530E-03	2.3500E-03	2.9949E-06	7.4687E-11	5.8906E-07
1.3000E-01	2000000	3.3371E-02	7.6032E-02	2.3531E-03	2.3500E-03	3.1023E-06	8.1983E-11	6.2072E-07
1.3500E-01	2000000	3.4200E-02	7.7936E-02	2.3532E-03	2.3500E-03	3.2050E-06	8.9544E-11	6.4918E-07
1.4000E-01	2000000	3.5014E-02	8.0984E-02	2.3533E-03	2.3500E-03	3.2896E-06	9.7390E-11	6.7326E-07
1.4500E-01	2000000	3.5819E-02	8.2922E-02	2.3534E-03	2.3500E-03	3.3695E-06	1.0552E-10	6.9356E-07
1.5000E-01	2000000	3.6506E-02	8.5132E-02	2.3534E-03	2.3500E-03	3.4289E-06	1.1387E-10	7.1143E-07
1.5500E-01	2000000	3.7131E-02	8.7251E-02	2.3535E-03	2.3500E-03	3.4975E-06	1.2252E-10	7.2770E-07
1.6000E-01	2000000	3.7687E-02	8.9333E-02	2.3535E-03	2.3500E-03	3.5442E-06	1.3134E-10	7.4141E-07
1.6500E-01	2000000	3.8218E-02	9.1223E-02	2.3536E-03	2.3500E-03	3.6015E-06	1.4045E-10	7.5309E-07
1.7000E-01	2000000	3.8712E-02	9.2971E-02	2.3536E-03	2.3500E-03	3.6424E-06	1.4970E-10	7.6406E-07
1.7500E-01	2000000	3.9151E-02	9.4015E-02	2.3537E-03	2.3500E-03	3.6859E-06	1.5912E-10	7.7418E-07
1.8000E-01	2000000	3.9568E-02	9.6610E-02	2.3537E-03	2.3500E-03	3.7410E-06	1.6877E-10	7.8413E-07
1.8500E-01	2000000	3.9967E-02	9.8548E-02	2.3538E-03	2.3500E-03	3.8031E-06	1.7870E-10	7.9401E-07
1.9000E-01	2000000	4.0347E-02	1.0016E-01	2.3538E-03	2.3500E-03	3.8529E-06	1.8885E-10	8.0372E-07
1.9500E-01	2000000	4.0700E-02	1.0102E-01	2.3539E-03	2.3500E-03	3.8761E-06	1.9906E-10	8.0968E-07
2.0000E-01	2000000	4.1039E-02	1.0444E-01	2.3539E-03	2.3500E-03	3.9560E-06	2.0972E-10	8.1724E-07
2.0500E-01	2000000	4.1373E-02	1.0862E-01	2.3540E-03	2.3500E-03	4.0361E-06	2.2079E-10	8.2700E-07
2.1000E-01	2000000	4.1691E-02	1.1040E-01	2.3541E-03	2.3500E-03	4.0799E-06	2.3205E-10	8.3681E-07
2.1500E-01	2000000	4.1973E-02	1.1126E-01	2.3541E-03	2.3500E-03	4.1047E-06	2.4337E-10	8.4390E-07
2.2000E-01	2000000	4.2233E-02	1.1296E-01	2.3541E-03	2.3500E-03	4.1424E-06	2.5488E-10	8.4940E-07
2.2500E-01	2000000	4.2461E-02	1.1366E-01	2.3541E-03	2.3500E-03	4.1588E-06	2.6646E-10	8.5358E-07
2.3000E-01	2000000	4.2679E-02	1.1644E-01	2.3542E-03	2.3500E-03	4.2110E-06	2.7833E-10	8.5858E-07
2.3500E-01	2000000	4.2873E-02	1.1757E-01	2.3542E-03	2.3500E-03	4.2325E-06	2.9028E-10	8.6314E-07
2.4000E-01	2000000	4.3052E-02	1.1778E-01	2.3542E-03	2.3500E-03	4.2384E-06	3.0225E-10	8.6581E-07

Figure C.1: Figure shows a picture of the ignition probability log (donated ignprob.log) file for the container geometry- part 1

Prob_C_001,	Prob_D_001,	Prob_002 ,	Prob_C_002,	Prob_D_002,	Prob_003 ,	Prob_C_003,	Prob_D_003,
1.7374E-11,	0.0000E+00,	1.4961E-11,	1.4961E-11,	0.0000E+00,	3.0477E-10,	3.0477E-10,	0.0000E+00,
1.0252E-09,	8.6375E-14,	8.8284E-10,	8.8282E-10,	1.0547E-14,	1.7983E-08,	1.7983E-08,	1.0547E-14,
4.3621E-09,	4.0568E-13,	3.7565E-09,	3.7564E-09,	4.9627E-14,	7.6519E-08,	7.6519E-08,	4.9627E-14,
1.1380E-08,	1.0886E-12,	9.8004E-09,	9.8002E-09,	1.3312E-13,	1.9963E-07,	1.9963E-07,	1.3312E-13,
1.9248E-08,	1.8546E-12,	1.6576E-08,	1.6575E-08,	2.2682E-13,	3.0825E-07,	3.0825E-07,	2.2682E-13,
2.5200E-08,	2.4296E-12,	2.1701E-08,	2.1701E-08,	2.9710E-13,	3.4081E-07,	3.4081E-07,	2.9710E-13,
3.3045E-08,	3.1747E-12,	2.8457E-08,	2.8457E-08,	3.8824E-13,	3.8092E-07,	3.8092E-07,	3.8824E-13,
4.3059E-08,	4.1077E-12,	3.7080E-08,	3.7080E-08,	5.0238E-13,	4.7769E-07,	4.7769E-07,	5.0238E-13,
5.4641E-08,	5.1606E-12,	4.7055E-08,	4.7054E-08,	6.3116E-13,	5.9312E-07,	5.9312E-07,	6.3116E-13,
6.7962E-08,	6.3384E-12,	5.8526E-08,	5.8525E-08,	7.7516E-13,	7.1075E-07,	7.1075E-07,	7.7516E-13,
8.2909E-08,	7.6320E-12,	7.1397E-08,	7.1396E-08,	9.3336E-13,	8.1242E-07,	8.1242E-07,	9.3336E-13,
1.0052E-07,	9.1818E-12,	8.6559E-08,	8.6558E-08,	1.1229E-12,	8.9596E-07,	8.9596E-07,	1.1229E-12,
1.2050E-07,	1.0993E-11,	1.0377E-07,	1.0377E-07,	1.3444E-12,	9.7096E-07,	9.7096E-07,	1.3444E-12,
1.4320E-07,	1.3061E-11,	1.2332E-07,	1.2332E-07,	1.5974E-12,	1.0425E-06,	1.0425E-06,	1.5974E-12,
1.6909E-07,	1.5435E-11,	1.4562E-07,	1.4561E-07,	1.8877E-12,	1.1245E-06,	1.1245E-06,	1.8877E-12,
1.9627E-07,	1.7931E-11,	1.6902E-07,	1.6902E-07,	2.1930E-12,	1.1736E-06,	1.1736E-06,	2.1930E-12,
2.2672E-07,	2.0733E-11,	1.9524E-07,	1.9524E-07,	2.5356E-12,	1.2597E-06,	1.2597E-06,	2.5356E-12,
2.6058E-07,	2.3884E-11,	2.2440E-07,	2.2440E-07,	2.9210E-12,	1.3388E-06,	1.3388E-06,	2.9210E-12,
2.9591E-07,	2.7182E-11,	2.5483E-07,	2.5483E-07,	3.3243E-12,	1.3951E-06,	1.3951E-06,	3.3243E-12,
3.3429E-07,	3.0785E-11,	2.8787E-07,	2.8787E-07,	3.7651E-12,	1.4636E-06,	1.4636E-06,	3.7651E-12,
3.7564E-07,	3.4678E-11,	3.2349E-07,	3.2348E-07,	4.2412E-12,	1.5211E-06,	1.5211E-06,	4.2412E-12,
4.2113E-07,	3.9015E-11,	3.6301E-07,	3.6301E-07,	4.7716E-12,	1.6183E-06,	1.6183E-06,	4.7716E-12,
4.6664E-07,	4.3734E-11,	4.0540E-07,	4.0539E-07,	5.3488E-12,	1.7005E-06,	1.7005E-06,	5.3488E-12,
5.1114E-07,	4.8891E-11,	4.4871E-07,	4.4870E-07,	5.9796E-12,	1.7838E-06,	1.7838E-06,	5.9796E-12,
5.5256E-07,	5.4319E-11,	4.9029E-07,	4.9028E-07,	6.6434E-12,	1.8356E-06,	1.8356E-06,	6.6434E-12,
5.8900E-07,	6.0009E-11,	5.2861E-07,	5.2861E-07,	7.3392E-12,	1.8773E-06,	1.8773E-06,	7.3392E-12,
6.2066E-07,	6.5871E-11,	5.6191E-07,	5.6190E-07,	8.0561E-12,	1.9198E-06,	1.9198E-06,	8.0561E-12,
6.4910E-07,	7.1946E-11,	5.9150E-07,	5.9149E-07,	8.7992E-12,	1.9644E-06,	1.9644E-06,	8.7992E-12,
6.7318E-07,	7.8249E-11,	6.1867E-07,	6.1867E-07,	9.5701E-12,	1.9978E-06,	1.9978E-06,	9.5701E-12,
6.9348E-07,	8.4778E-11,	6.4248E-07,	6.4247E-07,	1.0369E-11,	2.0335E-06,	2.0335E-06,	1.0369E-11,
7.1134E-07,	9.1490E-11,	6.6203E-07,	6.6202E-07,	1.1189E-11,	2.0555E-06,	2.0555E-06,	1.1189E-11,
7.2760E-07,	9.8438E-11,	6.8053E-07,	6.8052E-07,	1.2039E-11,	2.0894E-06,	2.0894E-06,	1.2039E-11,
7.4130E-07,	1.0553E-10,	6.9641E-07,	6.9640E-07,	1.2907E-11,	2.1065E-06,	2.1065E-06,	1.2907E-11,
7.5298E-07,	1.1285E-10,	7.1047E-07,	7.1045E-07,	1.3801E-11,	2.1381E-06,	2.1381E-06,	1.3801E-11,
7.6394E-07,	1.2028E-10,	7.2338E-07,	7.2337E-07,	1.4711E-11,	2.1552E-06,	2.1551E-06,	1.4711E-11,
7.7406E-07,	1.2785E-10,	7.3567E-07,	7.3565E-07,	1.5636E-11,	2.1762E-06,	2.1762E-06,	1.5636E-11,
7.8400E-07,	1.3560E-10,	7.4778E-07,	7.4776E-07,	1.6584E-11,	2.2092E-06,	2.2092E-06,	1.6584E-11,
7.9387E-07,	1.4358E-10,	7.5861E-07,	7.5859E-07,	1.7560E-11,	2.2507E-06,	2.2507E-06,	1.7560E-11,
8.0357E-07,	1.5173E-10,	7.6867E-07,	7.6865E-07,	1.8557E-11,	2.2807E-06,	2.2806E-06,	1.8557E-11,
8.0952E-07,	1.5994E-10,	7.7652E-07,	7.7650E-07,	1.9561E-11,	2.2901E-06,	2.2901E-06,	1.9561E-11,
8.1707E-07,	1.6850E-10,	7.8527E-07,	7.8525E-07,	2.0608E-11,	2.3537E-06,	2.3537E-06,	2.0608E-11,
8.2682E-07,	1.7740E-10,	7.9551E-07,	7.9549E-07,	2.1696E-11,	2.4138E-06,	2.4138E-06,	2.1696E-11,
8.3663E-07,	1.8644E-10,	8.0587E-07,	8.0584E-07,	2.2802E-11,	2.4374E-06,	2.4374E-06,	2.2802E-11,
8.4371E-07,	1.9554E-10,	8.1412E-07,	8.1410E-07,	2.3915E-11,	2.4469E-06,	2.4469E-06,	2.3915E-11,
8.4919E-07,	2.0479E-10,	8.2019E-07,	8.2016E-07,	2.5046E-11,	2.4731E-06,	2.4731E-06,	2.5046E-11,
8.5336E-07,	2.1409E-10,	8.2501E-07,	8.2499E-07,	2.6184E-11,	2.4805E-06,	2.4805E-06,	2.6184E-11,
8.5836E-07,	2.2363E-10,	8.3059E-07,	8.3056E-07,	2.7350E-11,	2.5221E-06,	2.5221E-06,	2.7350E-11,
8.6291E-07,	2.3323E-10,	8.3519E-07,	8.3516E-07,	2.8524E-11,	2.5344E-06,	2.5344E-06,	2.8524E-11,
8.6556E-07,	2.4284E-10,	8.3848E-07,	8.3845E-07,	2.9700E-11,	2.5344E-06,	2.5344E-06,	2.9700E-11,

Figure C.2: Figure shows a picture of the ignition probability log (donated ignprob.log) file for the container geometry- part 2

ftf_vol ,	LeL_vol ,	LeakRate
2.7706E-05,	2.7706E-05,	1.0000E-01
1.5794E-03,	1.6072E-03,	1.0000E-01
3.7143E-03,	5.3214E-03,	1.0000E-01
5.9663E-03,	1.1192E-02,	1.0000E-01
3.3352E-03,	1.2547E-02,	1.0000E-01
0.0000E+00,	9.4918E-03,	1.0000E-01
3.6469E-03,	1.2511E-02,	1.0000E-01
5.5834E-03,	1.5968E-02,	1.0000E-01
6.2659E-03,	1.8471E-02,	1.0000E-01
7.0235E-03,	2.1243E-02,	1.0000E-01
7.2150E-03,	2.3836E-02,	1.0000E-01
6.8033E-03,	2.8077E-02,	1.0000E-01
6.8182E-03,	3.1873E-02,	1.0000E-01
6.5066E-03,	3.6202E-02,	1.0000E-01
7.4536E-03,	4.1287E-02,	1.0000E-01
4.4621E-03,	4.3337E-02,	1.0000E-01
7.7974E-03,	4.8535E-02,	1.0000E-01
6.8802E-03,	5.3652E-02,	1.0000E-01
4.4303E-03,	5.5320E-02,	1.0000E-01
5.1630E-03,	5.9100E-02,	1.0000E-01
2.0152E-03,	6.0640E-02,	1.0000E-01
6.2531E-03,	6.5307E-02,	1.0000E-01
5.1403E-03,	6.9300E-02,	1.0000E-01
3.9654E-03,	7.2837E-02,	1.0000E-01
2.4442E-03,	7.5002E-02,	1.0000E-01
2.3720E-03,	7.7805E-02,	1.0000E-01
1.7988E-03,	7.8598E-02,	1.0000E-01
2.4790E-03,	8.0501E-02,	1.0000E-01
2.3835E-03,	8.3550E-02,	1.0000E-01
1.5057E-03,	8.5487E-02,	1.0000E-01
1.2275E-03,	8.7697E-02,	1.0000E-01
1.3498E-03,	8.9816E-02,	1.0000E-01
1.2763E-03,	9.1898E-02,	1.0000E-01
1.1431E-03,	9.3788E-02,	1.0000E-01
1.3035E-03,	9.5536E-02,	1.0000E-01
8.5278E-04,	9.6580E-02,	1.0000E-01
2.5949E-03,	9.9175E-02,	1.0000E-01
1.9387E-03,	1.0111E-01,	1.0000E-01
1.5098E-03,	1.0272E-01,	1.0000E-01
8.5822E-04,	1.0358E-01,	1.0000E-01
3.4182E-03,	1.0700E-01,	1.0000E-01
4.1851E-03,	1.1119E-01,	1.0000E-01
1.5183E-03,	1.1297E-01,	1.0000E-01
8.6090E-04,	1.1383E-01,	1.0000E-01
1.5852E-03,	1.1553E-01,	1.0000E-01
5.3302E-04,	1.1623E-01,	1.0000E-01
2.7806E-03,	1.1901E-01,	1.0000E-01
1.1217E-03,	1.2013E-01,	1.0000E-01
0.0000E+00,	1.2035E-01,	1.0000E-01

Figure C.3: Figure shows a picture of the ignition probability log (donated ignprob.log) file for the container geometry- part 3